Supporting Information

Understanding and Controlling the Emission Brightness and Color of Molecular Cerium Luminophores

Yusen Qiao,[†,§] Dumitru-Claudiu Sergentu,[‡,§] Haolin Yin,[†] Alexander V. Zabula,[†] Thibault Cheisson,[†] Alex McSkimming,[†] Brian C. Manor,[†] Patrick J. Carroll,[†] Jessica M. Anna,[†,*] Jochen Autschbach,[‡,*] and Eric J. Schelter[†,*]

[†]*P. Roy and Diana T. Vagelos Laboratories, Department of Chemistry, University of Pennsylvania, 231 South 34 Street, Philadelphia, PA 19104, United States*

[‡]*Department of Chemistry, University at Buffalo, State University of New York, Buffalo, NY 14260, United States*

[§]*These authors contributed equally*

**Corresponding authors. E-mail: jmanna@sas.upenn.edu, jochena@buffalo.edu, schelter@sas.upenn.edu*

Table of Contents

1. Materials and Methods

General Methods. All reactions and manipulations were performed under an inert atmosphere (N_2) using standard Schlenk techniques or in a Vacuum Atmospheres, Inc. Nexus II drybox equipped with a molecular sieves 13X / Q5 Cu–0226S catalyst purifier system. Glassware was oven-dried for 3 hours at 150 °C prior to use. ^{1}H spectra were obtained on a Bruker DMX–300 Fourier transform NMR spectrometer at 300 MHz. Chemical shifts were recorded in units of parts per million referenced to residual solvent peaks (^{1}H). Elemental analyses were performed at Midwest Microlab, Inc (Indianopolis, Indiana) and a Costech ECS 4010 analyzer at the Earth & Environmental Science Department of the University of Pennsylvania.

Materials. Toluene, THF, CH_2Cl_2, hexanes, and *n*-pentane were purchased from Fisher Scientific. The solvents were sparged for 20 min with dry N_2 and dried using a commercial two column solvent purification system comprising columns packed with Q5 reactant and neutral alumina respectively (for hexanes and *n*-pentane), or two columns of neutral alumina (for toluene, THF and CH_2Cl_2). Benzene-d_6 was purchased from Cambridge Isotopes and dried over potassium mirror for 24 hours before use. Pyridine-d_5 was purchased from Cambridge Isotope S5 Laboratories, Inc. and stored over molecular sieves overnight prior to use. CeI_3 was purchased from Alfa Aesar and used as received. *n*-Butyllithium solution (1.6 M in hexanes) was purchased from Sigma-Aldrich and used as received. $NaN(SiMe_3)_2$ and $Li(THF)N^iPr_2$ solutions (1.5 M in cyclohexane) were purchased from Acros Organics and used as received. Ferrocene (Fc) was purchased from Acros Organics and purified by sublimation before use. $KN(SiMe_3)_2{}^t$Bu,[1] di(-1-adamantyl)amine ($HN(C_{10}H_{15})_2$),[2] $Li(THF)(NC_9H_{18})$ (HNC_9H_{18} = 2,2,6,6-tetramethylpiperidine),[3] $LiNC_5H_{10}$ (HNC_5H_{10} = piperidine),[4] $Ce(BH_4)_3(THF)_3$,[5] $Ce_2(NPh_2)_6$,[6] $[(Me_3Si)_2NC(N^iPr)_2]_3Ce$,[7] and $[^nPr_4N][BAr^F{}_4]$[8] were prepared according to literature procedures. $Li[N(C_{10}H_{15})_2]$ was prepared by deprotonation of di(-1-adamantyl)amine with ^{n}BuLi and was used without further purification. $KN(SiMe_3)_2{}^i$Pr was prepared in similar to prepare $KN(SiMe_3)_2{}^t$Bu but using $HN(SiMe_3)_2{}^i$Pr as the starting material.

Absorption and Emission Spectroscopy. 10 mm path length quartz cells fused with a J-Young valve (Figure S1) were used for UV-vis and luminescence studies of air and moisture sensitive compounds.

Figure S1. 10 mm pathlength quartz cell fused with a J-Young valve used for luminescence data collection of air sensitive compounds.

Electronic absorption spectra (UV-Vis) were collected on a Perkin Elmer 950 UV-Vis/NIR spectrophotometer. Emission and excitation spectra were collected on Fluorolog®-3 spectrofluorometer (HORIBA Jobin Yvon, Inc.) using an R928 PMT detector. Deconvolution of the spectra was accomplished with Gaussian functions using fityk program.[9] Lifetime measurements were performed on a PTI PicoMaster TCSPC lifetime fluorometer with a 380 nm wavelength source. Quantum yields of samples (Φ_X) were measured using a comparative method[10,11] and calculated against 9,10-diphenylanthracene (Φ_{ST} = 0.97 in cyclohexane)[12] with the following equation:

$$\Phi_x = \Phi_{ST}\left(\frac{\mathrm{Grad_x}}{\mathrm{Grad_{ST}}}\right)\left(\frac{\eta_x^2}{\eta_{ST}^2}\right)$$

where subscripts ST and x denote the standard (9,10-diphenylanthracene) and a sample, respectively. Grad is the gradient obtained from the plot of integrated emission intensity versus absorbance. η is the diffraction index of the solvent.

2. Synthetic Details and Characterizations

Synthesis of [(Me$_3$SiN^{t}Bu)C(N^{i}Pr)$_2$]K. To a vial containing KN^{t}BuSiMe$_3$ (482 mg, 2.6 mmol, 1.00 equiv) in 3 mL THF, a 2 mL THF solution of ^{i}Pr−N=C=N−^{i}Pr (364 mg, 2.9 mmol, 1.10 equiv) were added dropwise. After stirring for 12 h, all volatiles were removed under reduced pressure. The resulting solid was collected on a medium size fritted filter and washed with hexanes (3×3 mL). The resulting white solid was dried under reduced pressure for 1 h. Yield: 619 mg, 79%. ^{1}H NMR (C_6D_6, 300 MHz, 300 K): δ 3.82 (m, 2H, –CH$^{i\text{Pr}}$), 1.41 (s, 9H, –CH$_3^{t\text{Bu}}$), 1.16 (m, 12H, –CH$_3^{i\text{Pr}}$), 0.39 (s, 9H, –CH$_3^{\text{SiMe3}}$). Elemental analysis found (calculated) for $C_{14}H_{32}LiN_3O$: C, 54.28 (54.31), H, 10.15 (10.42), N, 13.08 (13.57).

Synthesis of {[(C$_{10}$H$_{15}$)$_2$N]C(N^{i}Pr)$_2$}Li. To a vial containing Li[N(C$_{10}$H$_{15}$)$_2$] (291 mg, 1.00 mmol, 1.00 equiv) in 3 mL toluene, a 3 mL toluene solution of ^{i}Pr−N=C=N−^{i}Pr (139 mg, 1.10 mmol, 1.10 equiv) were added dropwise. After stirring for 12 h, the resulting precipitate was collected on a medium size fritted filter and washed with hexanes (3×3 mL). The resulting white solid was dried under reduced pressure for 1 h. Yield: 350 mg, 84%. ^{1}H NMR (pyridine-d_5, 300 MHz, 300 K): δ 3.97 (m, 2H, –CH$^{i\text{Pr}}$), 2.40 (s, 12H, –CH$_2^{\text{Ad}}$), 2.13 (s, 6H, –CH$^{\text{Ad}}$), 1.70 (dd, 12H, –CH$_2^{\text{Ad}}$), 1.27 (d, 12H, J = 6.0 Hz, –CH$_3^{i\text{Pr}}$). Elemental analysis found (calculated) for $C_{27}H_{44}LiN_3$: C, 77.66 (77.66), H, 10.12 (10.62), N, 9.38 (10.06).

Synthesis of [(C$_9$H$_{18}$N)C(N^{i}Pr)$_2$]Li(THF). To a vial containing Li(THF)(NC$_9$H$_{18}$) (2.190 g, 10.00 mmol, 1.00 equiv) in 5 mL THF, a 5 mL THF solution of ^{i}Pr−N=C=N−^{i}Pr (1.390 g, 11.00 mmol, 1.10 equiv) were added dropwise. After stirring for 12 h, all volatiles were removed under reduced pressure. The resulting solid was collected on a medium size fritted filter and washed with hexanes (3×3 mL). The resulting white solids were dried under reduced pressure for 1 h. Yield: 1.951 g, 57%. ^{1}H NMR (C_6D_6, 300 MHz, 300 K): δ 4.00 (m, 2H, –CH$^{i\text{Pr}}$), 3.56 (m, 4H, THF), 1.81 (br, 2H, –CH$_2$), 1.59 (br, 4H, –CH$_2$), 1.41 (s, 12H, –CH$_3$), 1.38 (m, 4H, THF), 1.26 (d, 12H, J = 6.0 Hz, –CH$_3^{i\text{Pr}}$). Elemental analysis found (calculated) for $C_{20}H_{40}LiN_3O$: C, 69.62 (69.53), H, 11.98 (11.67), N, 12.35 (12.16).

Synthesis of **[(Me$_3$SiN^{i}Pr)C(N^{i}Pr)$_2$]K**. To a vial containing KN^{i}PrSiMe$_3$ (339 mg, 2.0 mmol, 1.00 equiv) in 3 mL THF, a 2 mL THF solution of ^{i}Pr−N=C=N−^{i}Pr (277 mg, 2.2 mmol, 1.10 equiv) was added dropwise. After stirring for 12 h, all volatiles were removed under reduced pressure. The resulting solid was collected on a medium size fritted filter and washed with hexanes (3×3 mL).

The resulting white solid was dried under reduced pressure for 1 h. Yield: 410 mg, 70%. ^{1}H NMR (C_6D_6, 300 MHz, 300 K): δ 3.78 (m, 2H, –C$H^{i\text{Pr}}$), 3.45 (m, 1H, –C$H^{i\text{Pr}}$), 1.26 (m, 6H, –$CH_3{}^{i\text{Pr}}$), 1.16 (m, 12H, –$CH_3{}^{i\text{Pr}}$), 0.36 (s, 9H, –$CH_3{}^{\text{SiMe3}}$). Elemental analysis found (calculated) for $C_{13}H_{30}KN_3Si$: C, 53.17 (52.82), H, 10.04 (10.23), N, 14.29 (14.22).

Synthesis of [(^{i}Pr$_2$N)C(N^{i}Pr)$_2$]Li(THF). To a vial containing 2.70 mL Li(THF)N^{i}Pr$_2$ cyclohexane solution (1.5 M in cyclohexane, 4.000 mmol, 1.00 equiv) and 2 mL THF, a 1 mL THF solution of ^{i}Pr−N=C=N−^{i}Pr (0.554 g, 4.400 mmol, 1.10 equiv) was added dropwise. After stirring for 12 h, all volatiles were removed under reduced pressure. The resulting solid was collected on a medium size fritted filter and washed with hexanes (3×3 mL). The resulting white solid was dried under reduced pressure for 1 h. Yield: 0.650 g, 54%. ^{1}H NMR (C_6D_6, 300 MHz, 300 K): δ 3.82 (s, 2H, –C$H^{i\text{Pr}}$), 3.60 (m, 4H, THF), 3.54 (m, 2H, –C$H^{i\text{Pr}}$), 1.32 (m, 4H, THF), 1.36−1.20 (m, 24H, –$CH_3{}^{i\text{Pr}}$). Elemental analysis found (calculated) for $C_{17}H_{36}LiN_3O$: C, 66.45 (66.85), H, 11.67 (11.88), N, 14.08 (13.76).

Synthesis of [(C_5H_{10}N)C(N^{i}Pr)$_2$]Li(THF). To a vial containing $LiNC_5H_{10}$ (0.455 g, 5.000 mmol, 1.00 equiv) in 2 mL THF, a 1 mL THF solution of ^{i}Pr−N=C=N−^{i}Pr (0.756 g, 6.000 mmol, 1.20 equiv) was added dropwise. After stirring for 12 h, all volatiles were removed under reduced pressure. The resulting solid was collected on a medium size fritted filter and washed with hexanes (3×3 mL). The resulting white solid was dried under reduced pressure for 1 h. Yield: 0.725 g, 50%. ^{1}H NMR (C_6D_6, 300 MHz, 300 K): δ 3.87 (m, 2H, –C$H^{i\text{Pr}}$), 3.58 (m, 4H, THF), 3.11 (br, 4H, –CH_2), 1.66 (br, 4H, –CH_2), 1.46 (br, 2H, –CH_2), 1.42 (m, 4H, THF) 1.31 (d, 24H, J = 6.0 Hz, –$CH_3{}^{i\text{Pr}}$). Elemental analysis found (calculated) for $C_{16}H_{32}LiN_3O$: C, 66.09 (66.41), H, 11.12 (11.15), N, 14.46 (14.52).

Synthesis of [(Me$_3$SiN^{t}Bu)C(N^{i}Pr)$_2$]$_3$Ce$^{\text{III}}$ (2). To a vial containing CeI_3 (0.052 g, 0.100 mmol, 1.00 equiv) suspended in 3 mL toluene and three drops of THF, a 2 mL toluene solution of [(Me$_3$SiN^{t}Bu)C(N^{i}Pr)$_2$]K (0.093 g, 0.300 mmol, 3.00 equiv) were added. After stirring for 12 h, all volatiles were removed under reduced pressure. The resulting mixture was extracted into 5 mL *n*-pentane and filtered through Celite packed on a coarse size fritted filter. The filtrate was concentrated to 1 mL and stored at -25 °C for 12 h to yield pale yellow crystalline product. The product was collected on a medium size fritted filter and dried under reduced pressure for 1 h. Yield: 0.041 g, 0.044 mmol, 44%. Elemental analysis found (calculated) for $C_{42}H_{96}CeN_9Si_3$•$(C_7H_8)_{0.5}$: C, 54.98 (54.77), H, 9.69 (10.10), N, 12.92 (12.63). Single crystals

suitable for X-ray analysis were obtained by storing an *n*-pentane solution at –25 °C.

Synthesis of {[$(C_{10}H_{15})_2$N]C($N^iPr)_2$}$_3$$Ce^{III}$ (3). To a 10 ml glass bomb containing $Ce(BH_4)_3(THF)_3$ (0.004 g, 0.010 mmol, 1.00 equiv) suspended in 1 mL toluene, a 1 mL toluene suspension of {[$(C_{10}H_{15})_2$N]C($N^iPr)_2$}Li (0.013 g, 0.030 mmol, 3.00 equiv) was added. Two parallel syntheses were set up at the same time and were combined together for efficient recrystallization of the product. After stirring for 72 h at 40 °C, the reaction mixtures from the three glass bombs were combined, and the volatiles were removed under reduced pressure. The resulting product was extracted into 5 mL *n*-pentane and filtered through Celite packed on a pipet. The filtrate was concentrated to 1 mL and stored at -25 °C overnight to yield pale yellow crystalline products. The supernatant solution was removed and the products were dried under reduced pressure for 1 h. Yield: 0.015 g, 0.011 mmol, 36%. ^{1}H NMR (C_6D_6, 300 MHz, 300 K): δ 10.60 (s, 2H, –CH^{iPr}), 7.24 (s, 6H, –CH_2^{Ad}), 5.67 (s, 6H, –CH_2^{Ad}), 3.65 (s, 6H, –CH^{Ad}), 3.31 (d, 6H, –CH_2^{Ad}), 2.81 (d, 6H, –CH_2^{Ad}), 2.20 (s, 6H, –CH_3^{iPr}), -12.43 (s, 6H, –CH_3^{iPr}). Elemental analysis found (calculated) for $C_{81}H_{132}CeN_9$: C, 70.97 (70.90), H, 9.90 (9.70), N, 9.34 (9.19). Single crystals suitable for X-ray analysis were obtained by storing an *n*-pentane solution at –25 °C.

Synthesis of [$(C_9H_{18}N)$C($N^iPr)_2$]$_3$$Ce^{III}$ (4). To a vial containing CeI_3 (0.052 g, 0.100 mmol, 1.00 equiv) suspended in 3 mL toluene and three drops of DME, a 2 mL toluene solution of [$(C_9H_{18}N)$C($N^iPr)_2$]Li(THF) (0.087 g, 0.300 mmol, 3.00 equiv) was added. After stirring for 12 h, all volatiles were removed under reduced pressure. The resulting mixture was extracted into 5 mL *n*-pentane and filtered through Celite packed on a coarse size fritted filter. The filtrate was concentrated to 1 mL and stored at -25 °C for 12 h to yield pale yellow crystalline product. The product was collected on a medium size fritted filter and dried under reduced pressure for 1 h. Yield: 0.046 g, 0.060 mmol, 60%. ^{1}H NMR (C_6D_6, 300 MHz, 300 K): δ 10.74 (s, 2H, –CH^{iPr}), 6.60 (br, 2H, –CH_2^{TMP}), 5.60 (s, 6H, –CH_3^{TMP}), 4.40 (s, 6H, –CH_3^{TMP}), 3.36 (br, 2H, –CH_2^{TMP}), 3.22 (br, 2H, –CH_2^{TMP}), 2.02 (s, 6H, –CH_3^{iPr}), -10.67 (s, 6H, –CH_3^{iPr}). Elemental analysis found (calculated) for $C_{48}H_{96}CeN_9$: C, 60.98 (61.37), H, 10.11 (10.30), N, 12.99 (13.42). Single crystals suitable for X-ray analysis were obtained by storing an *n*-pentane solution at –25 °C.

Synthesis of [(Me_3SiN^iPr)C($N^iPr)_2$]$_3$$Ce^{III}$ (5). To a vial containing CeI_3 (0.052 g, 0.100 mmol, 1.00 equiv) suspended in 3 mL toluene and three drops of THF, a 2 mL toluene solution of [(Me_3SiN^iPr)C($N^iPr)_2$]K (0.088 g, 0.300 mmol, 3.00 equiv) was added. After stirring for 12 h, all volatiles were removed under reduced pressure. The resulting mixture was extracted into 5 mL

n-pentane and filtered through Celite packed on a coarse size fritted filter. The filtrate was concentrated to 1 mL and stored at -25 °C overnight to yield pale yellow crystalline product. The product was collected on a medium size fritted filter and dried under reduced pressure for 1 h. Yield: 0.041 g, 0.045 mmol, 45%. ^{1}H NMR (toluene-d_8, 300 MHz, 370 K): δ 9.04 (s, 2H, –CH$^{i\text{Pr}}$), 7.65 (s, 1H, –CH$^{i\text{Pr}}$), 3.44 (m, 6H, –CH$_3^{i\text{Pr}}$), 1.76 (s, 9H, –CH$_3^{\text{SiMe3}}$), -2.28 (m, 12H, –CH$_3^{i\text{Pr}}$). Elemental analysis found (calculated) for $C_{39}H_{90}CeN_9Si_3$: C, 51.26 (51.50), H, 9.68 (9.97), N, 14.12 (13.86). Single crystals suitable for X-ray analysis were obtained by storing an *n*-pentane solution at –25 °C.

Synthesis of [(Ph$_2$N)C(N^{i}Pr)$_2$]$_3$Ce^{III} (6). To a vial containing $Ce_2(NPh_2)_6$ (0.129 g, 0.100 mmol, 1.00 equiv) dissolved in 2 mL toluene, ^{i}PrN=C=N^{i}Pr (0.080 g, 0.600 mmol, 6.00 equiv) was added. After stirring for 2 h, all volatiles were removed under reduced vacuum. Resulting mixture was then extracted into 10 mL pentane and filtered through Celite packed on a coarse size fritted filter. The filtrate was concentrated to 1 mL and stored at -25 °C for 12 h to yield yellow crystals. The product was collected on a medium size fritted filter and dried under reduced vacuum for 1 h. Yield: 0.145 g, 0.142 mmol, 71%. ^{1}H NMR (C_6D_6, 300 MHz, 300 K): δ 11.00 (d, 4H, Ph, *J* = 3.0 Hz), 10.08 (s, 2H, -CH$^{i\text{Pr}}$), 8.08 (d, 4H, Ph, *J* = 3.0 Hz), 7.42 (t, 2H, Ph, *J* = 3.0 Hz), 2.50 (br, 6H, CH$_3^{i\text{Pr}}$), -7.42 (br, 6H, CH$_3^{i\text{Pr}}$). Elemental analysis found (calculated) for $C_{57}H_{72}CeN_9$: C, 67.11(66.90), H, 6.92(7.09), N, 12.17(12.32). Single crystals suitable for X-ray analysis were obtained by storing a pentane solution at –25 °C.

Synthesis of [(^{i}Pr$_2$N)C(N^{i}Pr)$_2$]$_3$Ce^{III} (7). To a vial containing CeI_3 (0.052 g, 0.100 mmol, 1.00 equiv) suspended in 3 mL toluene, a 2 mL toluene solution of [(^{i}Pr$_2$N)C(N^{i}Pr)$_2$]Li(THF) (0.092 g, 0.300 mmol, 3.00 equiv) was added. After stirring for 12 h, all volatiles were removed under reduced pressure. The resulting mixture was extracted into 5 mL *n*-pentane and filtered through Celite packed on a coarse size fritted filter. The filtrate was concentrated to 1 mL and stored at -25 °C overnight to yield pale yellow crystalline product. The product was collected on a medium size fritted filter and dried under reduced pressure for 1 h. Yield: 0.051 g, 0.062 mmol, 62%. ^{1}H NMR (C_6D_6, 300 MHz, 300 K): δ 10.67 (s, 6H, –CH$^{i\text{Pr}}$), 7.89 (s, 6H, –CH$^{i\text{Pr}}$), 3.95 (s, 18H, –CH$_3^{i\text{Pr}}$), 3.34 (s, 18H, –CH$_3^{i\text{Pr}}$), 2.56 (s, 18H, –CH$_3^{i\text{Pr}}$), -8.03 (s, 18H, –CH$_3^{i\text{Pr}}$). Elemental analysis found (calculated) for $C_{39}H_{84}CeN_9$: C, 57.08 (57.18), H, 10.54 (10.33), N, 15.32 (15.39). Single crystals suitable for X-ray analysis were obtained by storing an *n*-pentane solution at –25 °C.

Synthesis of [(C$_5$H$_{10}$N)C(N^{i}Pr)$_2$]$_3$Ce^{III} (8). To a vial containing CeI_3 (0.052 g, 0.100 mmol, 1.00

equiv) suspended in 3 mL toluene, a 2 mL toluene solution of $[(C_5H_{10}N)C(N^iPr)_2]Li(THF)$ (0.087 g, 0.300 mmol, 3.00 equiv) was added. After stirring for 12 h, all volatiles were removed under reduced pressure. The resulting mixture was extracted into 5 mL *n*-pentane and filtered through Celite packed on a coarse size fritted filter. The filtrate was concentrated to 1 mL and stored at -25 °C for 12 h to yield pale yellow crystalline product. The product was collected on a medium size fritted filter and dried under reduced pressure for 1 h. Yield: 0.046 g, 0.060 mmol, 60%. ^{1}H NMR (C_6D_6, 300 MHz, 300 K): δ 9.79 (s, 6H, $-CH^{iPr}$), 6.60 (s, 12H, $-CH_2$), 3.29 (s, 12H, $-CH_2$), 2.81 (s, 6H, $-CH_2$), -2.75 (br, 36H, $-CH_3^{iPr}$). Elemental analysis found (calculated) for $C_{36}H_{72}CeN_9$: C, 56.36 (56.07), H, 9.11 (9.41), N, 15.89 (16.35). Single crystals suitable for X-ray analysis were obtained by storing an *n*-pentane solution at –25 °C.

Synthesis of $\{[(C_{10}H_{15})_2N]C(N^iPr)_2\}_2Ce^{III}(\mu^2\text{–}I)_2Li(THF)_2$ (3-I). To a vial containing CeI_3 (0.052 g, 0.100 mmol, 1.00 equiv) suspended in 3 mL toluene and three drops of THF, a 2 mL toluene suspension of $\{[(C_{10}H_{15})_2N]C(N^iPr)_2\}Li$ (0.418 g, 0.300 mmol, 3.00 equiv) was added. After stirring for 3 h, all volatiles were removed under reduced pressure. The resulting mixture was extracted into 20 mL *n*-pentane and filtered through Celite packed on a coarse size fritted filter. The filtrate was concentrated to 3 mL and stored at -25 °C overnight to yield pale yellow crystalline product. The product was collected on a medium size fritted filter and dried under reduced pressure for 1 h. Yield: 0.067 g, 0.049 mmol, 49%. Elemental analysis found (calculated) for $C_{62}H_{104}CeI_2LiN_6O_2 \bullet C_7H_8$: C, 57.20 (56.82), H, 7.40 (7.74), N, 5.48 (5.76). Single crystals suitable for X-ray analysis were obtained by storing an *n*-pentane solution at –25 °C.

Figure S2. Syntheses of Cerium(III) *Tris*-(guanidinate) complexes **3** and **6**.

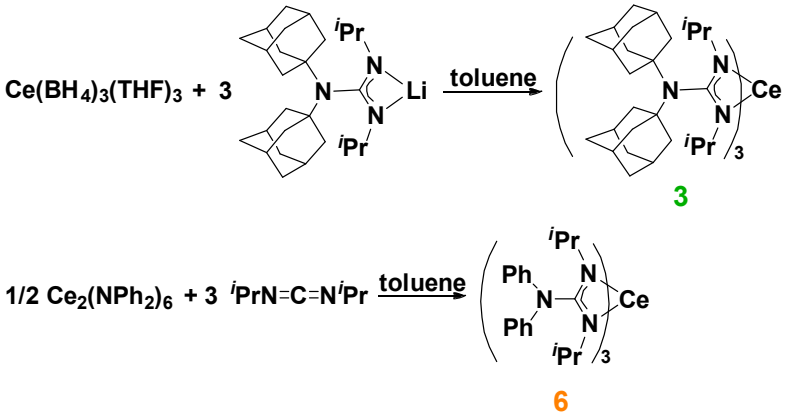

3. NMR Spectra

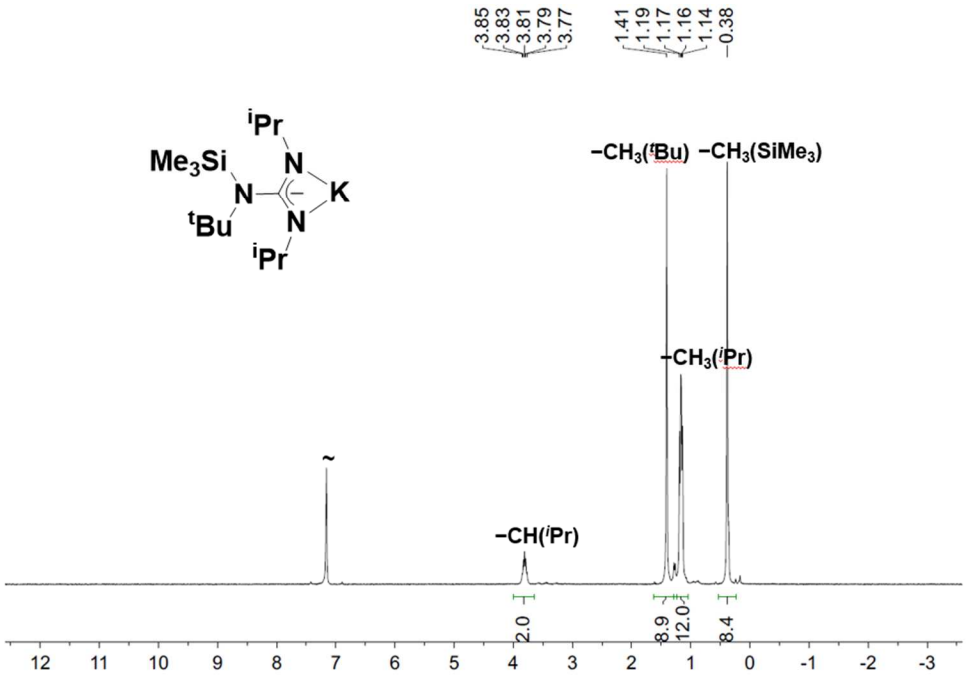

Figure S3. ^{1}H NMR spectrum of [(Me$_3$SiN^{t}Bu)C(N^{i}Pr)$_2$]K in C_6D_6. Peak of C_6D_5H is noted as ~.

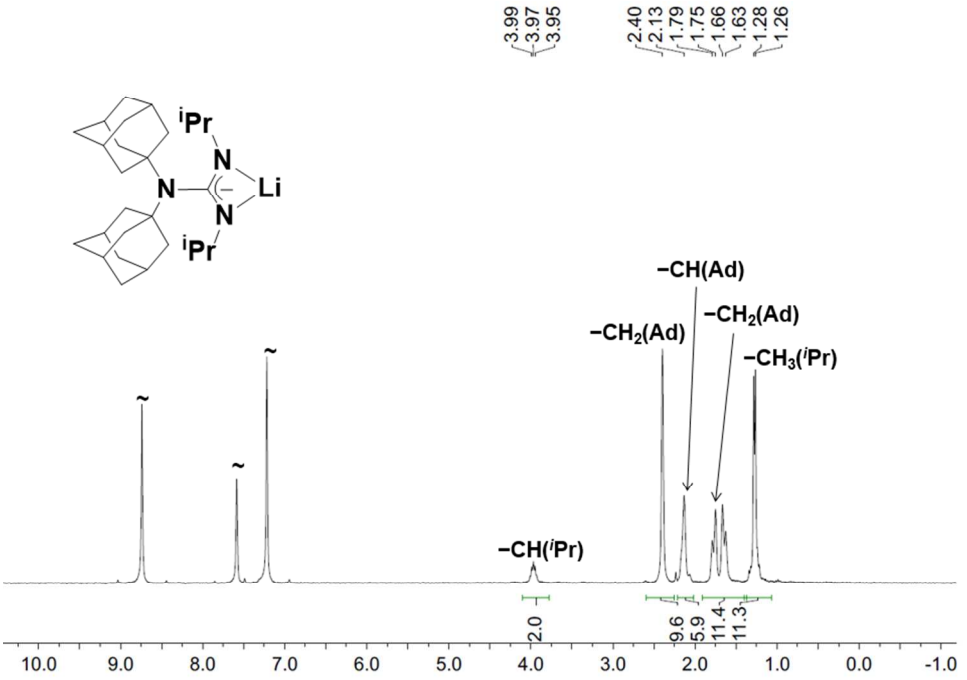

Figure S4. ^{1}H NMR spectrum of {[(C$_{10}$H$_{15}$)$_2$N]C(N^{i}Pr)$_2$}Li in pyridine-d$_5$. Proteo- peaks of pyridine-d_4 are noted as ~.

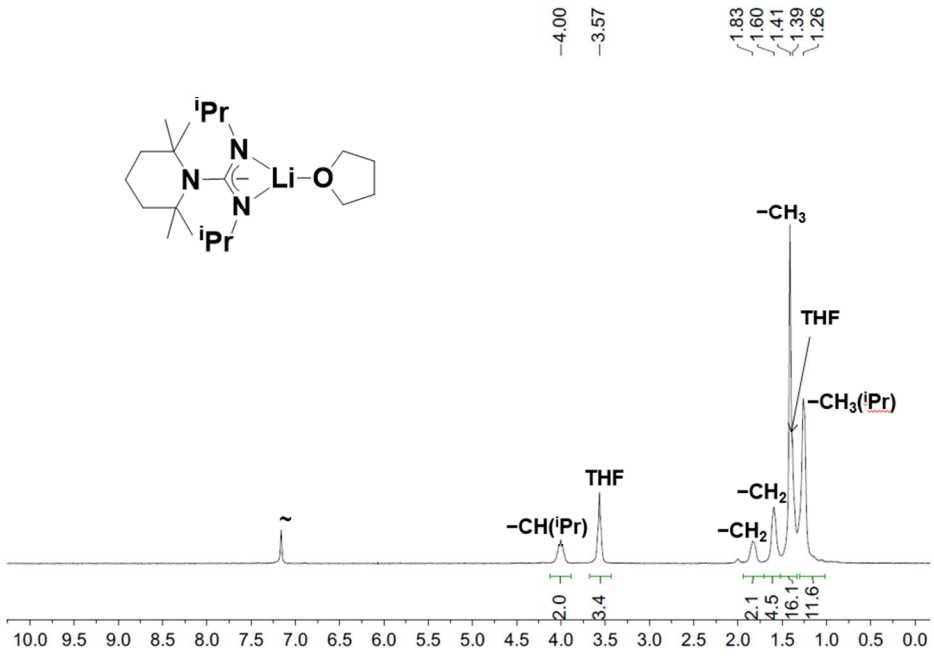

Figure S5. ^{1}H NMR spectrum of $[(C_9H_{18}N)C(N^{i}Pr)_2]Li(thf)$ in C_6D_6. Peak of C_6D_5H is noted as ~.

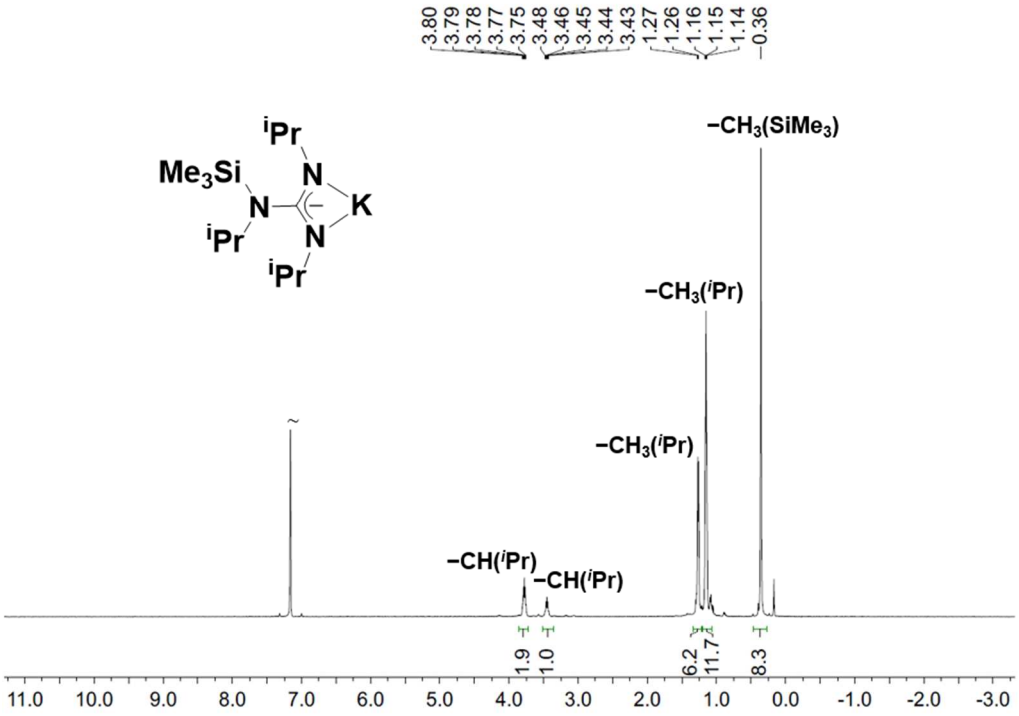

Figure S6. ^{1}H NMR spectrum of **$[(Me_3SiN^{i}Pr)C(N^{i}Pr)_2]K$** in C_6D_6. Peak of C_6D_5H is noted as ~.

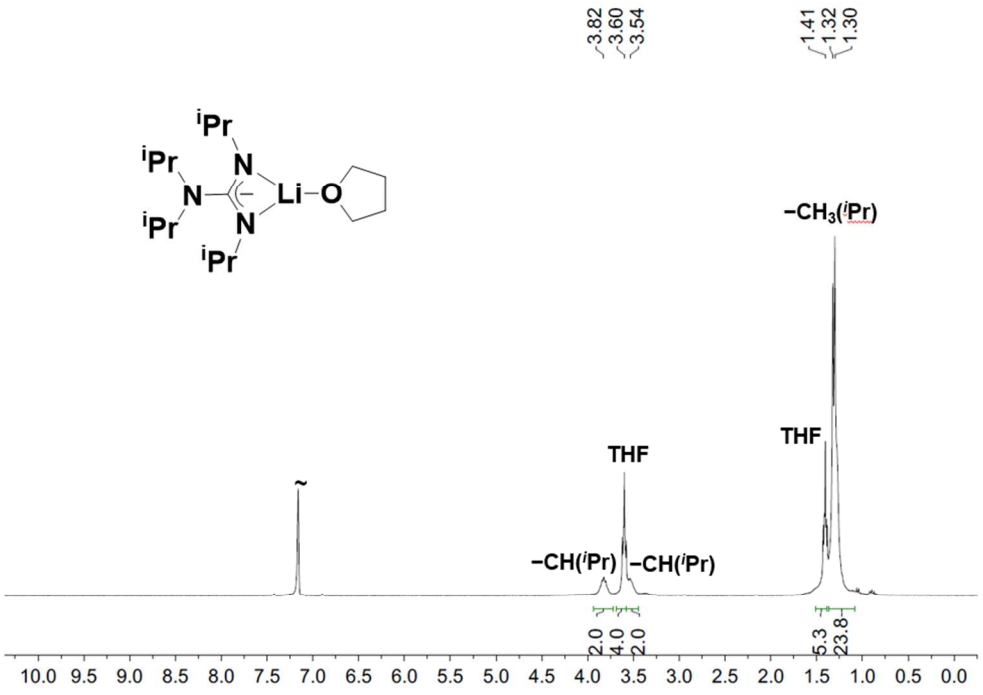

Figure S7. ^{1}H NMR of **[(^{i}Pr$_2$N)C(N^{i}Pr)$_2$]Li(THF)** in C_6D_6. Peak of C_6D_5H was noted by ~.

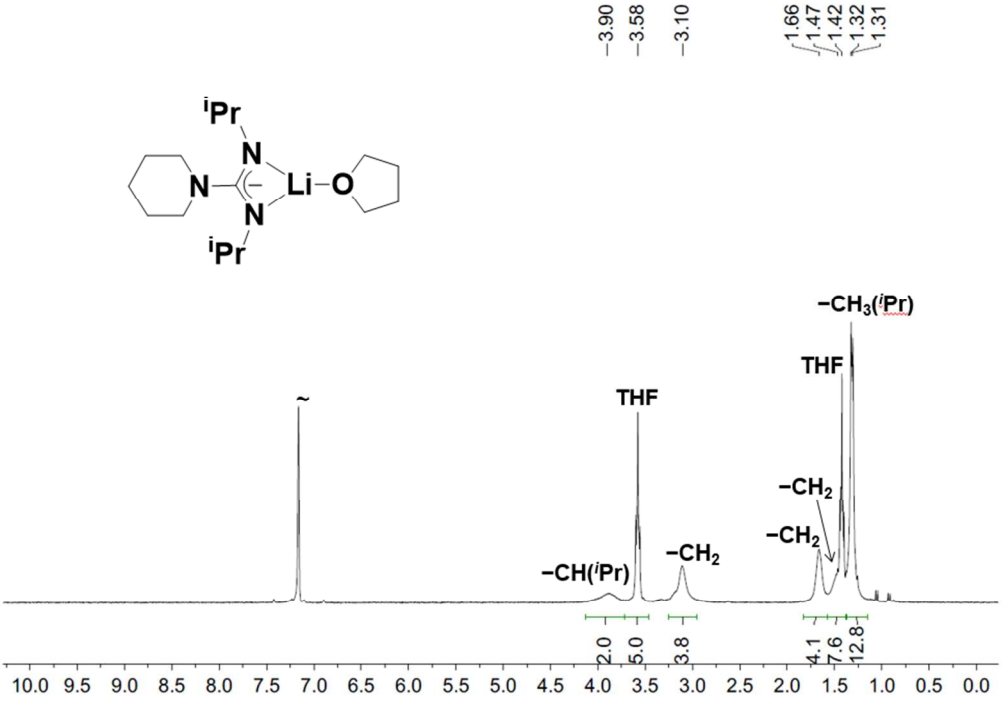

Figure S8. ^{1}H NMR of **[(C$_5$H$_{10}$N)C(N^{i}Pr)$_2$]Li(THF)** in C_6D_6. Peak of C_6D_5H was noted by ~.

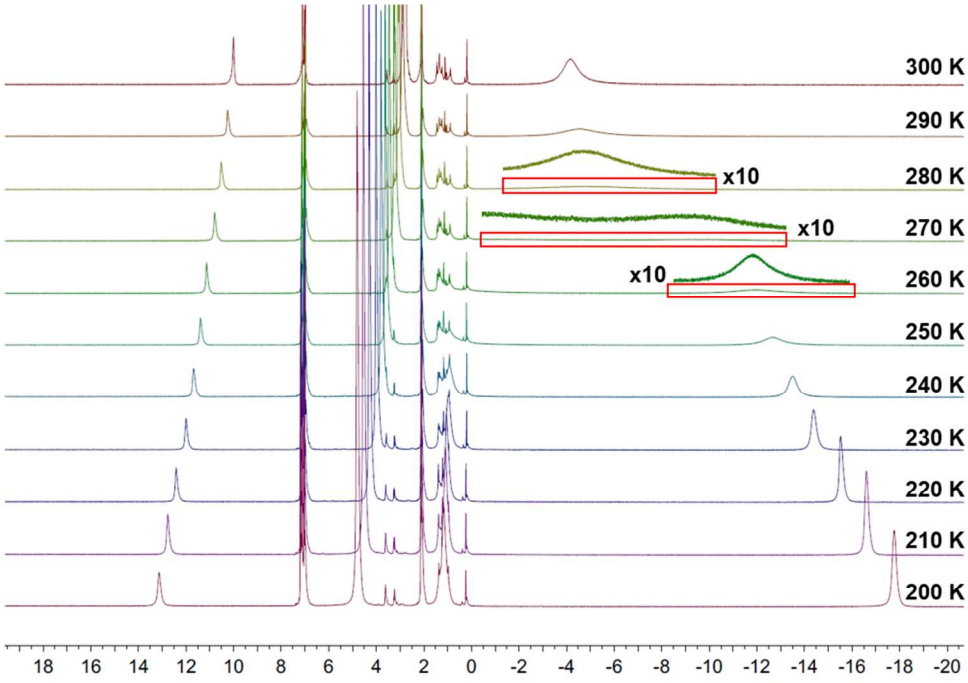

Figure S9. Variable temperature ^{1}H NMR spectra of **[(Me$_3$Si)$_2$NC(N^{i}Pr)$_2$]$_3$Ce^{III}** in toluene-d_8 from 200–300 K.

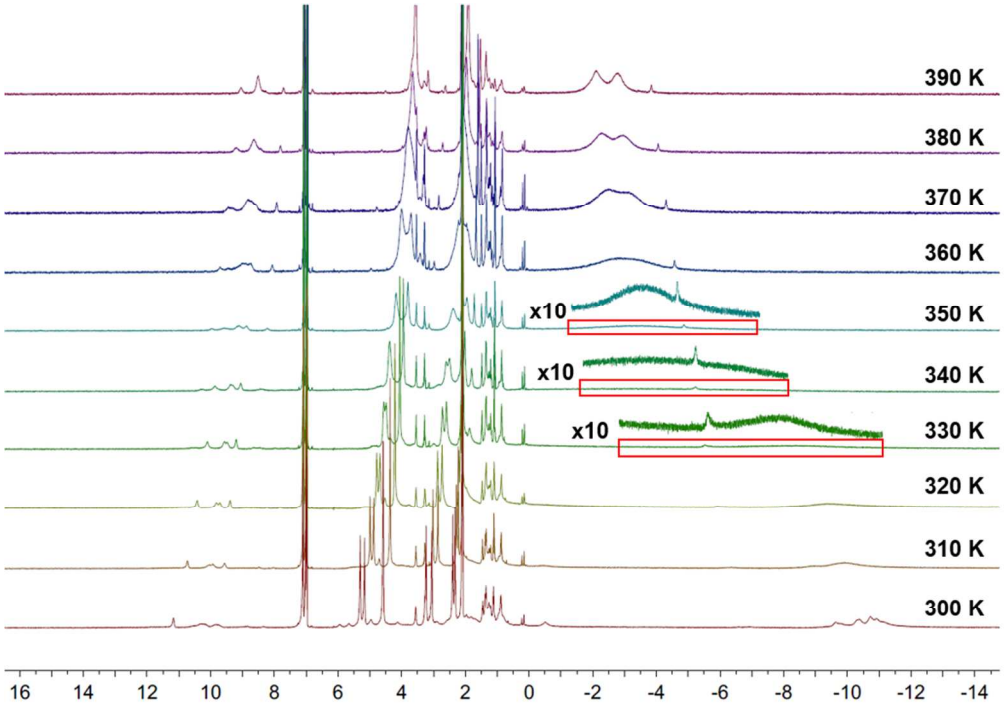

Figure S10. Variable temperature ^{1}H NMR spectra of **[(Me$_3$SiN^{t}Bu)C(N^{i}Pr)$_2$]$_3$Ce^{III}** in toluene-d_8 from 300–390 K.

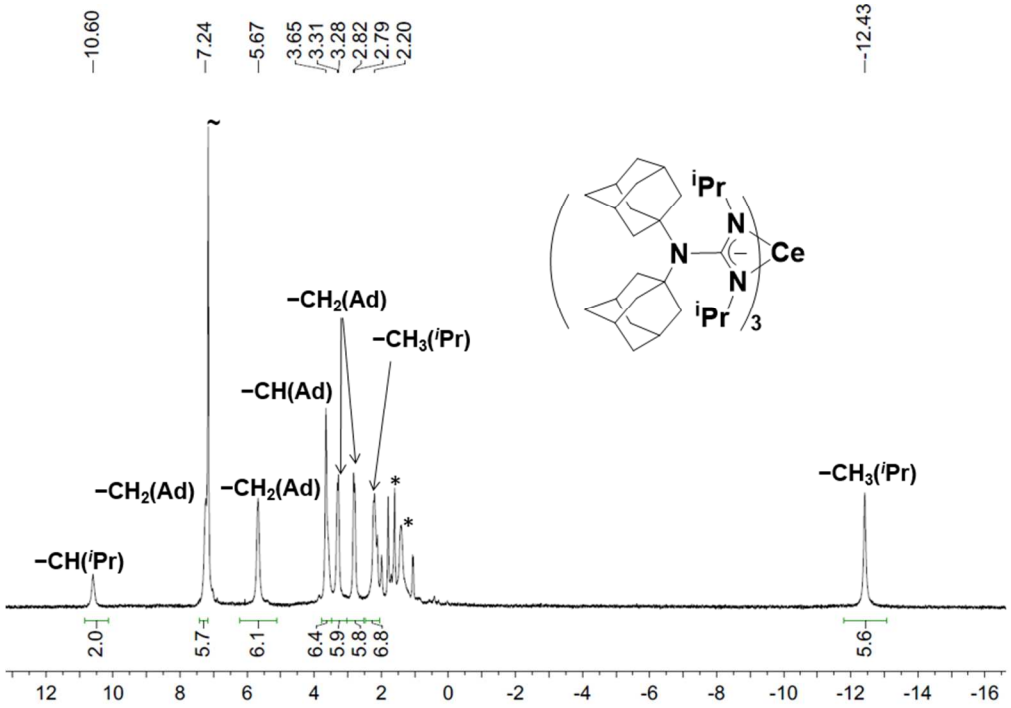

Figure S11. ^{1}H NMR of **{[($C_{10}H_{15}$)$_2$N]C(N^{i}Pr)$_2$}$_3$Ce^{III}** in C_6D_6. Peak of C_6D_5H was noted by ~. Protonated ligand resonance is marked as *.

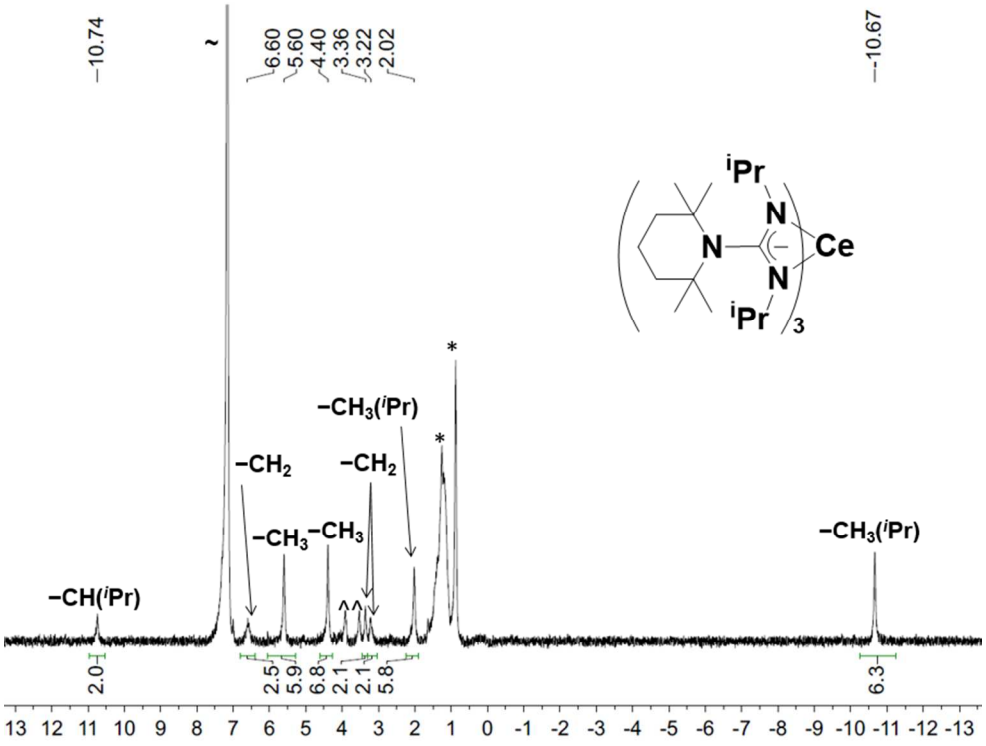

Figure S12. ^{1}H NMR of **[(C_9H_{18}N)C(N^{i}Pr)$_2$]$_3$Ce^{III}** in C_6D_6. Peak of C_6D_5H was noted by ~. Signals of *n*-pentane were noted by *. Protonated ligand resonance is marked as ^.

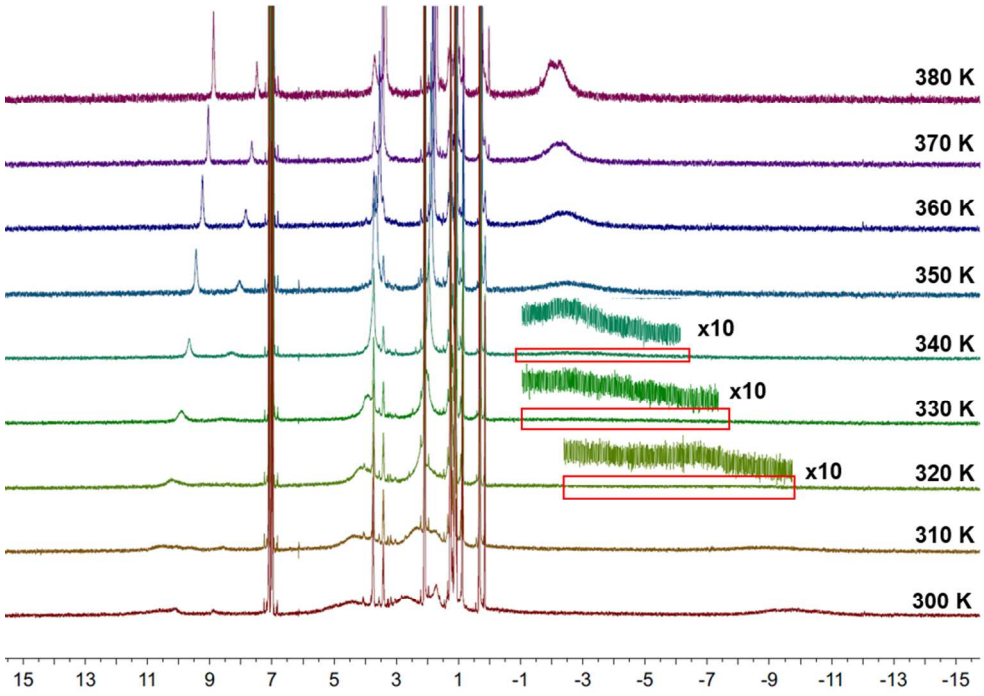

Figure S13. Variable temperature ^{1}H NMR spectra of **[(Me$_3$SiN^{i}Pr)C(N^{i}Pr)$_2$]$_3$Ce^{III}** in toluene-d_8 from 300–380 K.

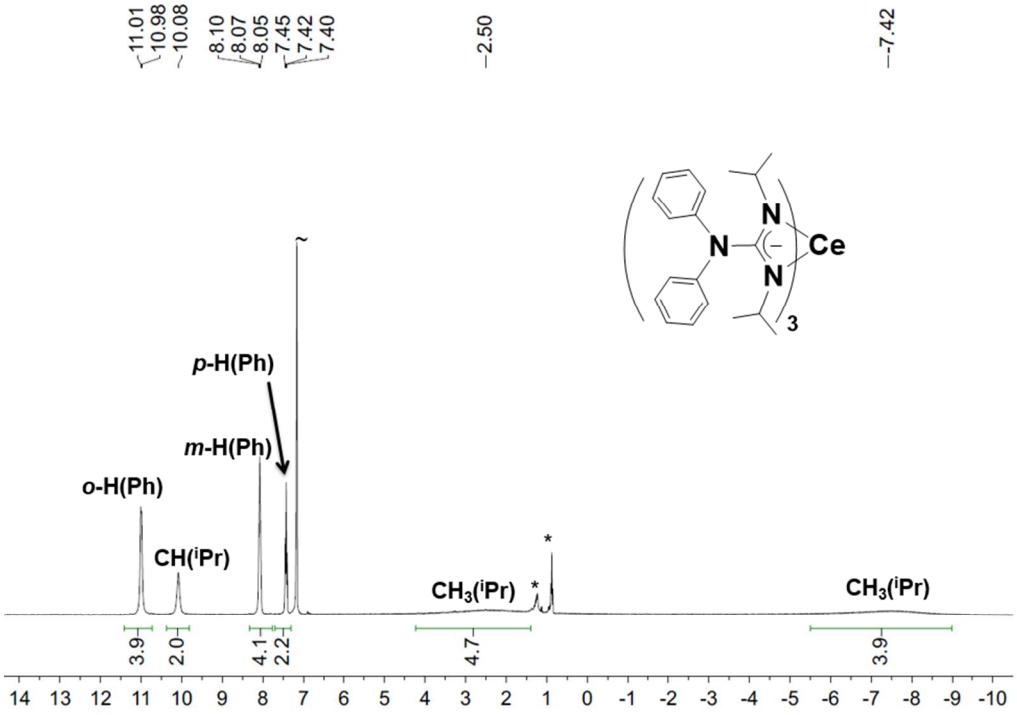

Figure S14. ^{1}H NMR spectrum of **[(Ph$_2$N)C(N^{i}Pr)$_2$]$_3$Ce^{III}** in C_6D_6. Peak of C_6D_5H was noted by ~. Signals of *n*-pentane were noted by *.

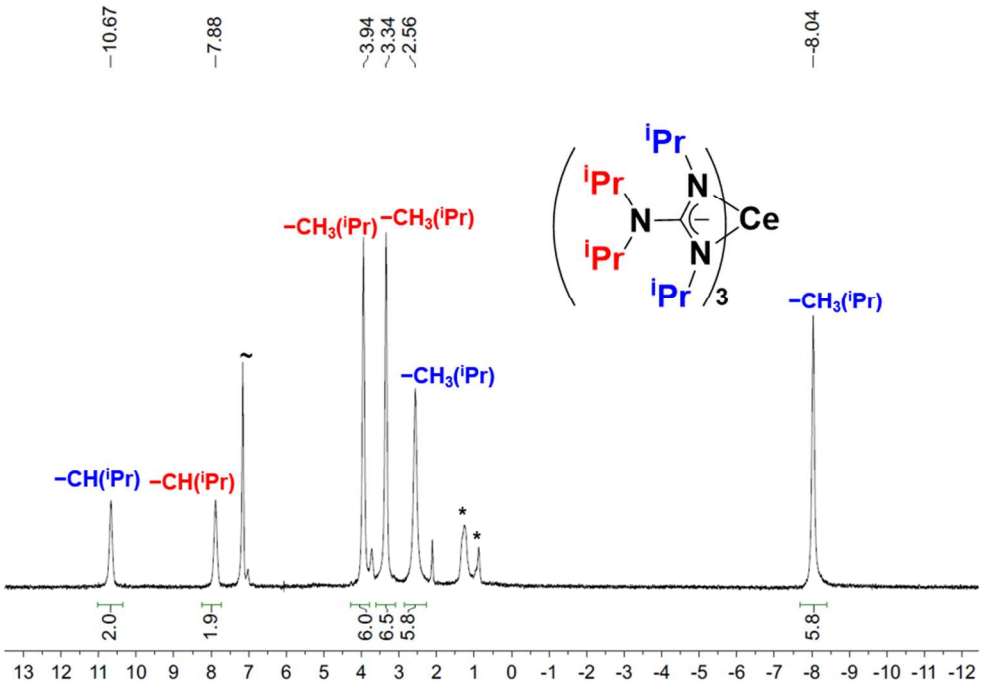

Figure S15. ^{1}H NMR spectrum of **[(^{i}Pr$_2$N)C(N^{i}Pr)$_2$]$_3$Ce^{III}** in C_6D_6. Peak of C_6D_5H was noted by ~. Signals of *n*-pentane were noted by *.

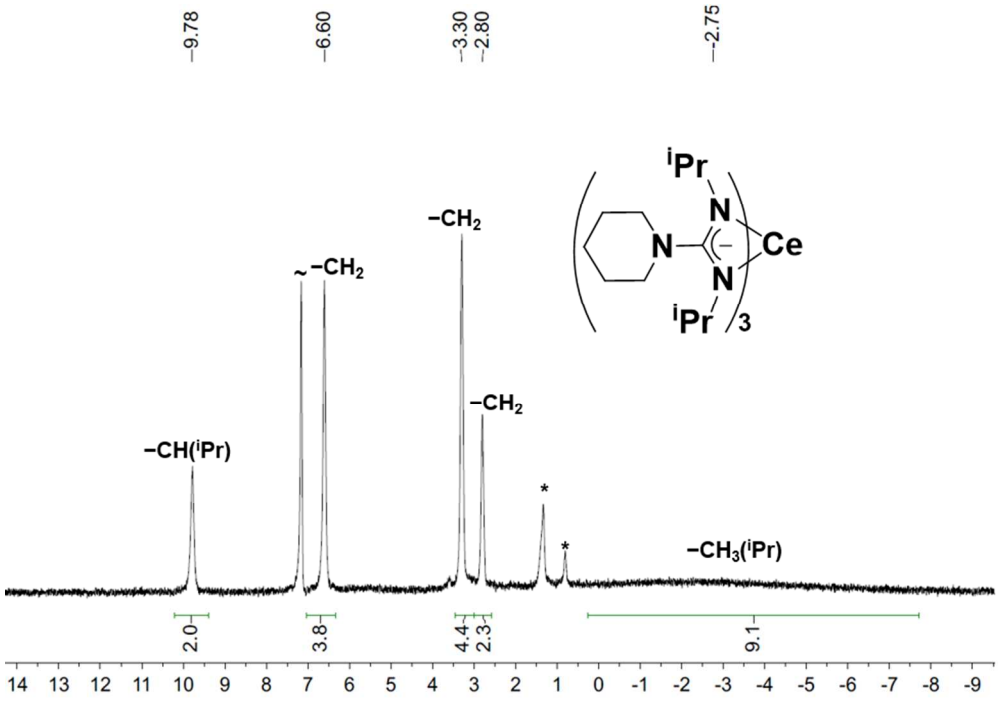

Figure S16. ^{1}H NMR spectrum of **[(C$_5$H$_{10}$N)C(N^{i}Pr)$_2$]$_3$Ce^{III}** in C_6D_6. Peak of C_6D_5H was noted by ~. Signals of *n*-pentane were noted by *.

4. X-ray Diffraction Studies

X-ray intensity data were collected on a Bruker APEXII CCD area detector employing graphite-monochromated Mo-Kα radiation (λ=0.71073 Å) at a temperature of 100(1) K or 143(1) K. Preliminary indexing was performed from a series of thirty-six 0.5° rotation frames with exposures of 10 seconds. Following full data collection, rotation frames were integrated using SAINT,[13] producing a listing of unaveraged F^2 and $\sigma(F^2)$ values which were then passed to the SHELXTL[14] program package for further processing and structure solution. The intensity data were corrected for Lorentz and polarization effects and for absorption using SADABS[15] or TWINABS[16]. The structure was solved by direct methods (SHELXS-97[17]). Refinement was by full-matrix least squares based on F^2 using SHELXL-2014.[18] All reflections were used during refinement. Non-hydrogen atoms were refined anisotropically and hydrogen atoms were refined using a riding model.

Table S1. Crystallographic Data for **2-8, 3-I**.

parameter	**2**	**3**	**4**	**6**	**7**	**8**	**3-I**
CCDC number	1576110	1576112	1576108	1576105	1576107	1576106	1576111
formula	$C_{42}H_{96}CeN_9Si_3$	$C_{81}H_{132}CeN_9$	$C_{48}H_{96}CeN_9$	$C_{57}H_{72}CeN_9$	$C_{39}H_{84}CeN_9$	$C_{36}H_{72}CeN_9$	$C_{67}H_{116}CeI_2LiN_6O_2$
M_r	951.66	1372.07	939.45	1023.35	819.27	771.15	1438.51
a [Å]	12.8493(7)	44.203(5)	24.249(2)	18.626(3)	13.2861(6)	10.0315(4)	20.8203(17)
b [Å]	10.7028(6)	44.203(5)	13.9439(12)	18.626(3)	19.9413(10)	11.8803(4)	15.8035(12)
c [Å]	39.410(2)	26.080(3)	18.4167(16)	55.983(11)	18.6655(9)	17.8420(7)	20.8531(18)
α [deg]	90	90	90	90	90	82.423(2)	90
β [deg]	93.013(2)	90	115.072(4)	90	109.946(2)	85.788(2)	90.547(3)
γ [deg]	90	120	90	120	90	89.638(2)	90
V [Å^3]	5412.3(5)	44131(11)	5640.4(8)	16820(6)	4648.6(4)	2102.09(14)	6861.1(10)
Z	4	18	4	12	4	2	4
space group	$P2_1/c$	$R3/c$	$C2/c$	$R\text{-}3/c$	$P2_1/c$	$P\text{-}1$	$P2_1/n$
ρ_{calcd}, [g cm^{-3}]	1.168	0.929	1.106	1.212	1.171	1.218	1.393
μ [mm^{-1}]	0.942	0.501	0.843	0.854	1.013	1.117	1.608
2θ range [deg]	5.760–55.208	5.844–55.110	2.442–55.474	2.914–55.056	3.100–55.100	3.460–55.160	4.680–55.170
data collected	111005	168600	51889	123114	79464	50048	226632
no. unique data, R_{int}	12517, 0.0519	22056, 0.0539	6790, 0.0545	4292, 0.0120	10726, 0.0274	9601, 0.0243	15800, 0.0169
no. obsd data [$I \geq 2\sigma(I)$]	10933	18822	6412	3535	9305	8754	13720
R_1 (all data) [a]	0.1165	0.0533	0.0886	0.0479	0.0268	0.0259	0.0745
wR_2 (all data) [b]	0.1970	0.0795	0.2309	0.1051	0.0450	0.0482	0.1430
S[c]	1.454	1.040	1.111	1.120	1.023	1.028	1.166
no. of variables	772	871	278	206	467	428	781
peak/hole [e Å^{-3}]	1.115/–4.117	0.910/–0.652	2.524/–4.138	2.841/–0.853	0.652/–0.308	0.677/–0.369	2.341/–1.868

[a] $R_1 = \Sigma||F_o|-|F_c||/\Sigma|F_o|$. [b] $wR_2 = [\Sigma[w(F_o^2-F_c^2)^2]/\Sigma[w(F_o^2)^2]]^{½}$. [c] Quality-of-fit $[\Sigma[w(F_o^2-F_c^2)^2]/(N_{obs}-N_{params})]^{½}$, based on all data.

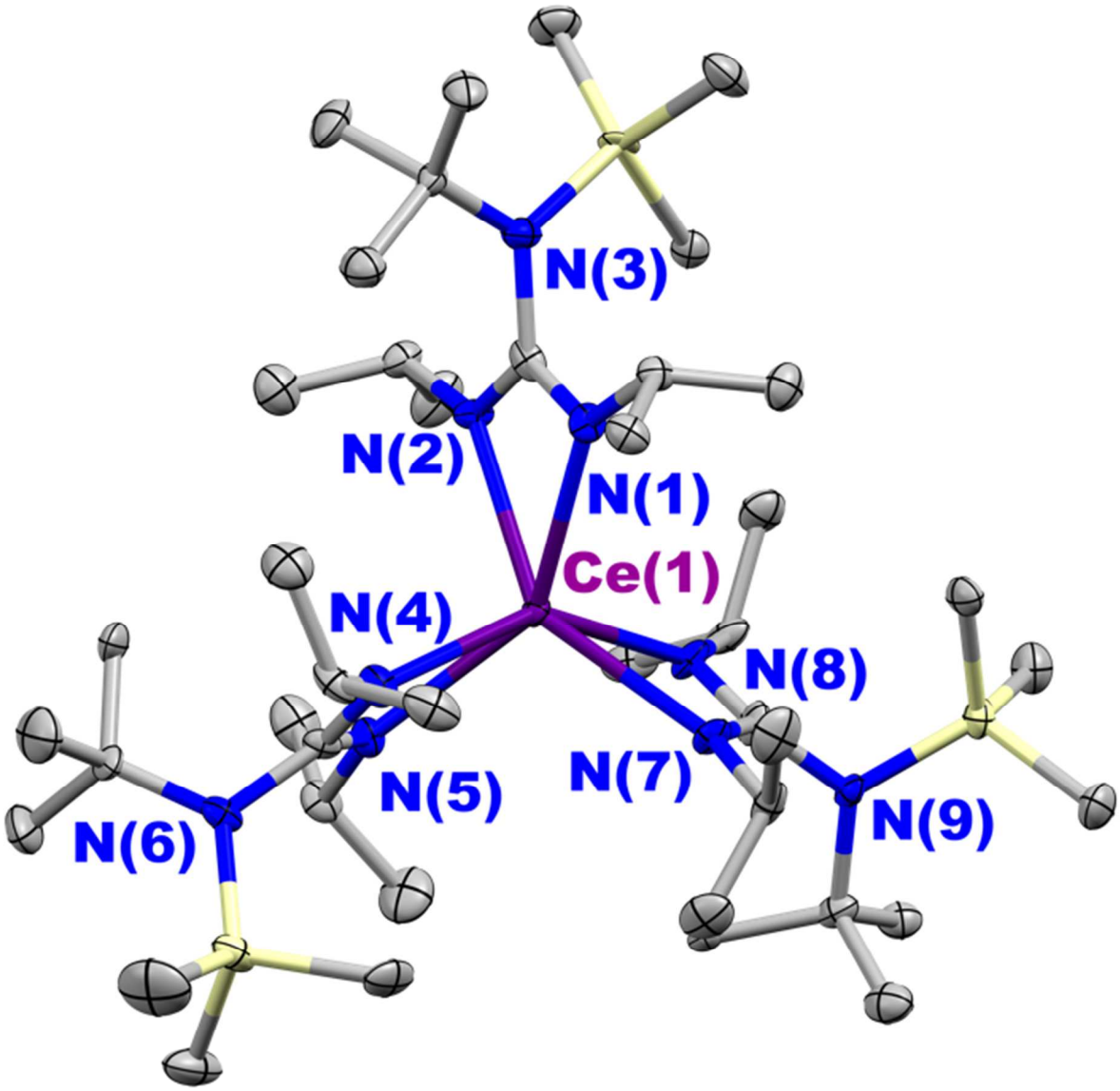

Figure S17. Thermal ellipsoid plot of **[(Me$_3$SiN^{t}Bu)C(N^{i}Pr)$_2$]$_3$Ce^{III}** at 30% probability level. Selected bond length (Å) and angles (deg): Ce(1)–N(1) 2.537(6), Ce(1)–N(2) 2.504(6), Ce(1)–N(4) 2.506(7), Ce(1)–N(5) 2.541(6), Ce(1)–N(7) 2.540(6), Ce(1)–N(8) 2.523(6); N(1)–Ce(1)–N(2) 53.0(2), N(4)–Ce(1)–N(5) 52.69(19), N(7)–Ce(1)–N(8) 53.3(2).

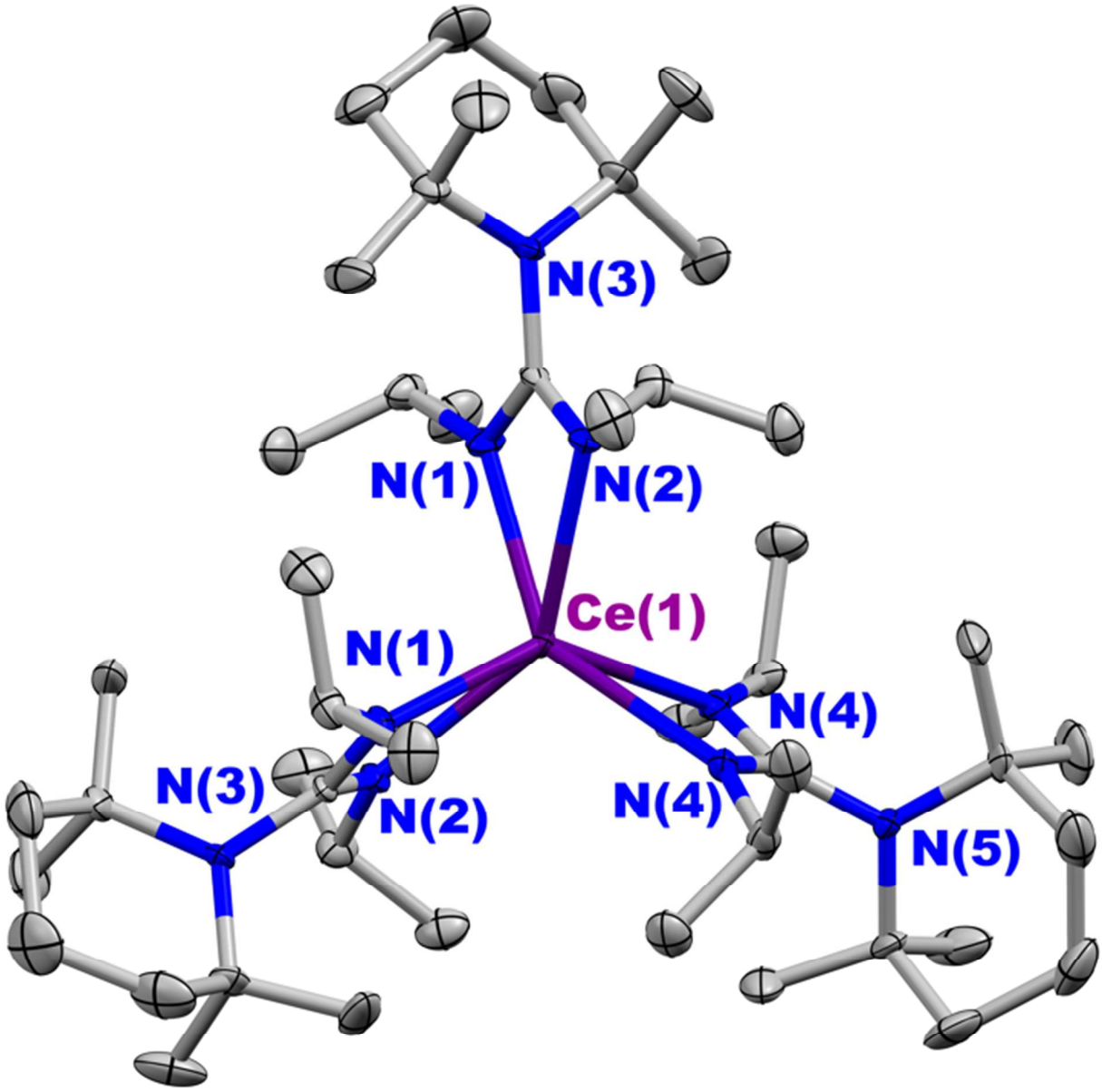

Figure S18. Thermal ellipsoid plot of **{[$(C_{10}H_{15})_2$N]C($N^iPr)_2$}$_3$Ce^{III}** at 30% probability level. Selected bond length (Å) and angles (deg): Ce(1)–N(1) 2.508(3), Ce(1)–N(2) 2.522(3), Ce(1)–N(4) 2.513(3), Ce(1)–N(5) 2.527(3), Ce(1)–N(7) 2.519(3), Ce(1)–N(8) 2.522(4); N(1)–Ce(1)–N(2) 52.60(11), N(4)–Ce(1)–N(5) 52.75(11), N(7)–Ce(1)–N(8) 52.91(10)

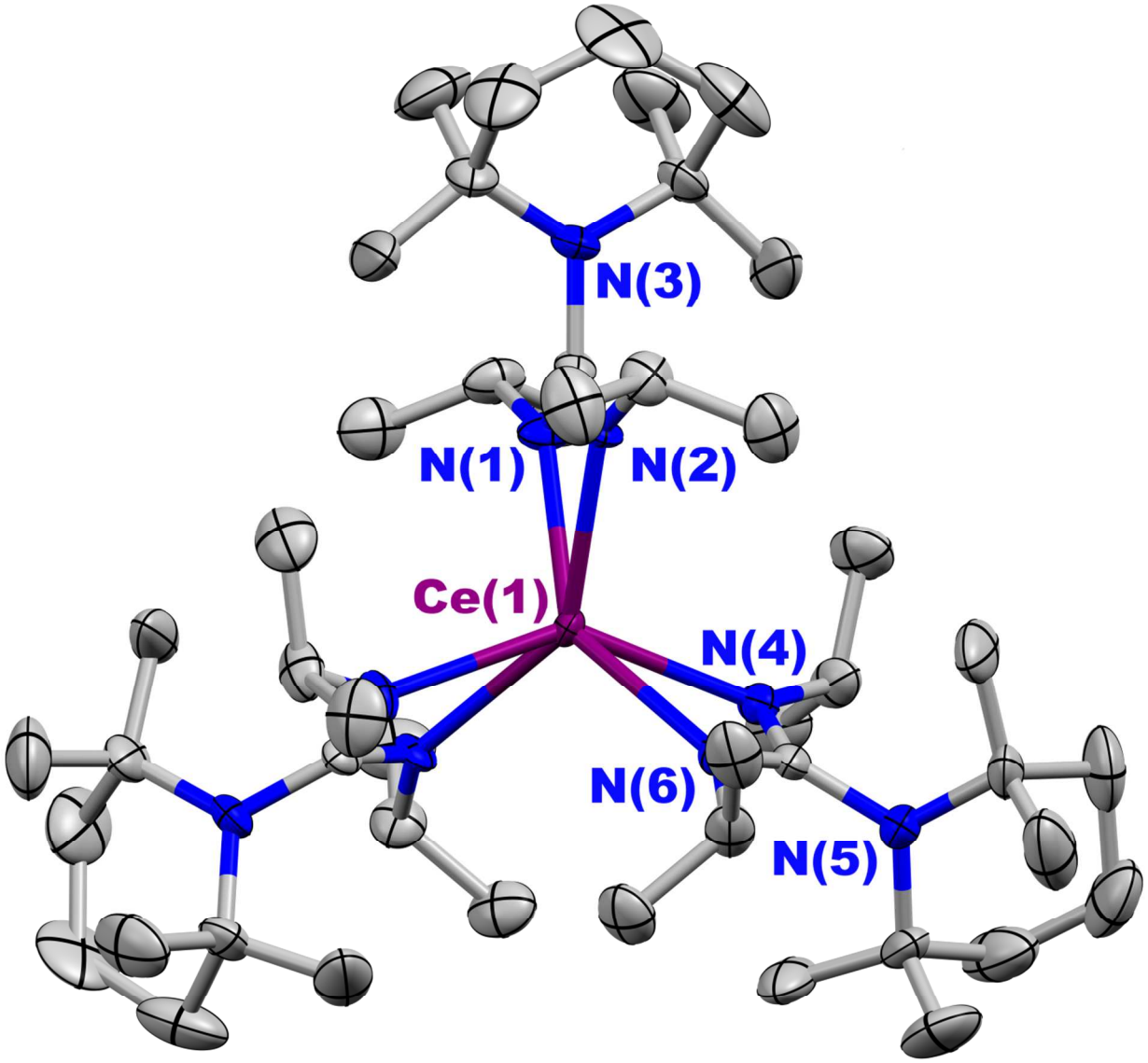

Figure S19. Thermal ellipsoid plot of **[$(C_9H_{18}N)C(N^iPr)_2]_3Ce^{III}$** at 30% probability level. Selected bond length (Å) and angles (deg): Ce(1)–N(1) 2.517(6), Ce(1)–N(2) 2.524(5), Ce(1)–N(4) 2.532 (5); N(1)–Ce(1)–N(2) 52.62(17), N(4)–Ce(1)–N(6) 52.1(3).

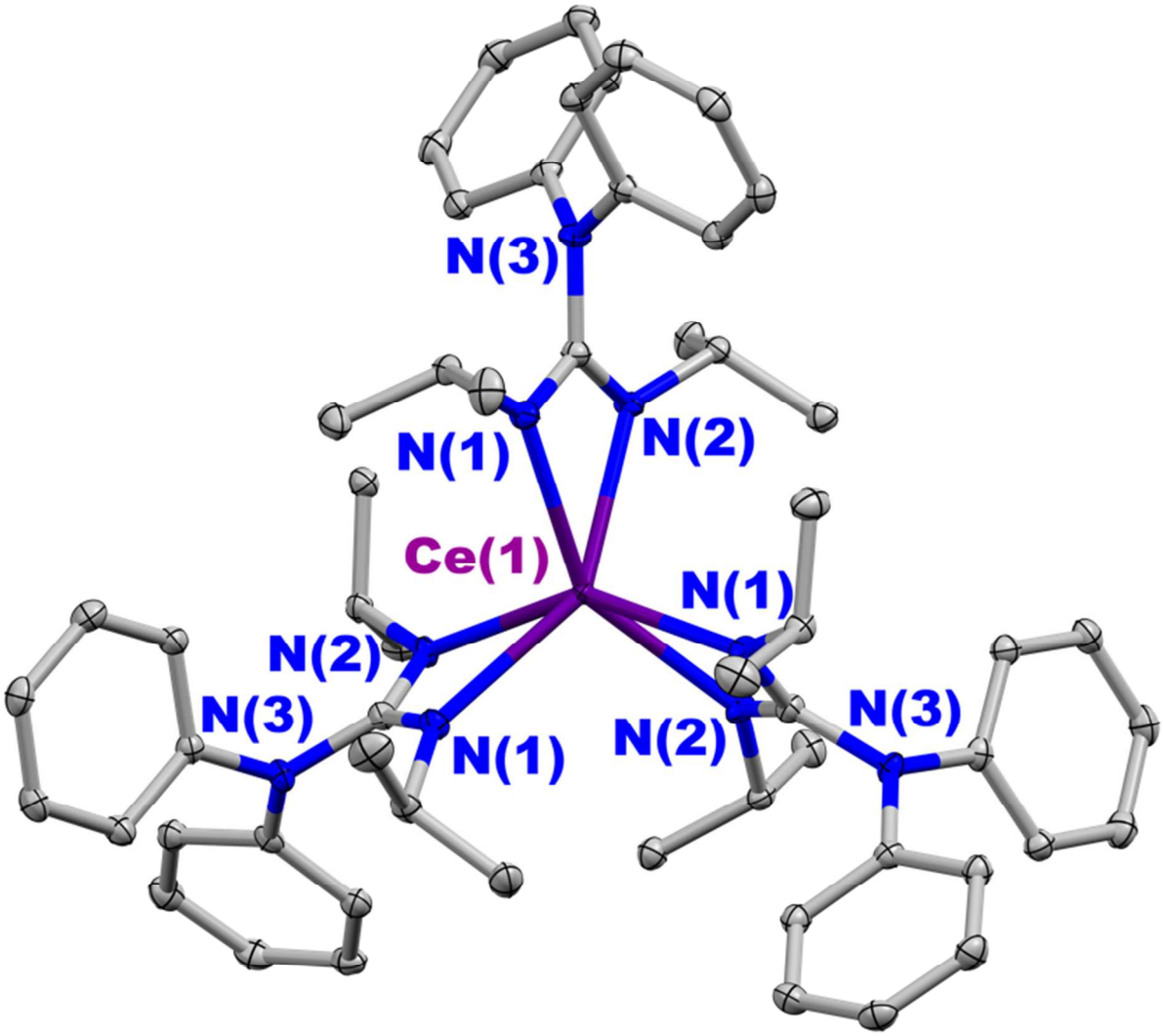

Figure S20. Thermal ellipsoid plot of **[(Ph$_2$N)C(N^{i}Pr)$_2$]$_3$Ce^{III}** at 30% probability level. Selected bond length (Å) and angles (deg): Ce(1)–N(1) 2.517(3), Ce(1)–N(2) 2.505(3); N(1)–Ce(1)–N(2) 53.55(8).

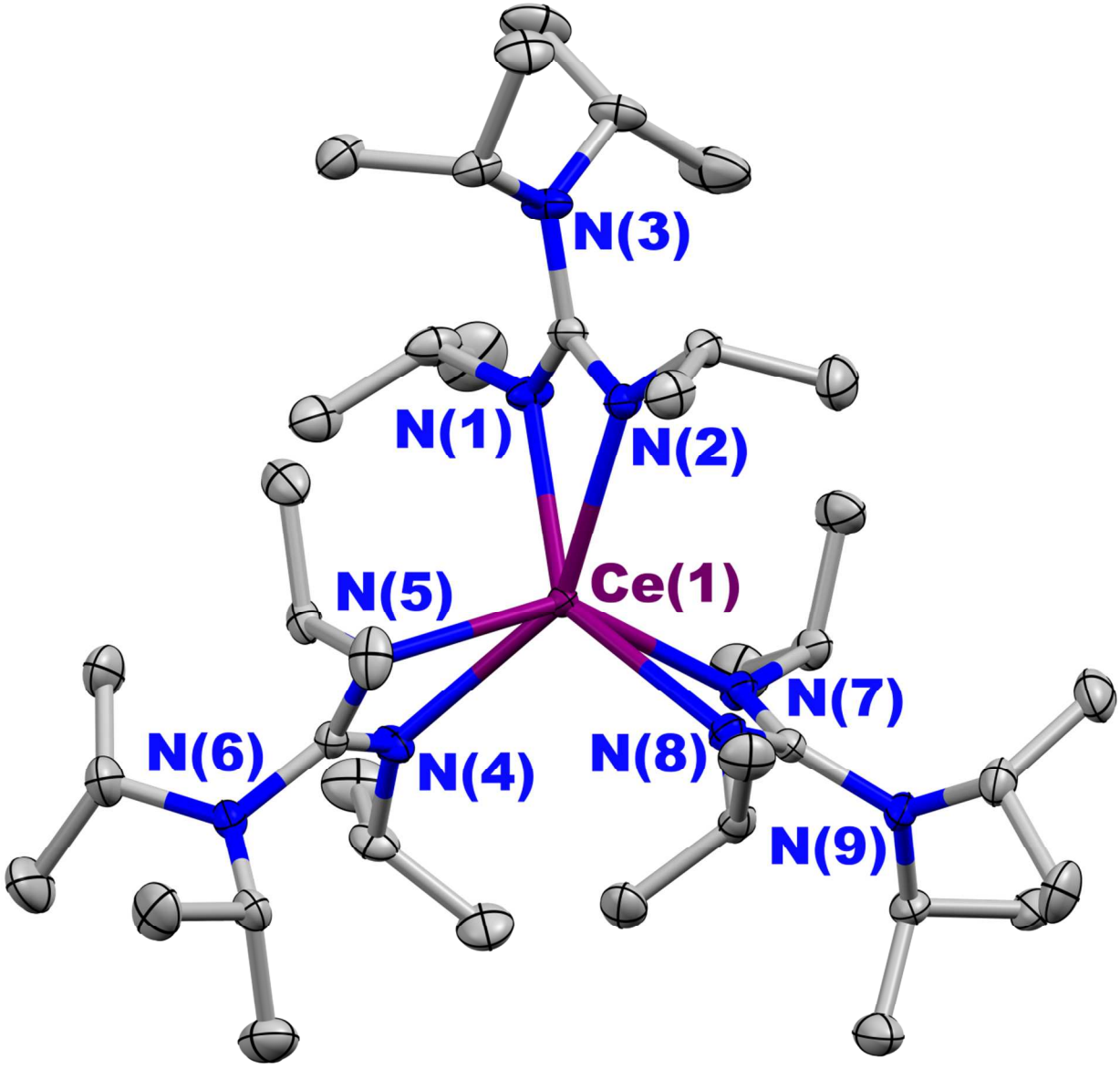

Figure S21. Thermal ellipsoid plot of **[(^{i}Pr$_2$N)C(N^{i}Pr)$_2$]$_3$Ce^{III}** at 30% probability level. Selected bond length (Å) and angles (deg): Ce(1)–N(1) 2.5098(11), Ce(1)–N(2) 2.4827(12), Ce(1)–N(4) 2.5313(12), Ce(1)–N(5) 2.4851(12), Ce(1)–N(7) 2.4841(12), Ce(1)–N(8) 2.4916(12); N(1)–Ce(1)–N(2) 53.65(4), N(4)–Ce(1)–N(5) 53.19(4), N(7)–Ce(1)–N(8) 53.91(4).

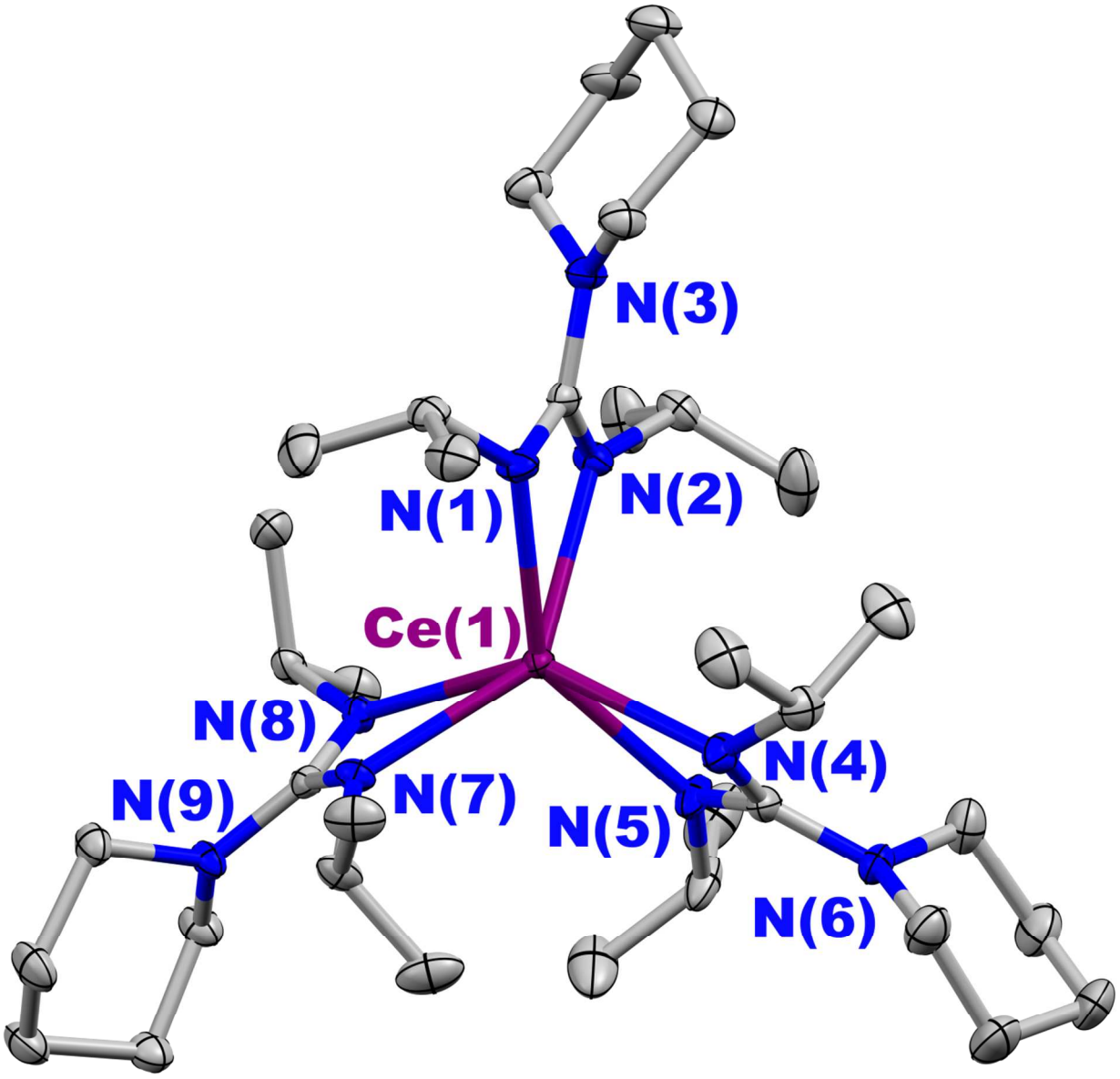

Figure S22. Thermal ellipsoid plot of **$[(C_5H_{10}N)C(N^iPr)_2]_3Ce^{III}$** at 30% probability level. Selected bond length (Å) and angles (deg): Ce(1)–N(1) 2.5036(13), Ce(1)–N(2) 2.4990(13), Ce(1)–N(4) 2.5215(13), Ce(1)–N(5) 2.5036(13), Ce(1)–N(7) 2.4979(13), Ce(1)–N(8) 2.4884(13); N(1)–Ce(1)–N(2) 53.79(4), N(4)–Ce(1)–N(5) 53.55(4), N(7)–Ce(1)–N(8) 53.89(4).

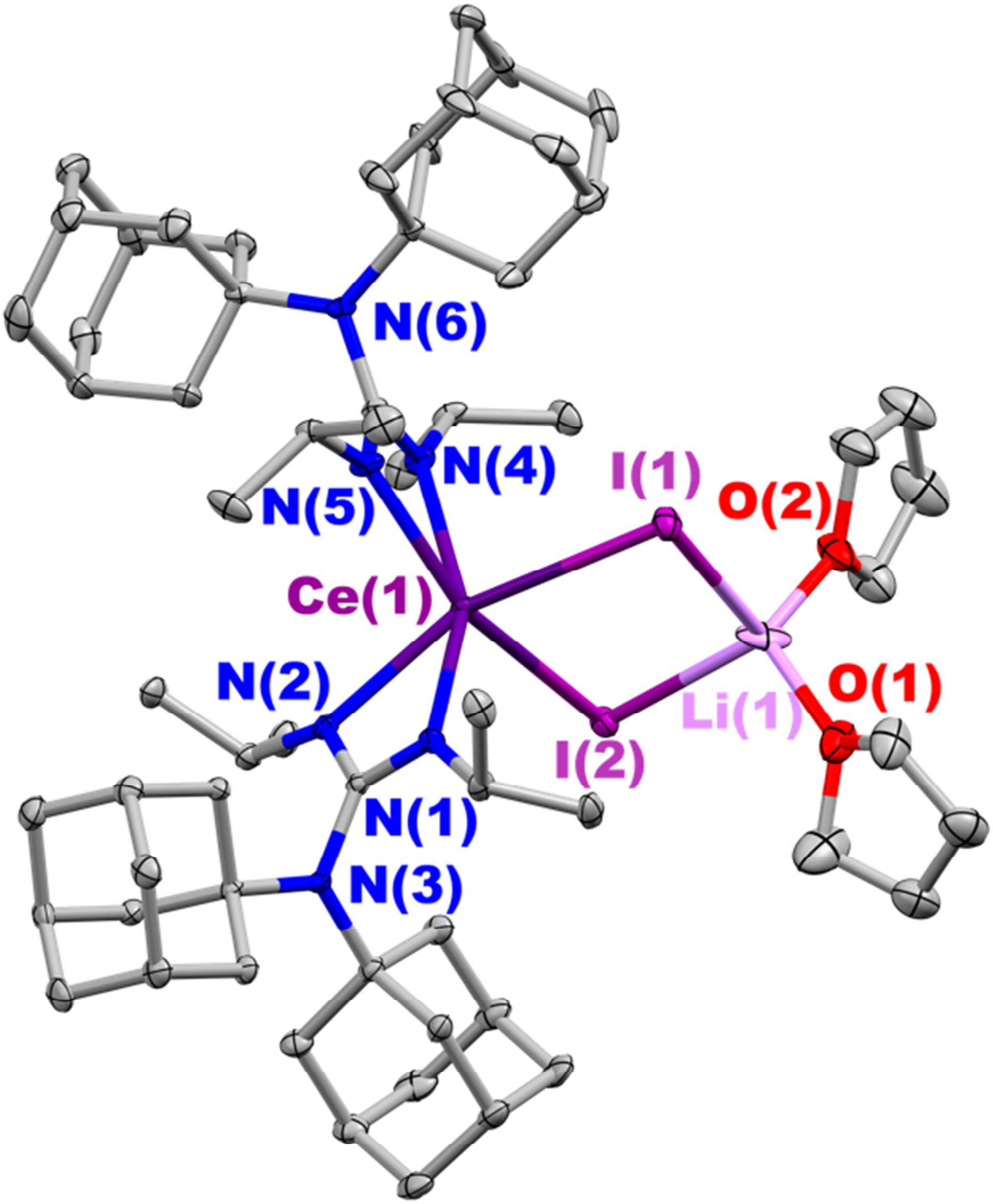

Figure S23. Thermal ellipsoid plot of **{[$(C_{10}H_{15})_2$N]C($N^iPr)_2$}$_2$$Ce^{III}$($\mu^2$–I)$_2$Li(THF)$_2$** at 30% probability level. Selected bond length (Å) and angles (deg): Ce(1)–N(1) 2.460(4), Ce(1)–N(2) 2.442(4), Ce(1)–N(4) 2.462(4), Ce(1)–N(5) 2.451(4), Ce(1)–I(1) 3.2306(5), Ce(1)–I(2) 3.2638(5); N(1)–Ce(1)–N(2) 53.90(13), N(4)–Ce(1)–N(5) 54.08(13), I(1)–Ce(1)–I(2) 86.604(11).

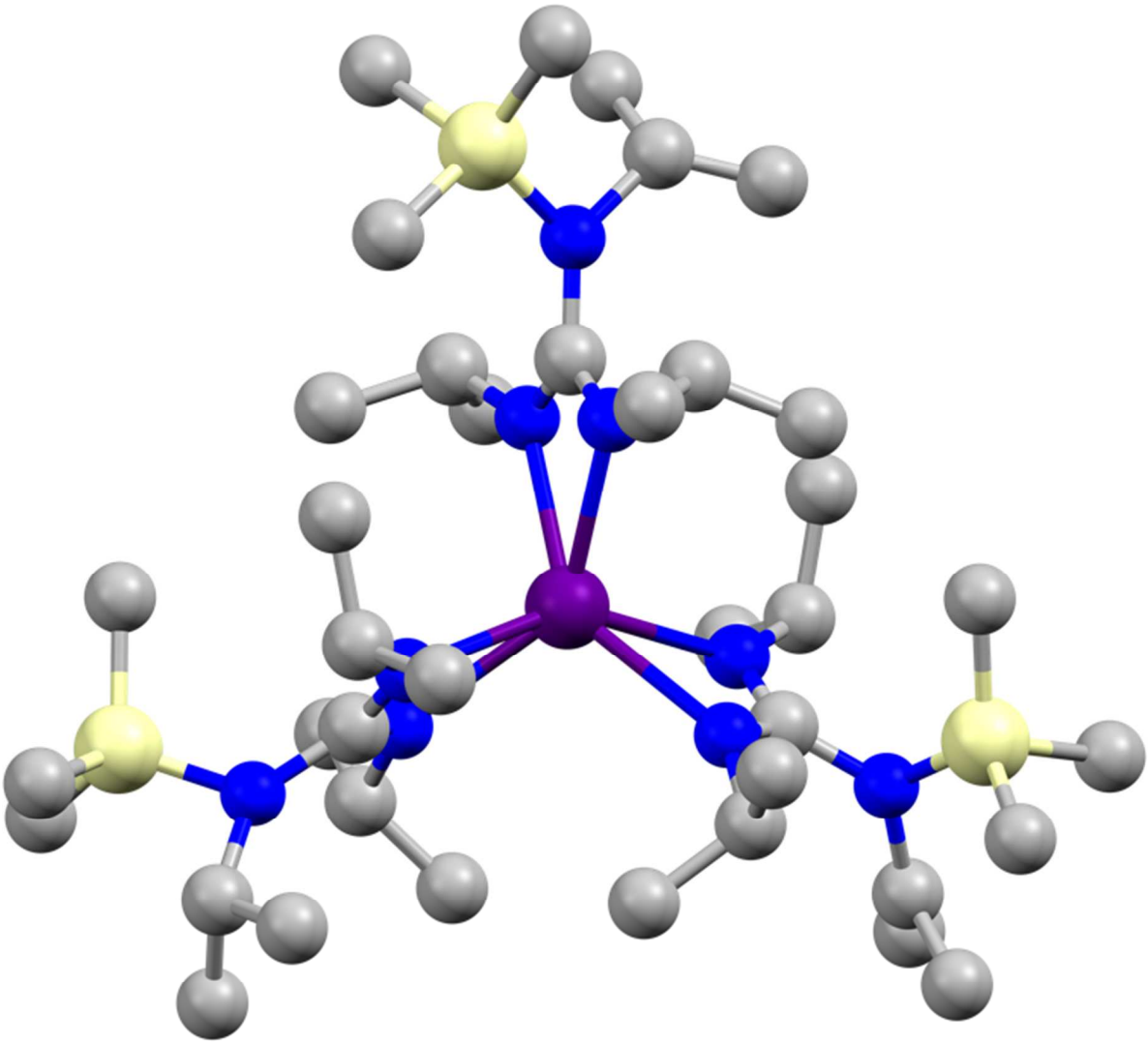

Figure S24. Ball and stick model of **[(Me$_3$SiN^{i}Pr)C(N^{i}Pr)$_2$]$_3$Ce^{III}**. The model has been refined isotropically due to excess amount of occupational disorders between the ^{i}Pr and SiMe$_3$ groups on each ligand.

5. Steady State Absorption and Emission Spectra

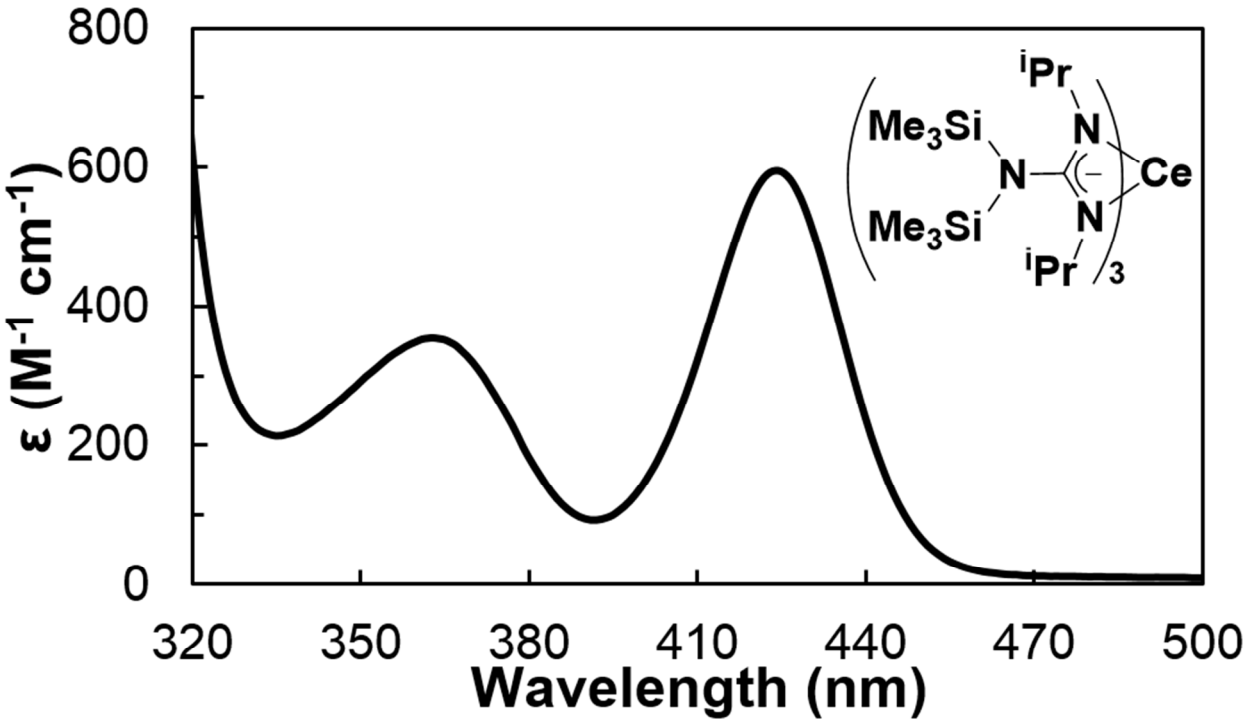

Figure S25. UV-vis spectrum of **$[(Me_3Si)_2NC(N^iPr)_2]_3Ce^{III}$** recorded in toluene.

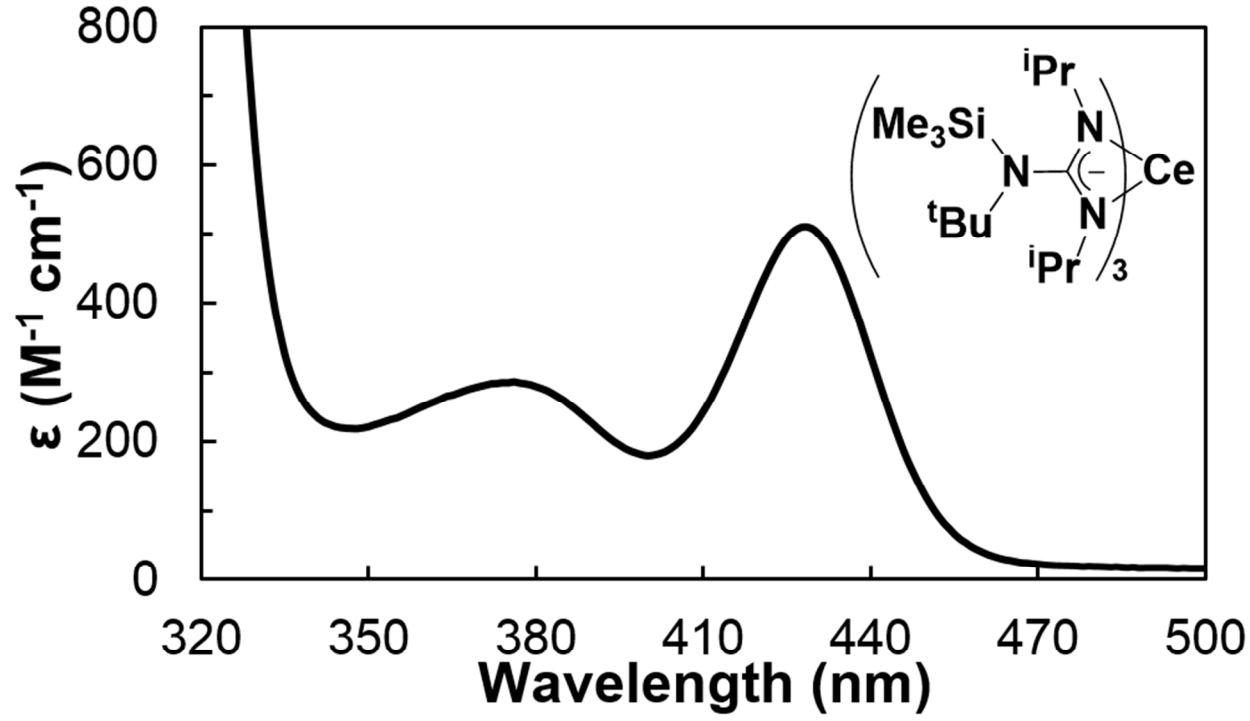

Figure S26. UV-vis spectrum of **$[(Me_3SiN^tBu)C(N^iPr)_2]_3Ce^{III}$** recorded in toluene.

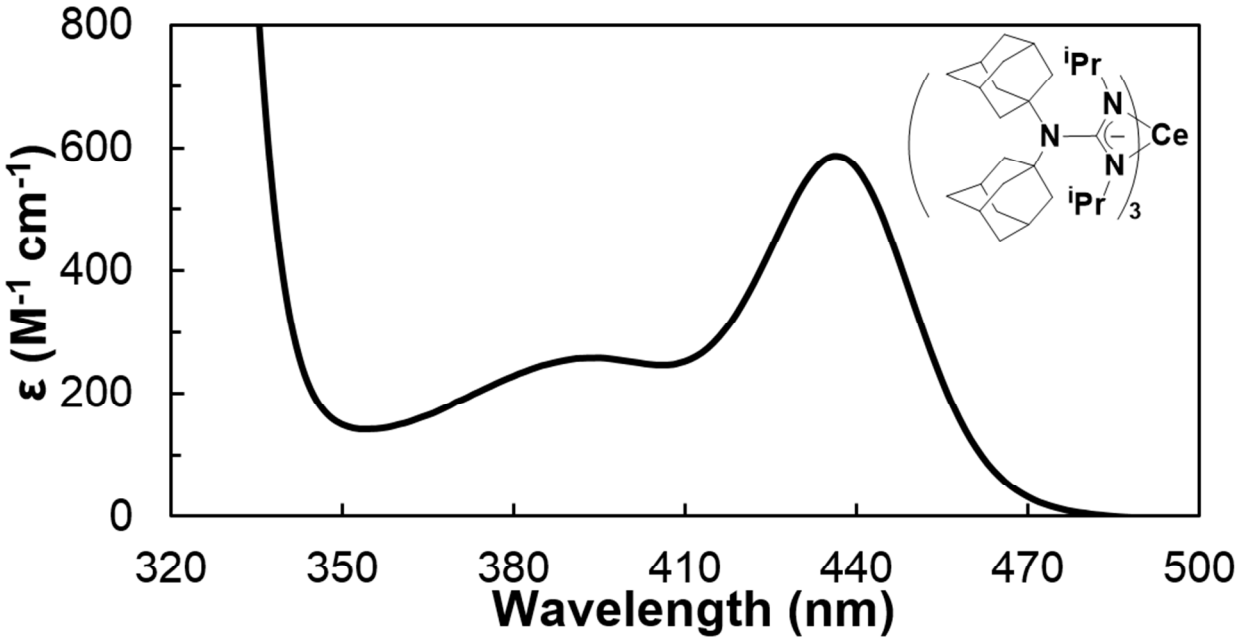

Figure S27. UV-vis spectrum of **{[($C_{10}H_{15}$)$_2$N]C(N^{i}Pr)$_2$}$_3$Ce^{III}** recorded in toluene.

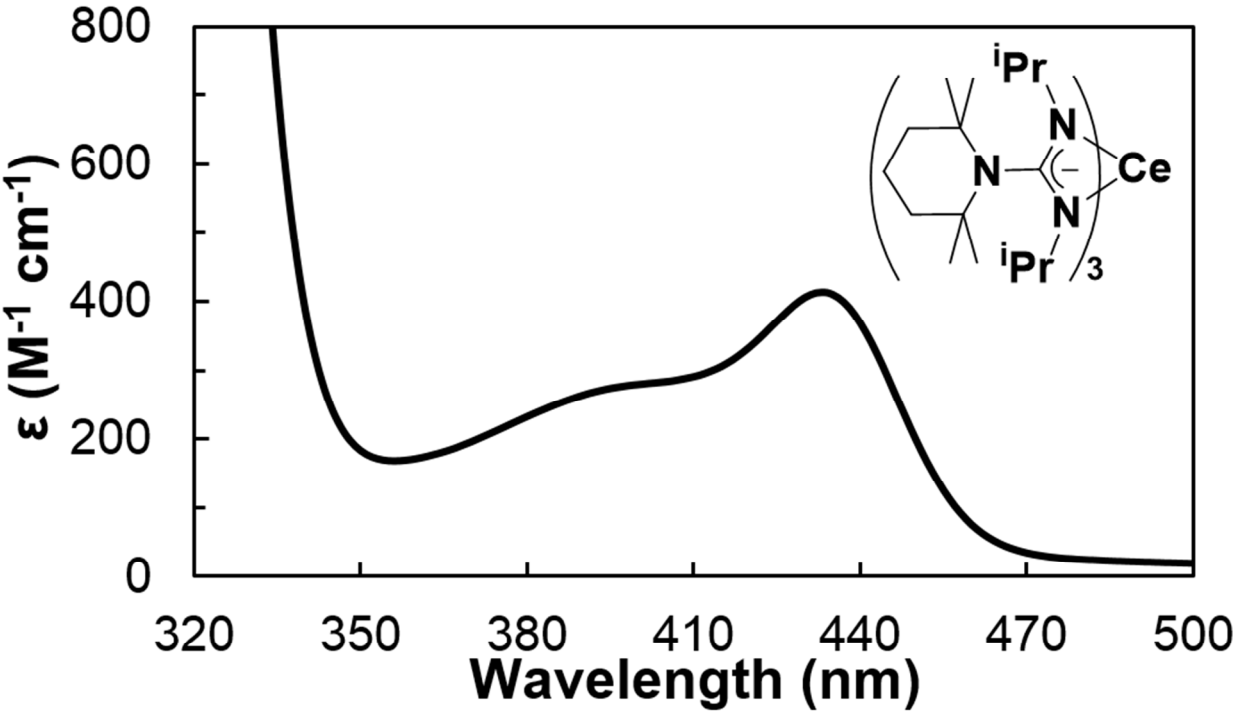

Figure S28. UV-vis spectrum of **[(C_9H_{18}N)C(N^{i}Pr)$_2$]$_3$Ce^{III}** recorded in toluene.

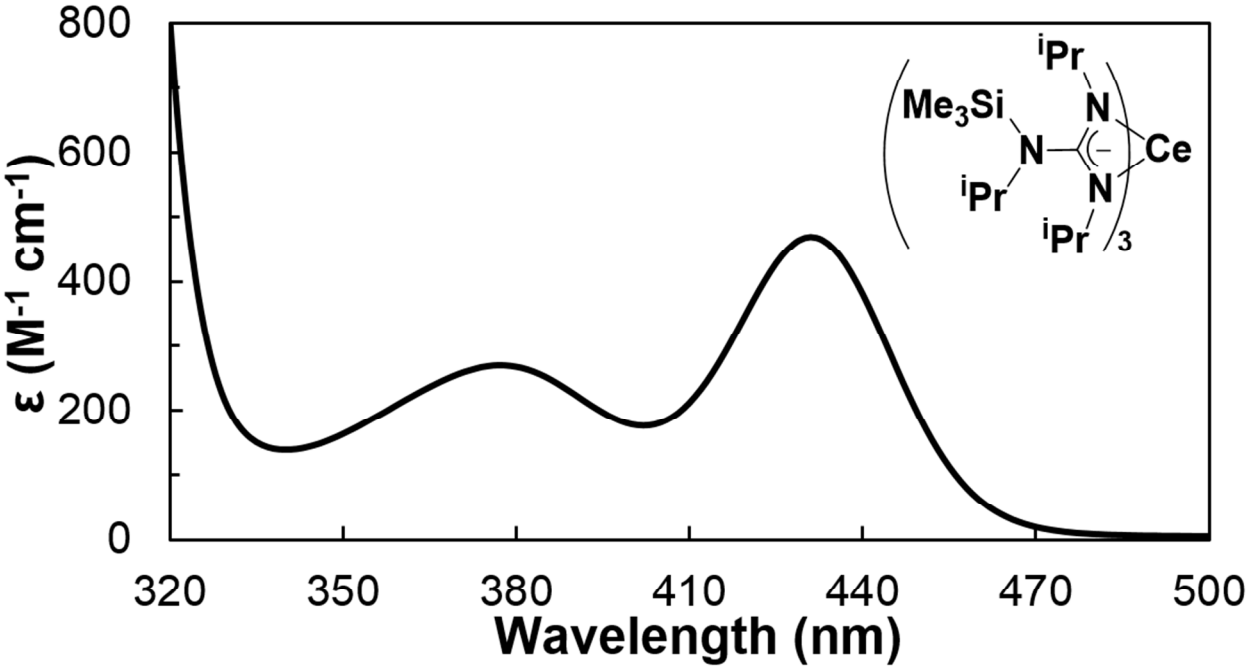

Figure S29. UV-vis spectrum of **[(Me$_3$SiN^{i}Pr)C(N^{i}Pr)$_2$]$_3$Ce^{III}** recorded in toluene.

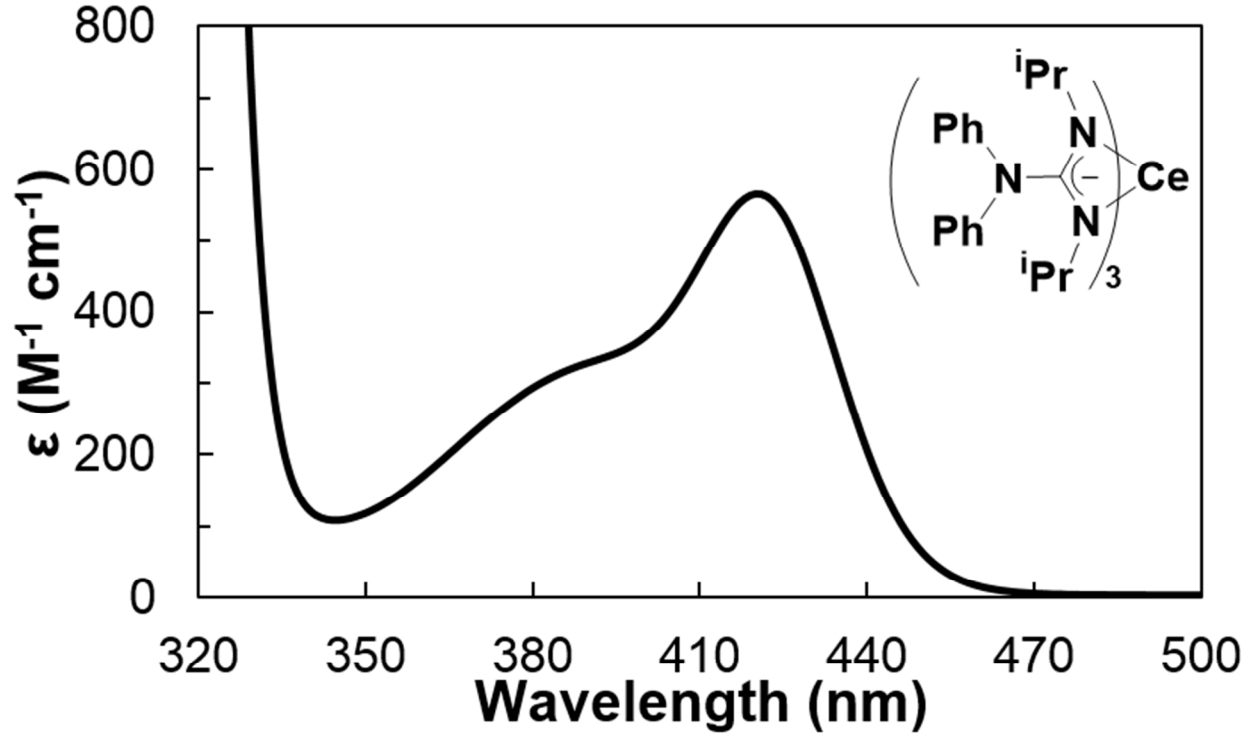

Figure S30. UV-vis spectrum of **[(Ph$_2$N)C(N^{i}Pr)$_2$]$_3$Ce^{III}** recorded in toluene.

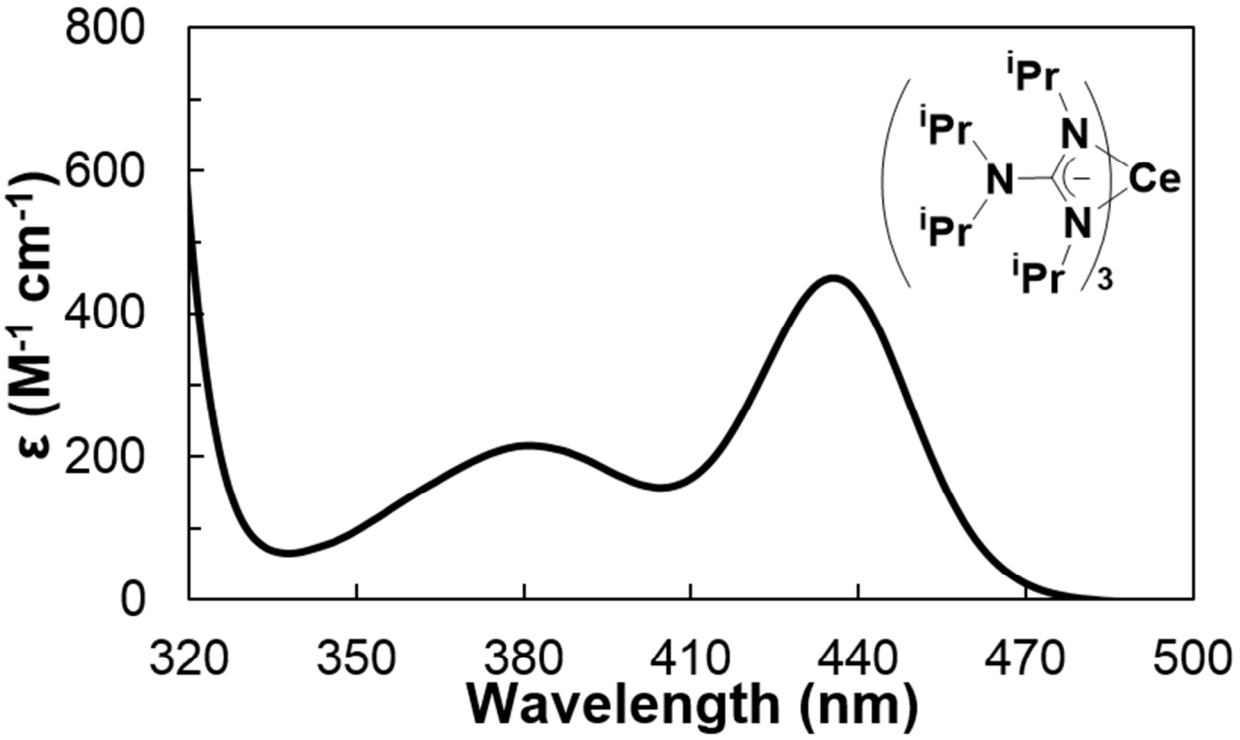

Figure S31. UV-vis spectrum of **[(^{i}Pr$_2$N)C(N^{i}Pr)$_2$]$_3$Ce^{III}** recorded in toluene.

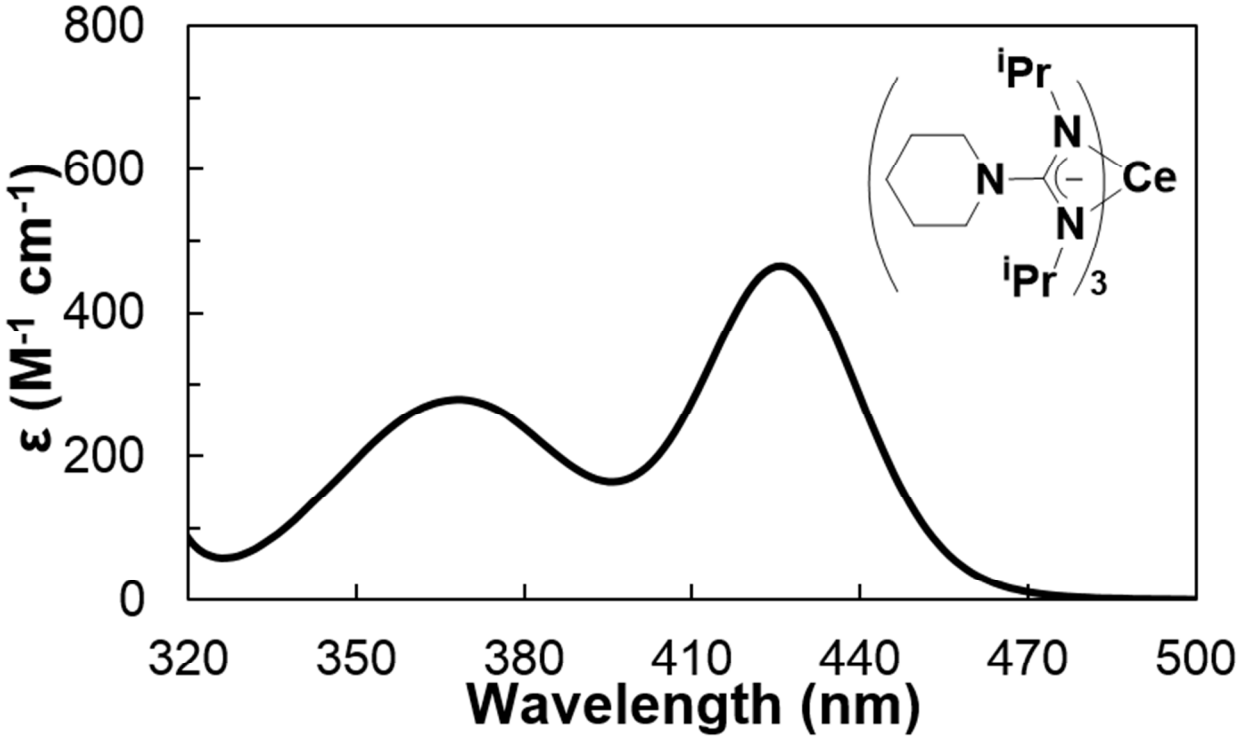

Figure S32. UV-vis spectrum of **[(C$_5$H$_{10}$N)C(N^{i}Pr)$_2$]$_3$Ce^{III}** recorded in toluene.

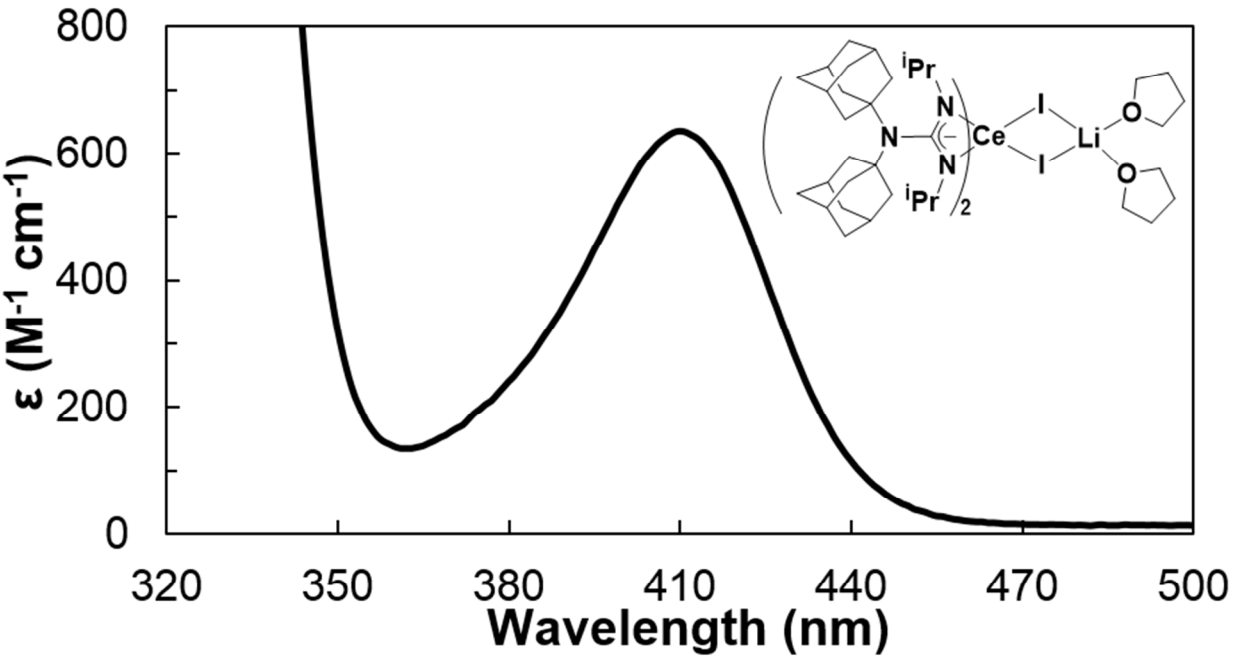

Figure S33. UV-vis spectrum of **{[$(C_{10}H_{15})_2$N]C($N^iPr)_2$}$_2$$Ce^{III}$($\mu^2$–I)$_2$Li(THF)$_2$** recorded in toluene.

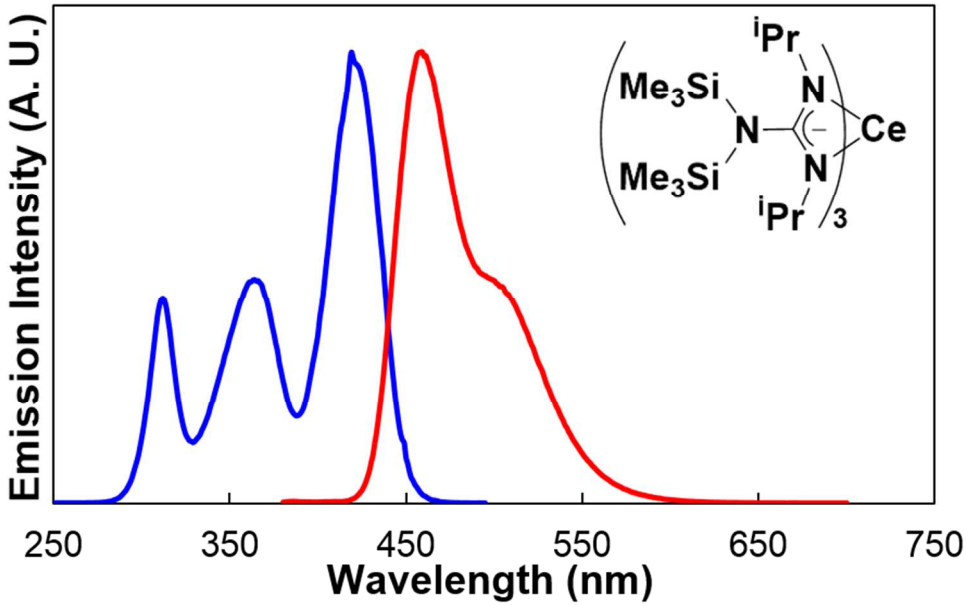

Figure S34. Normalized emission (red) and excitation (blue, uncorrected to lamp emission profile) spectra of **[$(Me_3Si)_2$NC($N^iPr)_2$]$_3$$Ce^{III}$** recorded in toluene.

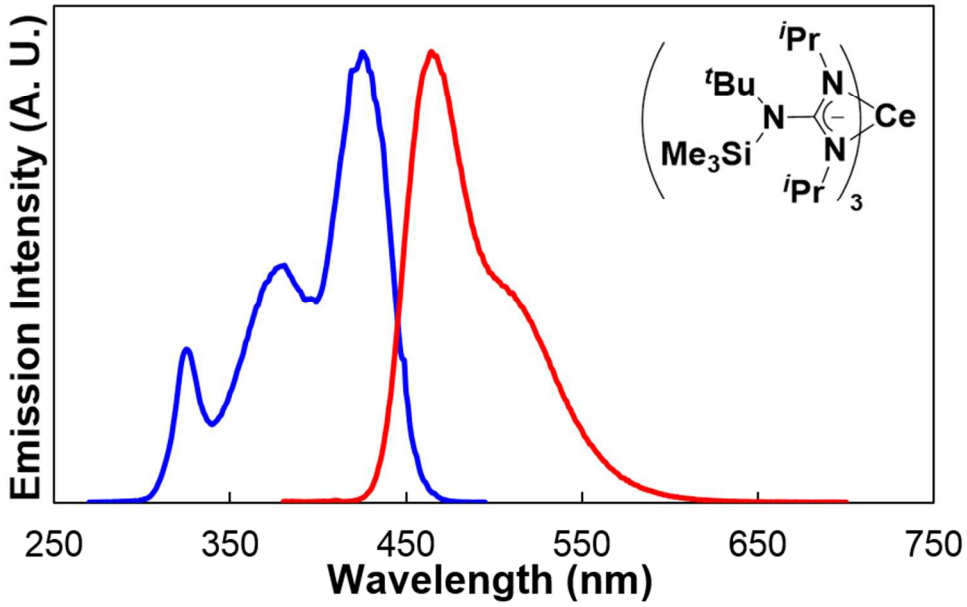

Figure S35. Normalized emission (red) and excitation (blue, uncorrected to lamp emission profile) spectra of **$[(Me_3SiN^tBu)C(N^iPr)_2]_3Ce^{III}$** recorded in toluene.

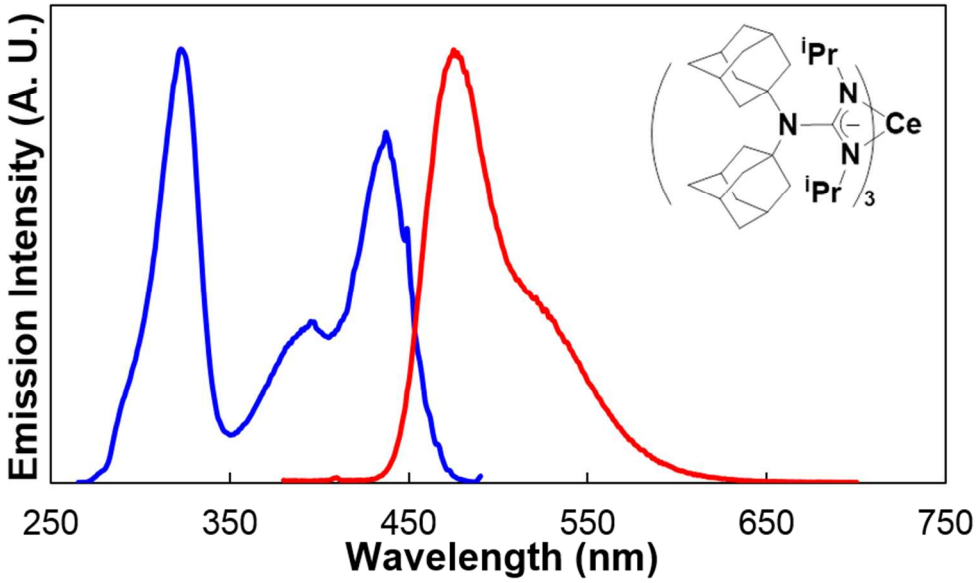

Figure S36. Normalized emission (red) and excitation (blue, uncorrected to lamp emission profile) spectra of **$\{[(C_{10}H_{15})_2N]C(N^iPr)_2\}_3Ce^{III}$** recorded in toluene.

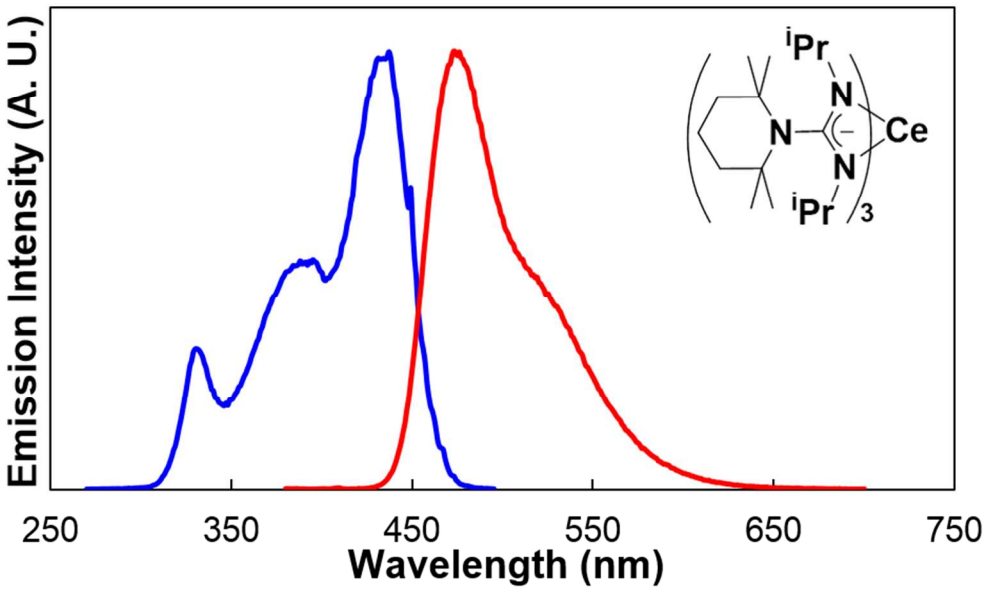

Figure S37. Normalized emission (red) and excitation (blue, uncorrected to lamp emission profile) spectra of **$[(C_9H_{18}N)C(N^iPr)_2]_3Ce^{III}$** recorded in toluene.

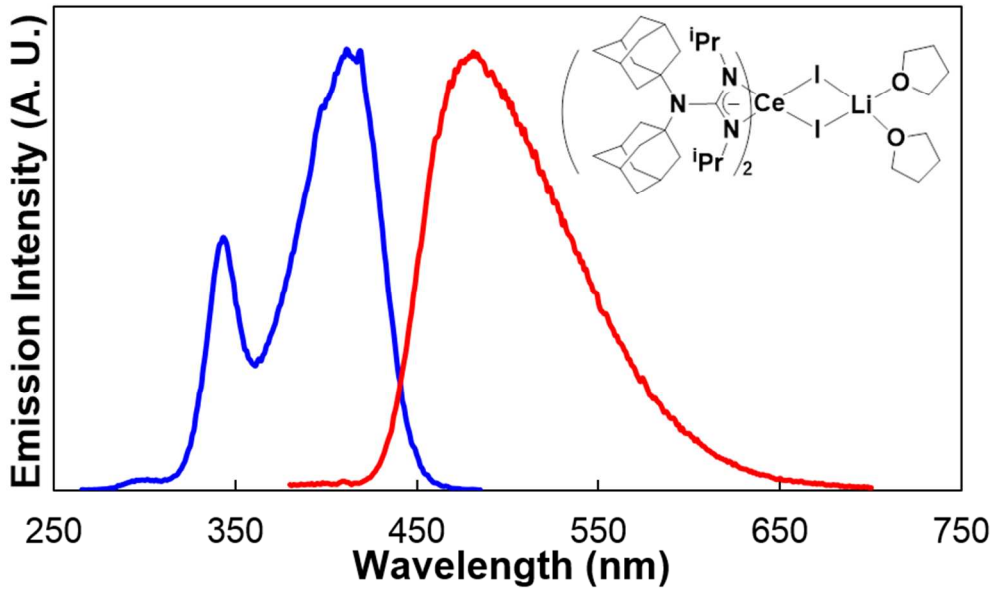

Figure S38. Normalized emission (red) and excitation (blue, uncorrected to lamp emission profile) spectra of **$\{[(C_{10}H_{15})_2N]C(N^iPr)_2\}_2Ce^{III}(\mu^2\text{–}I)_2Li(THF)_2$** recorded in toluene.

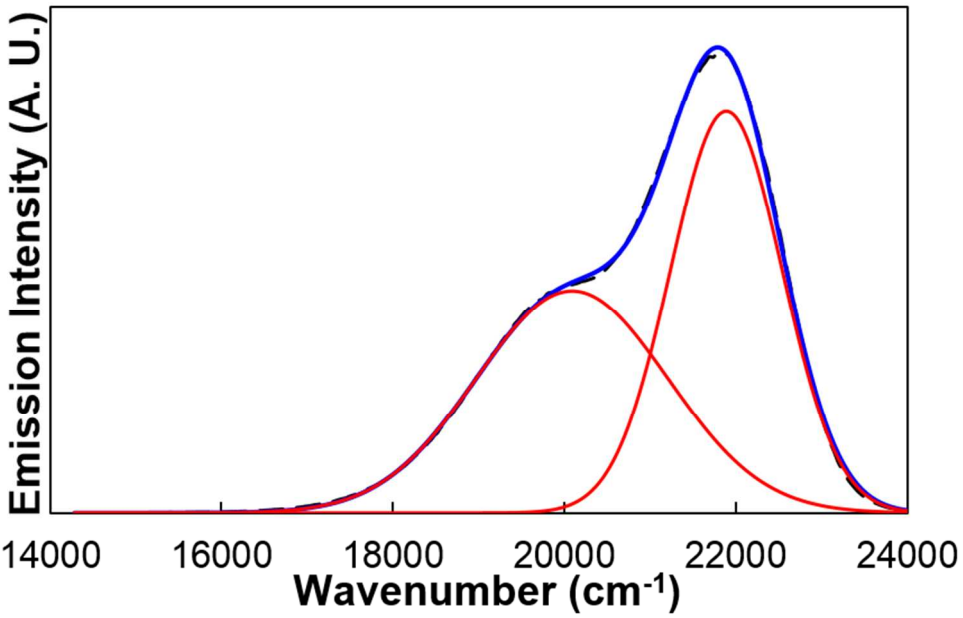

Figure S39. Fitting of emission spectrum of **$[(Me_3Si)_2NC(N^iPr)_2]_3Ce^{III}$** plotted in wavenumbers. Two Gaussian bands (red solid lines) were applied for each fitting, featuring transitions to $^2F_{5/2}$ and $^2F_{7/2}$. Sum of the fit (blue solid lines) is in good agreement with experimental spectra (black dashed lines).

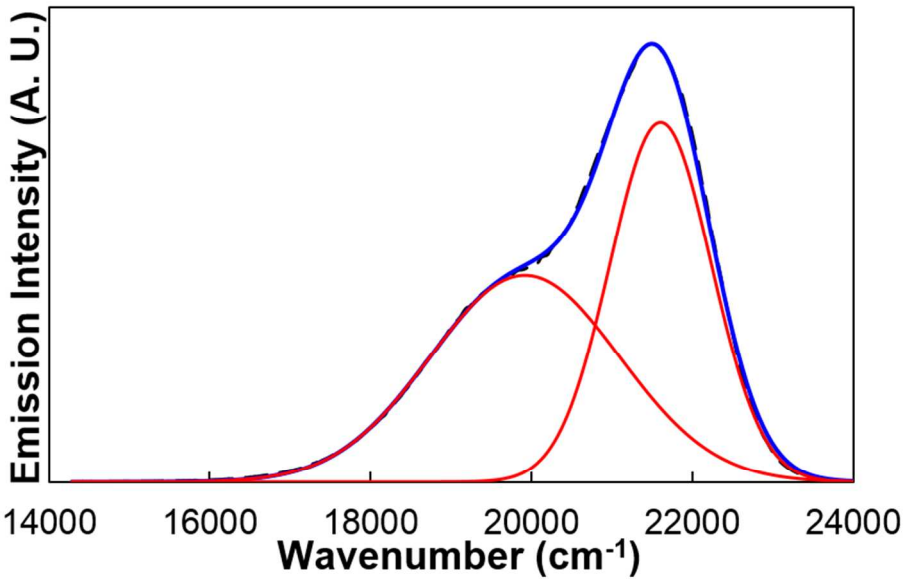

Figure S40. Fitting of emission spectrum of **$[(Me_3SiN^tBu)C(N^iPr)_2]_3Ce^{III}$** plotted in wavenumbers. Two Gaussian bands (red solid lines) were applied for each fitting, featuring transitions to $^2F_{5/2}$ and $^2F_{7/2}$. Sum of the fit (blue solid lines) is in good agreement with experimental spectra (black dashed lines).

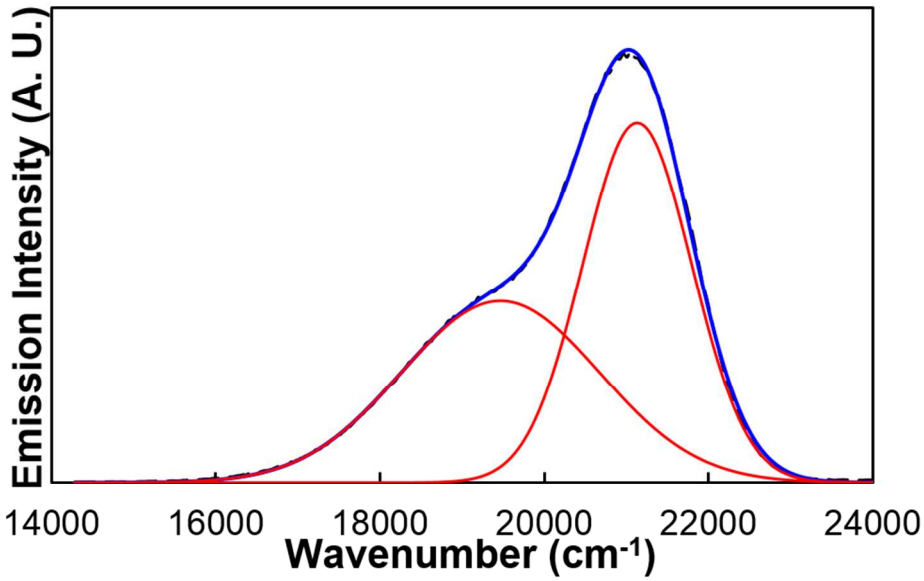

Figure S41. Fitting of emission spectrum of **{[($C_{10}H_{15}$)$_2$N]C(N^{i}Pr)$_2$}$_3$Ce^{III}** plotted in wavenumbers. Two Gaussian bands (red solid lines) were applied for each fitting, featuring transitions to $^2F_{5/2}$ and $^2F_{7/2}$. Sum of the fit (blue solid lines) is in good agreement with experimental spectra (black dashed lines).

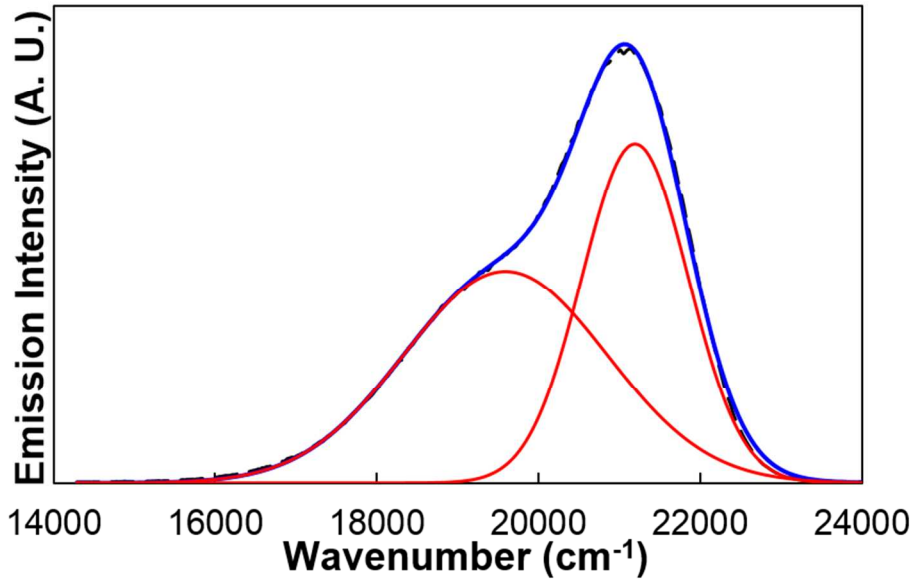

Figure S42. Fitting of emission spectrum of **[($C_9H_{18}N$)C(N^{i}Pr)$_2$]$_3$Ce^{III}** plotted in wavenumbers. Two Gaussian bands (red solid lines) were applied for each fitting, featuring transitions to $^2F_{5/2}$ and $^2F_{7/2}$. Sum of the fit (blue solid lines) is in good agreement with experimental spectra (black dashed lines).

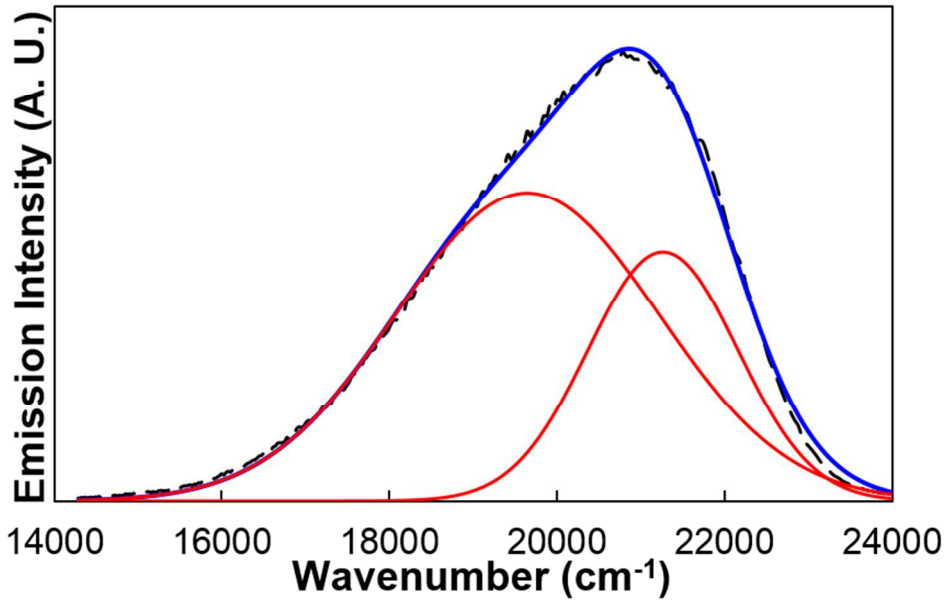

Figure S43. Fitting of emission spectrum of **{[$(C_{10}H_{15})_2$N]C($N^iPr)_2$}$_2$$Ce^{III}(\mu^2–I)_2Li(THF)_2$** plotted in wavenumbers. Two Gaussian bands (red solid lines) were applied for each fitting, featuring transitions to $^2F_{5/2}$ and $^2F_{7/2}$. Sum of the fit (blue solid lines) is in good agreement with experimental spectra (black dashed lines).

6. Computation Details for Cerium(III) *Tris*-(guanidinate) Complexes

For cerium(III) *tris*-(guanidinate) complexes **2**-**4**, Gaussian 09 Rev. A.02 was used for all electronic structure calculations.[19] The B3LYP hybrid DFT method was employed, with a 28-electron small core pseudopotential on cerium with published segmented natural orbital basis set incorporating quasi-relativistic effects,[20] and the 6-31G* basis set for all other atoms. Gas phase ground-state geometry optimization for **2, 3** and **4** were carried out starting from the coordinates of the crystal structure. The only constraint was the spin state (doublet). The frequency calculation was performed to indicate that the geometry was the minimum (no imaginary frequencies). Calculated metal-ligand bond lengths were within 0.05 A of the crystal structures in all cases. TD-DFT calculation was carried out for **2, 3,** and **4** in gas phase. Molecular orbitals were rendered with the program Chemcraft v1.6.[21] Natural Transition Orbitals (NTOs)[22] were calculated using keyword pop=NTO. Corresponding donor and acceptor orbitals from NTOs calculation were rendered with the program Chemcraft v1.6.[21] DFT and TD-DFT calculations on **1** was previously reported by us.[7]

Table S2. Cartesian coordinates of optimized gas phase structure for **2**

Ce	0.039062	-0.04275	-0.011862	C	4.725091	1.4018	1.318078
C	-2.002775	-2.266653	0.04278	H	4.387562	1.125728	2.321084
N	-1.792517	-1.456938	1.092106	H	3.860155	1.783759	0.769223
C	-2.605753	-1.513281	2.305136	H	5.441332	2.226234	1.426685
H	-3.244896	-2.402906	2.275095	C	6.837329	-0.753324	1.687021
C	-3.513448	-0.27558	2.405067	H	6.346529	-1.201856	2.557912
H	-4.201988	-0.214121	1.557292	H	7.466248	0.070108	2.051279
H	-2.908814	0.6362	2.407878	H	7.510072	-1.501598	1.253906
H	-4.108937	-0.294369	3.327013	C	6.615823	0.708127	-0.966174
C	-1.733813	-1.607043	3.567385	H	7.290293	-0.012077	-1.439368
H	-1.092049	-2.492576	3.555456	H	7.23812	1.513992	-0.554035
H	-2.36276	-1.657076	4.464779	H	5.993318	1.147059	-1.75246
H	-1.08962	-0.726203	3.663956	C	4.700508	-2.607253	-0.557027
N	-1.237499	-2.008247	-1.029956	C	5.100652	-3.553941	0.599093
C	-1.310775	-2.794516	-2.258314	H	4.264572	-3.745564	1.273927
H	-2.169901	-3.473133	-2.203942	H	5.926611	-3.147016	1.186068
C	-1.508425	-1.888876	-3.484557	H	5.426026	-4.519256	0.191891
H	-1.609143	-2.490541	-4.396549	C	5.888982	-2.540377	-1.540545

H	-0.646926	-1.225161	-3.621528	H	6.810963	-2.215674	-1.047836
H	-2.40267	-1.267171	-3.386116	H	5.684666	-1.859781	-2.372518
C	-0.038525	-3.637091	-2.460052	H	6.081621	-3.536506	-1.955256
H	0.143818	-4.307374	-1.614695	C	3.515699	-3.243503	-1.302492
H	0.835745	-2.98599	-2.559323	H	3.775454	-4.272263	-1.575483
H	-0.112552	-4.24692	-3.369677	H	3.278723	-2.702509	-2.220256
N	-2.997124	-3.329188	0.063809	H	2.615078	-3.279557	-0.684433
Si	-4.670134	-2.93427	-0.40436	C	-0.758913	2.88105	-0.033109
C	-4.668977	-1.252613	-1.262012	N	-0.247909	2.281196	1.052347
H	-4.123009	-0.484709	-0.707397	C	0.074413	3.007609	2.277838
H	-5.705398	-0.909451	-1.37292	H	-0.322844	4.027085	2.211823
H	-4.234655	-1.314696	-2.264088	C	1.596309	3.090952	2.48761
C	-5.41238	-4.173276	-1.638258	H	2.019416	2.086786	2.588664
H	-4.786831	-4.296895	-2.529532	H	1.838736	3.654702	3.397758
H	-6.383859	-3.782356	-1.969455	H	2.09712	3.575285	1.644078
H	-5.596202	-5.165944	-1.213022	C	-0.561607	2.33944	3.507495
C	-5.91303	-2.828202	1.03255	H	-0.169277	1.325664	3.647862
H	-6.113501	-3.795124	1.504618	H	-1.648739	2.269365	3.414405
H	-6.86785	-2.457905	0.635176	H	-0.333253	2.910442	4.416087
H	-5.597169	-2.133723	1.817287	N	-0.951442	2.071624	-1.087486
C	-2.578443	-4.707887	0.535523	C	-1.60111	2.526972	-2.314604
C	-1.213279	-4.660972	1.241279	H	-1.705024	3.617495	-2.288709
H	-0.908034	-5.681017	1.499168	C	-0.776456	2.159515	-3.558208
H	-1.25719	-4.080089	2.164187	H	-0.687717	1.071807	-3.65606
H	-0.437681	-4.229983	0.60326	H	0.23381	2.577263	-3.517698
C	-2.476028	-5.712036	-0.636978	H	-1.262745	2.533788	-4.467594
H	-2.238828	-6.711194	-0.25085	C	-3.010212	1.923757	-2.44999
H	-1.688923	-5.433824	-1.339833	H	-2.956037	0.831609	-2.496377
H	-3.415235	-5.786213	-1.189209	H	-3.502328	2.278267	-3.365
C	-3.605561	-5.265497	1.544595	H	-3.643536	2.189116	-1.598678
H	-3.256272	-6.229452	1.932212	N	-1.099307	4.296176	-0.065674
H	-4.58182	-5.441884	1.081749	Si	-2.745422	4.782581	0.409753
H	-3.742211	-4.587887	2.392851	C	-3.594519	3.320764	1.251325
C	2.955184	-0.812179	-0.032998	H	-3.507224	2.386827	0.689853

N	2.165647	-0.987692	1.037435	H	-4.663196	3.548358	1.354549
C	2.616517	-1.66315	2.250902	H	-3.197073	3.144967	2.254889
H	3.698847	-1.826048	2.195169	C	-2.77147	6.216806	1.655303
C	1.926085	-3.028718	2.411196	H	-3.806772	6.353965	1.995159
H	2.117074	-3.6816	1.554017	H	-2.443445	7.174823	1.236835
H	0.842828	-2.896366	2.489177	H	-2.160517	6.007894	2.54084
H	2.274229	-3.542567	3.316428	C	-3.870381	5.315625	-1.028701
C	2.337603	-0.807057	3.496722	H	-3.952541	4.543963	-1.800593
H	1.264088	-0.614778	3.606222	H	-3.548383	6.240901	-1.516098
H	2.849107	0.157902	3.444653	H	-4.879906	5.490796	-0.632921
H	2.676682	-1.323039	4.403613	C	-0.052249	5.289606	-0.529911
N	2.359844	-0.213856	-1.077219	C	0.534856	6.104506	0.646925
C	3.087246	0.159802	-2.288056	H	1.093572	5.471862	1.338782
H	4.08662	-0.289958	-2.266129	H	-0.244498	6.621051	1.211023
C	2.371111	-0.343937	-3.551336	H	1.225702	6.865275	0.262796
H	2.252837	-1.431371	-3.546396	C	-0.666863	6.290127	-1.533031
H	2.936738	-0.068564	-4.450124	H	-1.117298	5.77601	-2.387555
H	1.374568	0.102378	-3.638396	H	0.114687	6.958609	-1.912074
C	3.257895	1.686696	-2.376191	H	-1.430207	6.92179	-1.067954
H	3.811938	2.077859	-1.517871	C	1.112044	4.577898	-1.238697
H	2.279923	2.177891	-2.393401	H	0.788444	4.103481	-2.166606
H	3.798078	1.97018	-3.288768	H	1.56983	3.814857	-0.604187
N	4.351662	-1.219086	-0.057362	H	1.883708	5.314622	-1.487633
Si	5.586036	-0.037393	0.450641				

Table S3. Comparison of parameters between X-ray structure and optimized gas phase model for **2**

	X-ray structure	**Optimized model**
Average Ce−$N_{guanidine}$ (Å)	2.525(6)	2.56233
Average $N_{guanidine}$−Ce−$N_{guanidine}$ (°)	53.0(2)	52.37

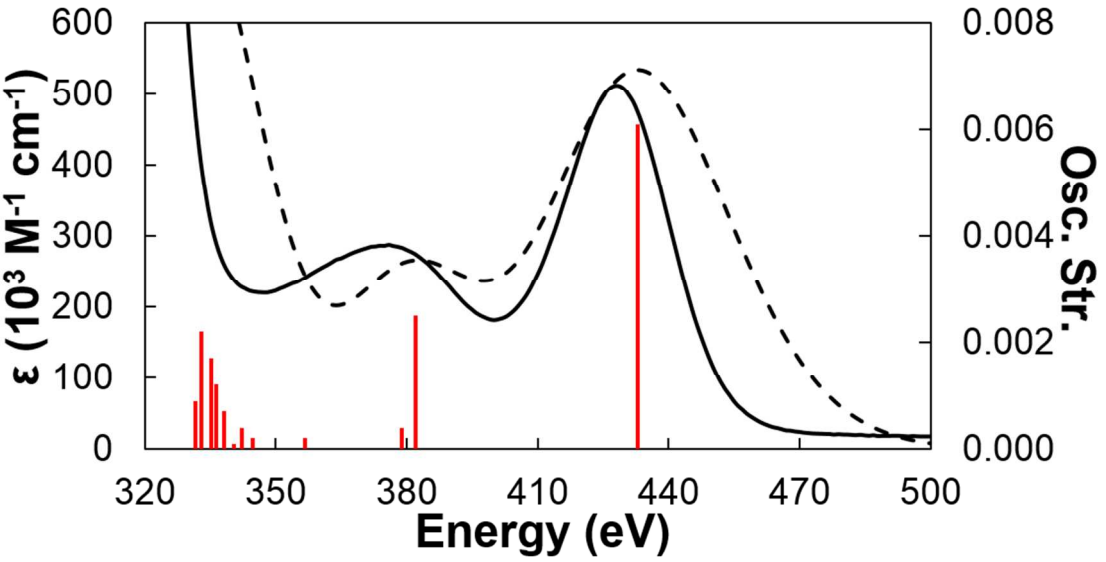

Figure S44. Experimental (black solid line) and TD-DFT predicted (black dashed line) absorption spectrum of **2**. The predicted spectra were rendered as Gaussian line shapes having a fwhm of 2500 cm^{-1}. Oscillator strengths for the electronic transitions are shown as red vertical lines.

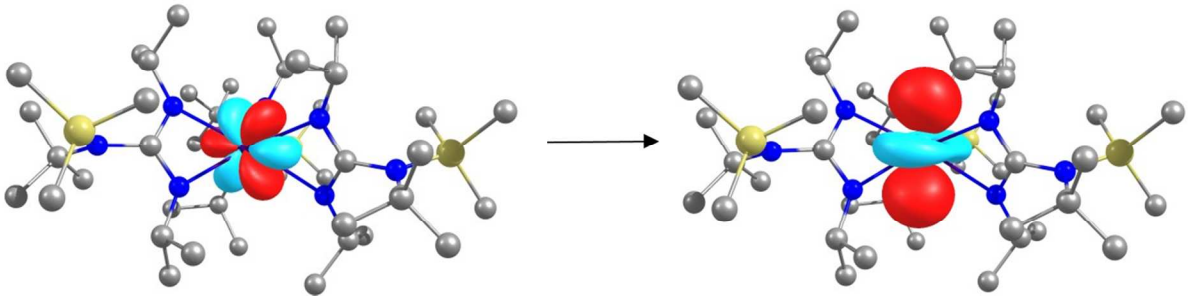

Figure S45. Calculated Natural Transition Orbitals (NTO) of **2** in gas phase with contour value of 0.05. The calculated transition shown is centered at 433 nm (oscillator strength 0.0061).

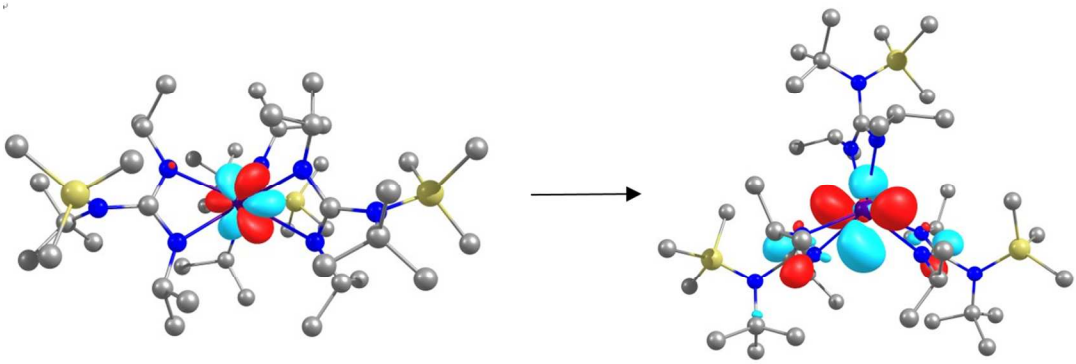

Figure S46. Calculated Natural Transition Orbitals (NTO) of **2** in gas phase with contour value of 0.05. The calculated transition shown is centered at 382 nm (oscillator strength 0.0025).

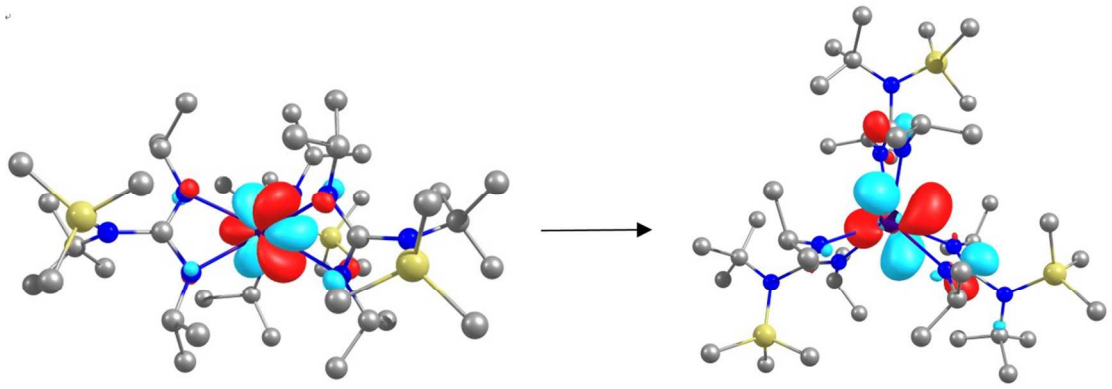

Figure S47. Calculated Natural Transition Orbitals (NTO) of **2** in gas phase with contour value of 0.05. The calculated transition shown is centered at 379 nm (oscillator strength 0.0004).

Table S4. Cartesian coordinates of optimized gas phase structure for **3**

Ce	-0.01151	-0.0049	-0.00714	H	4.72139	3.160102	-2.39436
N	-2.0647	-1.13994	-1.0488	C	2.9352	3.659995	-1.29762
N	-2.31454	-0.33798	1.039819	H	3.025121	2.777879	-0.65613
N	-4.28739	-1.40606	-0.0002	H	2.285625	3.383667	-2.12955
N	0.877168	2.156061	1.04833	C	5.275583	4.400709	-0.70029
N	0.027007	2.336273	-1.029	H	6.270744	4.654854	-1.09132
N	0.921415	4.395877	0.001833	H	5.407094	3.543835	-0.02494
N	1.972622	-1.24214	-1.05668	C	4.678982	5.594004	0.066309
N	1.44129	-1.85446	1.043007	H	5.335151	5.861968	0.905585
N	3.364143	-2.9979	-0.00501	C	4.536844	6.797206	-0.8841
C	-2.89135	-0.9623	-0.00351	H	4.13367	7.663418	-0.34077
C	-2.44152	-1.86471	-2.25788	H	5.520642	7.09424	-1.27342
H	-3.51745	-2.07292	-2.23786	C	3.29169	5.209692	0.630198
C	-2.14108	-1.04646	-3.52639	H	2.912325	6.046765	1.218182
H	-2.6396	-0.07327	-3.51855	H	3.407628	4.36791	1.316173
H	-2.47473	-1.58953	-4.41931	C	-0.13974	5.35385	0.506494
H	-1.06478	-0.87208	-3.63098	C	-1.22505	4.555357	1.279061
C	-1.68548	-3.20303	-2.35255	H	-1.66698	3.797485	0.624729
H	-0.60658	-3.02221	-2.38254	H	-0.75856	4.023988	2.110057
H	-1.96632	-3.75013	-3.26173	C	-2.34152	5.464558	1.834151
H	-1.88801	-3.84707	-1.49215	H	-3.06856	4.831608	2.360052
C	-3.03105	0.03316	2.255692	C	-1.73155	6.480487	2.815697

H	-4.03269	-0.41046	2.238753	H	-2.51583	7.126847	3.233606
C	-2.31241	-0.47705	3.517356	H	-1.26251	5.95724	3.66045
H	-2.17929	-1.56234	3.507328	C	-0.68559	7.323871	2.065501
H	-2.88604	-0.21531	4.415163	H	-0.22458	8.043878	2.755212
H	-1.32261	-0.01803	3.614644	C	0.424998	6.407668	1.503229
C	-3.17341	1.563104	2.362203	H	0.93381	5.894805	2.328453
H	-2.18402	2.028621	2.412977	H	1.16749	7.041152	1.010111
H	-3.73072	1.846367	3.264459	C	-3.03718	6.212335	0.683227
H	-3.69062	1.983842	1.495328	H	-3.83906	6.853441	1.075555
C	-4.58897	-2.79617	0.522453	H	-3.50812	5.497387	-0.00578
C	-3.35012	-3.34533	1.282402	C	-1.98912	7.056883	-0.06223
H	-3.10604	-2.67271	2.106035	H	-2.46517	7.585421	-0.89947
H	-2.48081	-3.36268	0.61792	C	-1.36654	8.078349	0.908194
C	-3.58915	-4.7603	1.850303	H	-2.13996	8.75399	1.299175
H	-2.67429	-5.08129	2.36576	H	-0.6325	8.703552	0.380526
C	-4.76114	-4.71963	2.847757	C	-0.88424	6.134166	-0.62713
H	-4.52354	-4.04851	3.684669	H	-0.18445	6.742499	-1.20136
H	-4.93622	-5.71682	3.275026	H	-1.33271	5.424039	-1.32553
C	-6.01847	-4.22561	2.111288	C	2.260503	-2.03364	-0.00684
H	-6.86232	-4.17136	2.812468	C	2.781198	-1.17742	-2.26919
C	-5.77025	-2.81253	1.536374	H	3.519678	-1.98689	-2.26081
H	-5.55921	-2.11266	2.353959	C	3.527534	0.167045	-2.35733
H	-6.69302	-2.47725	1.054131	H	2.808945	0.992482	-2.38399
C	-6.35863	-5.19627	0.964493	H	4.14087	0.219903	-3.26615
H	-7.26977	-4.86615	0.445813	H	4.181103	0.327709	-1.49529
H	-6.56433	-6.19909	1.364055	C	1.921093	-1.33619	-3.5359
C	-5.17561	-5.246	-0.02083	H	1.35867	-2.27389	-3.53955
H	-5.41448	-5.92554	-0.85024	H	2.552878	-1.31739	-4.43259
C	-3.91624	-5.74134	0.71098	H	1.203014	-0.51322	-3.62315
H	-3.07182	-5.80654	0.010843	C	1.488193	-2.66996	2.251895
H	-4.07709	-6.75157	1.112768	H	2.385962	-3.29861	2.234669
C	-4.92012	-3.8354	-0.59906	C	1.542323	-1.80099	3.521048
H	-4.09114	-3.8844	-1.30893	H	2.403781	-1.12773	3.526238
H	-5.80121	-3.52789	-1.1639	H	1.603632	-2.43433	4.414761

C	-5.34117	-0.44334	-0.51434	H	0.637904	-1.18961	3.612556
C	-6.34208	-1.11325	-1.50171	C	0.251652	-3.58418	2.343317
H	-5.78661	-1.58512	-2.32121	H	-0.65971	-2.97893	2.379493
H	-6.90907	-1.90141	-0.99803	H	0.285499	-4.2057	3.247413
C	-7.35481	-0.09606	-2.07598	H	0.172408	-4.24733	1.477384
H	-8.02988	-0.62992	-2.75853	C	4.713561	-2.53421	0.507759
C	-6.61093	1.01162	-2.84169	C	5.359165	-3.53874	1.508775
H	-6.04844	0.580842	-3.68163	H	5.558462	-4.49587	1.01813
H	-7.3262	1.728351	-3.26866	H	4.660786	-3.73439	2.331388
C	-5.65311	1.723217	-1.87015	C	6.695691	-3.01044	2.077044
H	-5.08935	2.497771	-2.40652	H	7.099231	-3.76328	2.767725
C	-4.64722	0.700866	-1.30241	C	7.692723	-2.77545	0.925961
H	-3.93392	1.219099	-0.65442	H	8.654857	-2.4245	1.324466
H	-4.07628	0.27407	-2.12835	H	7.890705	-3.71846	0.397266
C	-6.45848	2.362503	-0.72568	C	7.103099	-1.73626	-0.04492
H	-7.16961	3.099456	-1.12435	H	7.799962	-1.57241	-0.8782
H	-5.78669	2.902418	-0.04395	C	6.865047	-0.41183	0.701725
C	-7.20535	1.251689	0.033972	H	7.811564	-0.01904	1.098883
H	-7.77353	1.688842	0.866383	H	6.469135	0.346706	0.012118
C	-8.16779	0.529416	-0.92684	C	5.868344	-0.66289	1.84631
H	-8.90896	1.23477	-1.32788	H	5.662964	0.278248	2.373342
H	-8.72616	-0.24987	-0.38936	C	4.537298	-1.19859	1.280044
C	-6.18911	0.238712	0.61054	H	4.097522	-0.44503	0.619691
H	-6.73376	-0.5087	1.190435	H	3.837879	-1.34753	2.104298
H	-5.52597	0.755903	1.306782	C	5.766144	-2.26151	-0.61723
C	0.608994	2.965528	0.008506	H	5.965631	-3.16988	-1.18834
C	1.56647	2.596085	2.256987	H	5.368818	-1.52751	-1.3211
H	1.668531	3.687026	2.240892	C	6.458301	-1.68997	2.828855
C	0.789934	2.212786	3.529531	H	5.768536	-1.85005	3.669041
H	-0.2235	2.622677	3.535489	H	7.40068	-1.31743	3.253915
H	1.309601	2.584222	4.421479	C	3.0847	-4.39748	-0.51558
H	0.712874	1.124169	3.623441	C	4.160381	-4.89556	-1.52497
C	2.972679	1.974384	2.342893	H	5.139863	-4.95675	-1.04215
H	2.897969	0.88354	2.388607	H	4.249653	-4.17628	-2.34804

H	3.50033	2.318827	3.241599	C	3.820184	-6.29328	-2.08936
H	3.583848	2.226379	1.471626	H	4.615447	-6.58693	-2.78797
C	-0.39807	3.016966	-2.24793	C	2.470488	-6.24675	-2.82687
H	-0.03504	4.050905	-2.23314	H	2.522795	-5.54347	-3.66953
C	0.169373	2.332792	-3.50425	H	2.230915	-7.23372	-3.24632
H	1.261582	2.284205	-3.49152	C	1.380456	-5.80579	-1.83277
H	-0.1339	2.877961	-4.40669	H	0.413388	-5.73647	-2.34826
H	-0.21168	1.309691	-3.59505	C	1.730414	-4.40978	-1.27616
C	-1.93358	3.037957	-2.36171	H	1.775691	-3.70268	-2.10566
H	-2.31816	2.014649	-2.41394	H	0.92775	-4.07171	-0.61384
H	-2.25388	3.569725	-3.26689	C	1.28657	-6.82742	-0.68591
H	-2.39999	3.522236	-1.49916	H	1.028405	-7.82015	-1.08065
C	2.284903	4.826399	-0.50468	H	0.486992	-6.54284	0.011942
C	2.208607	6.033587	-1.48482	C	2.638314	-6.87329	0.04715
H	1.533114	5.789379	-2.31351	H	2.58334	-7.58501	0.882214
H	1.797183	6.911926	-0.97944	C	3.742052	-7.31	-0.93482
C	3.598812	6.413845	-2.04448	H	4.709338	-7.36881	-0.41619
H	3.476865	7.271058	-2.72045	H	3.52813	-8.31426	-1.32655
C	4.194323	5.223716	-2.81632	C	2.967501	-5.47324	0.614714
H	5.175199	5.490811	-3.23352	H	2.184873	-5.18013	1.318452
H	3.54681	4.957899	-3.66336	H	3.8953	-5.53877	1.184702
C	4.326715	4.030297	-1.85352				

Table S5. Comparison of parameters between X-ray structure and optimized gas phase model for **3**

	X-ray structure	**Optimized model**
Average Ce−$N_{guanidine}$ (Å)	2.518(3)	2.56266
Average $N_{guanidine}$−Ce−$N_{guanidine}$ (°)	52.75(11)	52.11

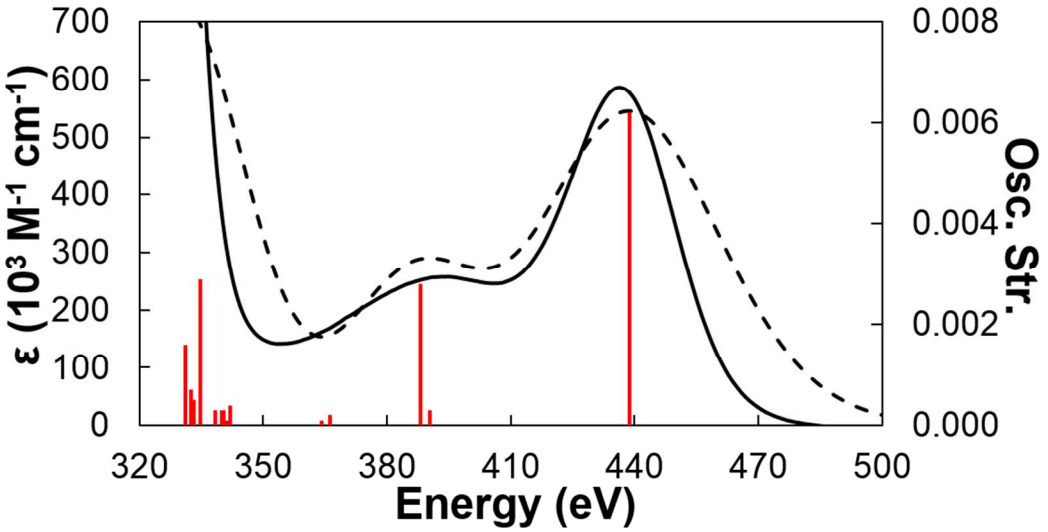

Figure S48. Experimental (black solid line) and TD-DFT predicted (black dashed line) absorption spectrum of **3**. The predicted spectra were rendered as Gaussian line shapes having a fwhm of 2500 cm^{-1}. Oscillator strengths for the electronic transitions are shown as red vertical lines.

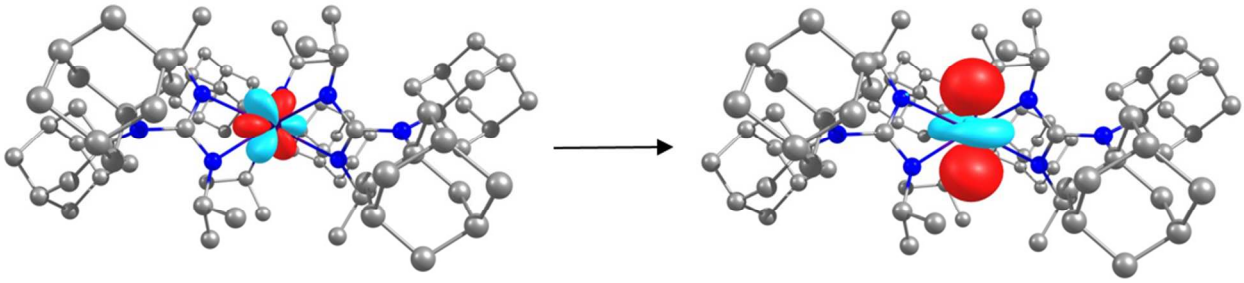

Figure S49. Calculated Natural Transition Orbitals (NTO) of **3** in gas phase with contour value of 0.05. The calculated transition shown is centered at 439 nm (oscillator strength 0.0062).

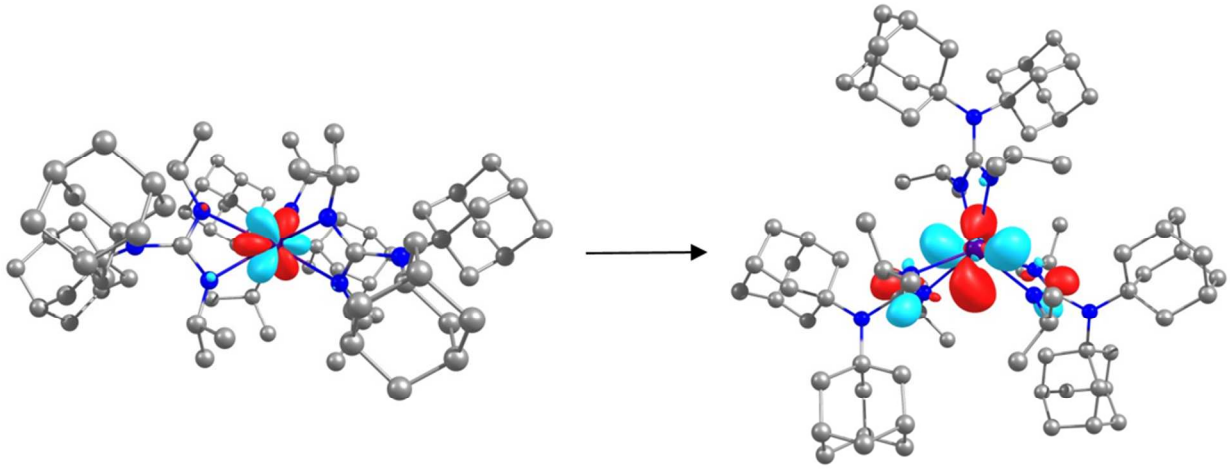

Figure S50. Calculated Natural Transition Orbitals (NTO) of **3** in gas phase with contour value

of 0.05. The calculated transition shown is centered at 390 nm (oscillator strength 0.0003).

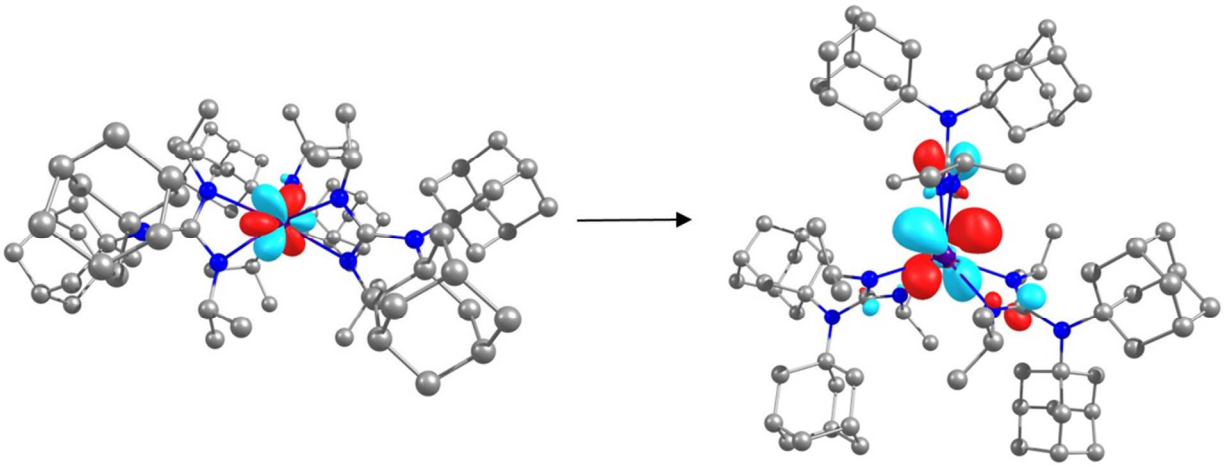

Figure S51. Calculated Natural Transition Orbitals (NTO) of **3** in gas phase with contour value of 0.05. The calculated transition shown is centered at 388 nm (oscillator strength 0.0028).

Table S6. Cartesian coordinates of optimized gas phase structure for **4**

Ce	-0.00622	0.00535	0.007151	N	0.708486	-2.18483	1.096312
N	-2.32752	0.408133	1.021339	C	0.401322	-2.99489	2.270491
N	-2.27935	-0.34683	-1.10409	H	0.945776	-3.94088	2.208662
N	-4.48528	0.089099	-0.12572	C	-1.10016	-3.32052	2.330874
N	1.461228	-1.82909	-1.00198	H	-1.41655	-3.88924	1.449972
N	2.094491	-3.94443	0.100631	H	-1.69135	-2.40032	2.363939
C	-3.03318	0.050851	-0.0655	H	-1.33903	-3.91433	3.222659
C	-2.90713	1.059604	2.19379	C	0.837781	-2.28783	3.563309
H	-3.9965	1.116721	2.079979	H	1.916369	-2.10025	3.571945
C	-2.35829	2.49015	2.362958	H	0.592531	-2.89795	4.441578
H	-2.5297	3.110428	1.48	H	0.327855	-1.32342	3.675436
H	-1.27841	2.458943	2.538298	C	3.470411	-4.06386	0.692435
H	-2.82573	2.985473	3.223367	C	4.400089	-4.76717	-0.33076
C	-2.59803	0.289661	3.492425	H	5.375989	-4.94402	0.140315
H	-2.99622	-0.72776	3.488212	H	4.57406	-4.08145	-1.17025
H	-3.02589	0.813217	4.356212	C	3.82633	-6.07999	-0.87059
H	-1.51502	0.221633	3.649883	H	3.774451	-6.83088	-0.07144
C	-2.85221	-0.95699	-2.30047	H	4.49925	-6.49571	-1.63153
H	-3.94265	-0.90027	-2.24509	C	2.439352	-5.84816	-1.47624

C	-2.41145	-0.21397	-3.57143	H	2.54396	-5.2211	-2.37134
H	-2.73816	0.830847	-3.55595	H	2.004759	-6.80012	-1.80884
H	-2.83585	-0.68823	-4.46507	C	4.055407	-2.67428	0.988986
H	-1.31987	-0.22462	-3.67669	H	4.084064	-2.04337	0.101826
C	-2.46603	-2.4416	-2.39872	H	5.081646	-2.79064	1.353538
H	-2.83128	-3.0038	-1.53276	H	3.482703	-2.15354	1.758985
H	-1.37853	-2.55472	-2.43575	N	0.937113	2.150616	-1.03784
H	-2.88835	-2.89829	-3.30312	N	1.496684	1.746478	1.110108
C	-5.29835	-1.05311	0.413037	N	2.38664	3.791635	0.090672
C	-6.37476	-0.50656	1.384873	C	1.606424	2.565947	0.051258
H	-5.87474	-0.15458	2.296886	C	0.725422	2.972447	-2.22721
H	-7.03488	-1.33096	1.685214	H	1.265811	3.920791	-2.11874
C	-7.19493	0.644273	0.794895	C	-0.77125	3.284125	-2.42515
H	-7.88911	1.032986	1.551057	H	-1.22	3.750506	-1.54481
H	-7.82065	0.284268	-0.03219	H	-1.32365	2.360647	-2.62615
C	-6.26899	1.765706	0.316038	H	-0.91752	3.956326	-3.28015
H	-6.85362	2.570916	-0.14794	C	1.224566	2.278071	-3.50859
H	-5.76452	2.204379	1.187096	H	2.296796	2.069115	-3.48952
C	-5.18864	1.290852	-0.69141	H	1.021892	2.905997	-4.38494
C	-4.40829	-2.0347	1.190781	H	0.702148	1.325391	-3.65665
H	-3.6385	-2.47771	0.552544	C	2.3008	1.9099	2.317629
H	-5.03041	-2.84817	1.579232	H	2.869538	2.840593	2.247089
H	-3.91459	-1.55617	2.033009	C	1.415684	1.999406	3.570802
C	-5.9919	-1.90372	-0.68773	H	0.736582	2.856656	3.521057
H	-6.76434	-1.36489	-1.23661	H	2.031231	2.107252	4.472601
H	-6.47678	-2.76928	-0.22055	H	0.808053	1.094162	3.689459
H	-5.26549	-2.28252	-1.41115	C	3.304423	0.755302	2.468729
C	-4.19741	2.447181	-0.89789	H	3.986021	0.70616	1.613202
H	-3.70392	2.728441	0.031079	H	2.777405	-0.20168	2.532222
H	-4.74232	3.322321	-1.26771	H	3.906757	0.874124	3.378506
H	-3.42913	2.193393	-1.63172	C	3.799735	3.806613	-0.41811
C	-5.85768	1.057412	-2.07523	C	3.975564	4.980585	-1.41473
H	-5.1369	0.688285	-2.80869	H	3.419378	4.745653	-2.33184
H	-6.25064	2.010625	-2.44891	H	5.034228	5.052574	-1.6968

C	1.423051	-2.65409	0.06036	C	3.47917	6.319403	-0.86282
C	2.298225	-2.04841	-2.17937	H	3.566987	7.096161	-1.63325
H	2.786005	-3.02781	-2.10673	H	4.112549	6.648152	-0.02895
C	3.392508	-0.96988	-2.30238	C	2.021389	6.199768	-0.41144
H	4.059018	-0.94852	-1.43701	H	1.678492	7.147125	0.024987
H	2.936345	0.020847	-2.39159	H	1.392866	6.013294	-1.29218
H	4.006085	-1.14368	-3.19544	C	1.77801	5.061439	0.614468
C	1.46903	-2.01432	-3.47756	C	4.125171	2.499322	-1.15723
H	0.684532	-2.77473	-3.49947	H	4.036334	1.628888	-0.5008
H	2.115428	-2.17342	-4.34939	H	5.158302	2.542682	-1.5183
H	0.987962	-1.03624	-3.59743	H	3.474023	2.344551	-2.01413
C	1.448736	-5.15883	-0.5019	C	4.871421	3.930187	0.702008
C	0.970235	-6.19856	0.551252	H	4.845801	4.884872	1.227943
H	1.787238	-6.69455	1.076181	H	5.868838	3.838176	0.2556
H	0.393528	-6.98326	0.047334	H	4.766938	3.133063	1.442415
H	0.318794	-5.73646	1.297301	C	0.258325	4.900612	0.782346
C	3.5296	-4.8354	2.04113	H	-0.22779	4.647145	-0.15888
H	2.865812	-4.38866	2.785355	H	-0.16408	5.848304	1.133026
H	4.551043	-4.78419	2.437289	H	0.011946	4.12969	1.516283
H	3.275789	-5.89204	1.953653	C	2.312281	5.510716	2.00364
C	0.193978	-4.7689	-1.29759	H	2.188569	4.724175	2.751786
H	-0.55845	-4.29341	-0.66192	H	1.739911	6.382428	2.342748
H	-0.25178	-5.67328	-1.72522	H	-6.69518	0.359873	-2.04317
H	0.426083	-4.09053	-2.11526	H	3.36232	5.804706	1.993296

Table S7. Comparison of parameters between X-ray structure and optimized gas phase model for **4**

	X-ray structure	**Optimized model**
Average Ce−$N_{guanidine}$ (Å)	2.524(5)	2.55691
Average $N_{guanidine}$−Ce−$N_{guanidine}$ (°)	52.45(21)	52.37

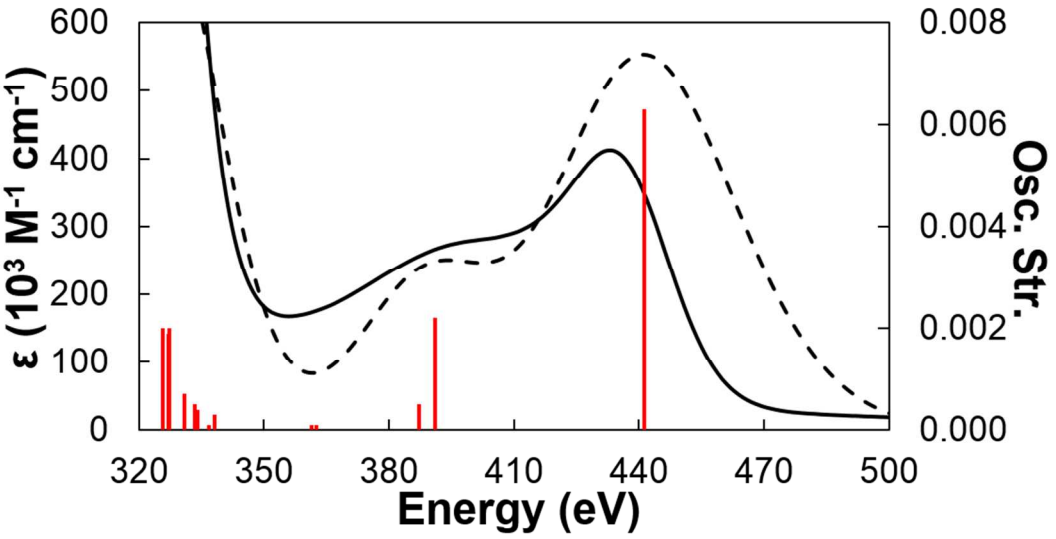

Figure S52. Experimental (black solid line) and TD-DFT predicted (black dashed line) absorption spectrum of **4**. The predicted spectra were rendered as Gaussian line shapes having a fwhm of 2500 cm^{-1}. Oscillator strengths for the electronic transitions are shown as red vertical lines.

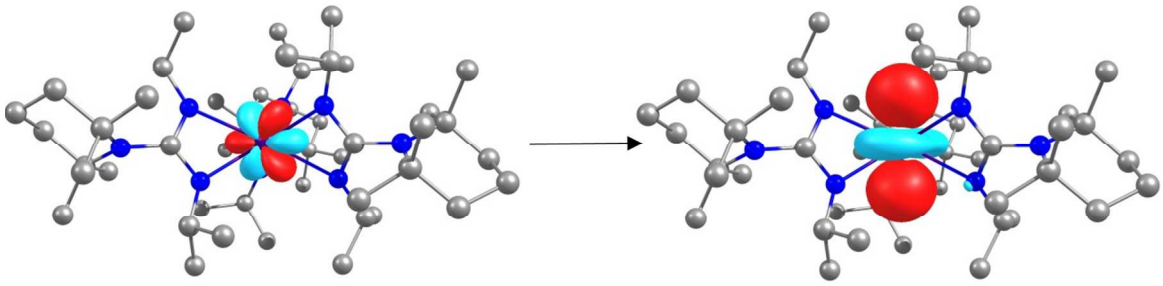

Figure S53. Calculated Natural Transition Orbitals (NTO) of **4** in gas phase with contour value of 0.05. The calculated transition shown is centered at 441 nm (oscillator strength 0.0063).

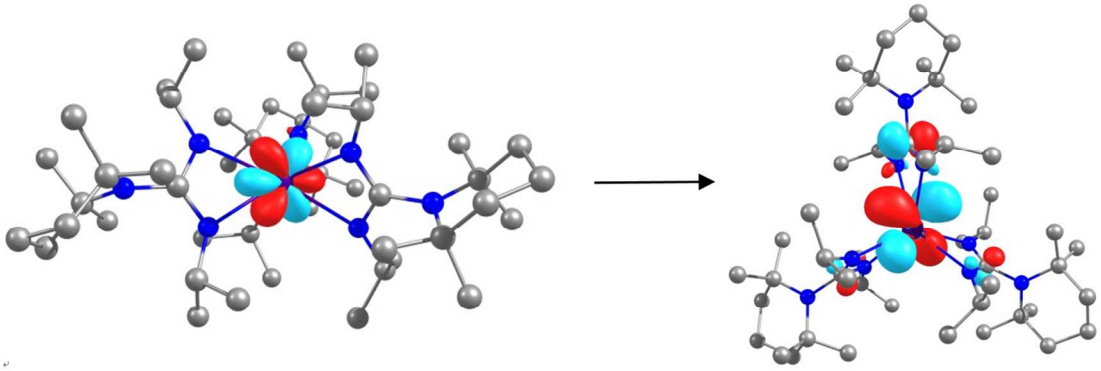

Figure S54. Calculated Natural Transition Orbitals (NTO) of **4** in gas phase with contour value of 0.05. The calculated transition shown is centered at 391 nm (oscillator strength 0.0022).

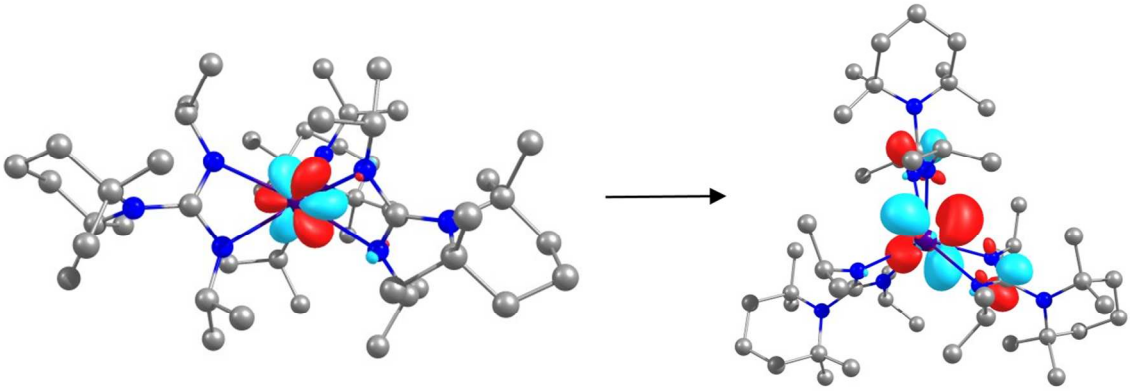

Figure S55. Calculated Natural Transition Orbitals (NTO) of **4** in gas phase with contour value of 0.05. The calculated transition shown is centered at 387 nm (oscillator strength 0.0005).

7. Lifetime Data

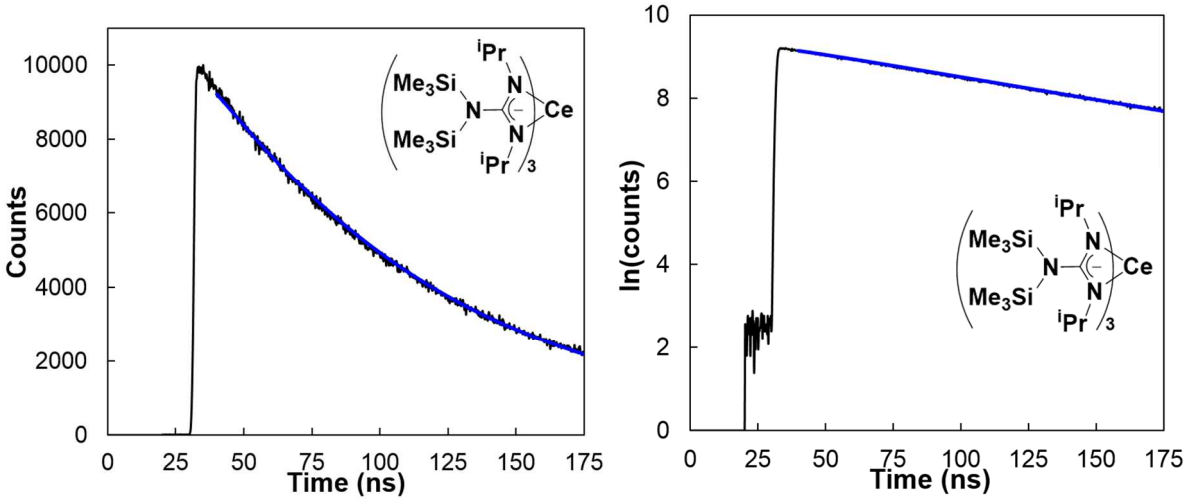

Figure S56. (left) Time-resolved emission intensity decay of **$[(Me_3Si)_2NC(N^iPr)_2]_3Ce^{III}$** in toluene shown in black trace. The decay data was collected at 460 nm upon 380 nm excitation. A single exponential fit from 40 ns to 175 ns is given as blue lines, affording τ = 88.8 ± 0.3 ns. (right) The ln(counts) versus time plot of time-resolved emission intensity decay for **$[(Me_3Si)_2NC(N^iPr)_2]_3Ce^{III}$** in toluene is shown in the black trace with the model shown as the blue solid line (R^2 = 0.9982).

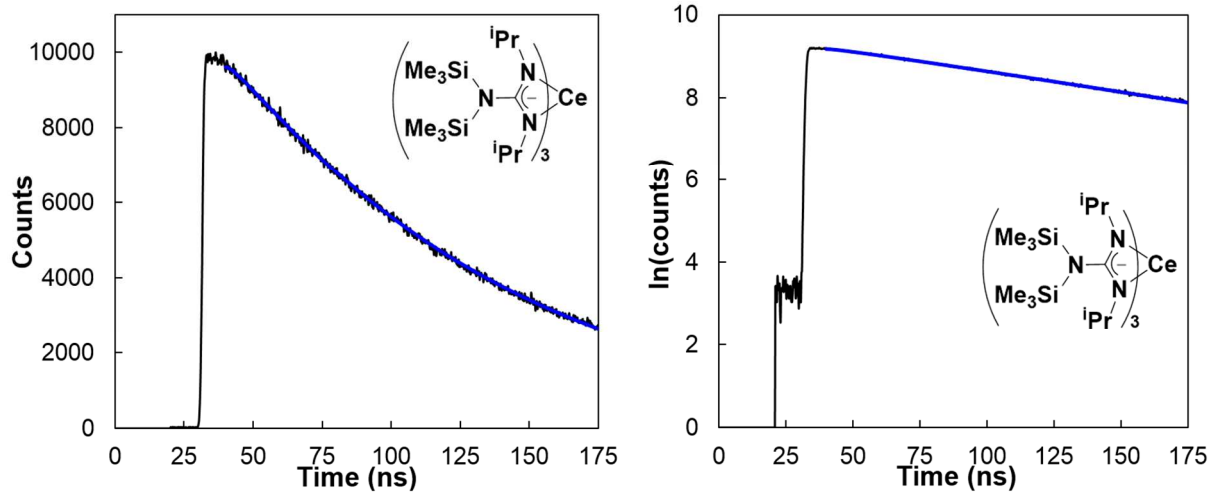

Figure S57. (left) Time-resolved emission intensity decay of **$[(Me_3Si)_2NC(N^iPr)_2]_3Ce^{III}$** in toluene-$d_8$ shown in black trace. The decay data was collected at 460 nm upon 380 nm excitation. A single exponential fit from 40 ns to 175 ns is given as blue lines, affording τ = 96.1 ± 0.1 ns. (right) The ln(counts) versus time plot of time-resolved emission intensity decay for **$[(Me_3Si)_2NC(N^iPr)_2]_3Ce^{III}$** in toluene is shown in the black trace with the model shown as the blue solid line (R^2 = 0.9985).

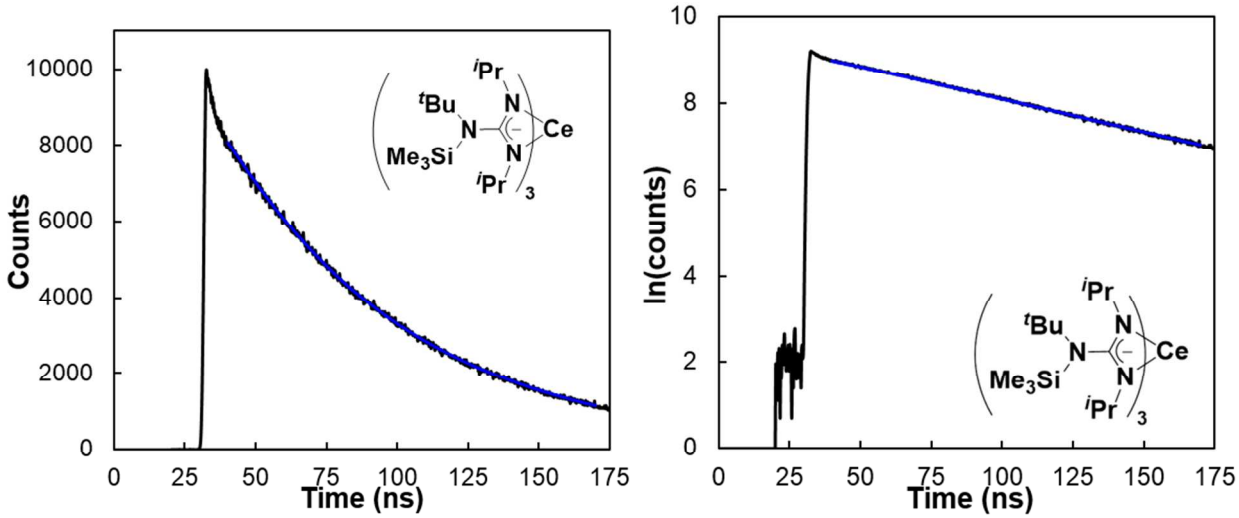

Figure S58. (left) Time-resolved emission intensity decay of **[(Me$_3$SiN^{t}Bu)C(N^{i}Pr)$_2$]$_3$Ce^{III}** in toluene shown in black trace. The decay data was collected at 480 nm upon 380 nm excitation. A single exponential fit from 40 ns to 175 ns is given as blue lines, affording τ = 63.8 ± 0.2 ns. (right) The ln(counts) versus time plot of time-resolved emission intensity decay for **[(Me$_3$SiN^{t}Bu)C(N^{i}Pr)$_2$]$_3$Ce^{III}** in toluene is shown in the black trace with the model shown as the blue solid line (R^2 = 0.9988).

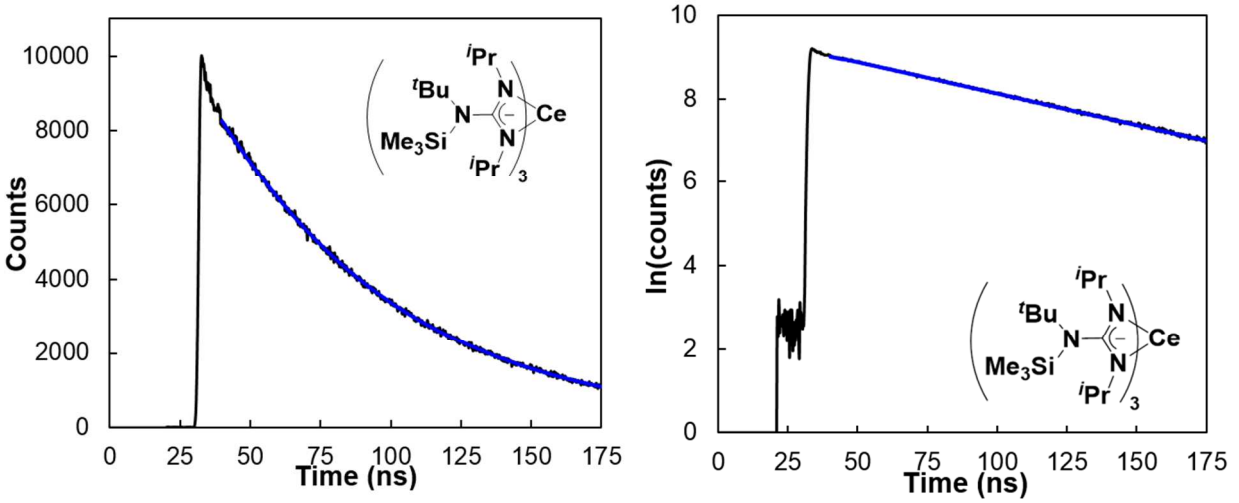

Figure S59. (left) Time-resolved emission intensity decay of **[(Me$_3$SiN^{t}Bu)C(N^{i}Pr)$_2$]$_3$Ce^{III}** in toluene-d_8 shown in black trace. The decay data was collected at 480 nm upon 380 nm excitation. A single exponential fit from 40 ns to 175 ns is given as blue lines, affording τ = 64.0 ± 0.1 ns. (right) The ln(counts) versus time plot of time-resolved emission intensity decay for **[(Me$_3$SiN^{t}Bu)C(N^{i}Pr)$_2$]$_3$Ce^{III}** in toluene is shown in the black trace with the model shown as the blue solid line (R^2 = 0.9981).

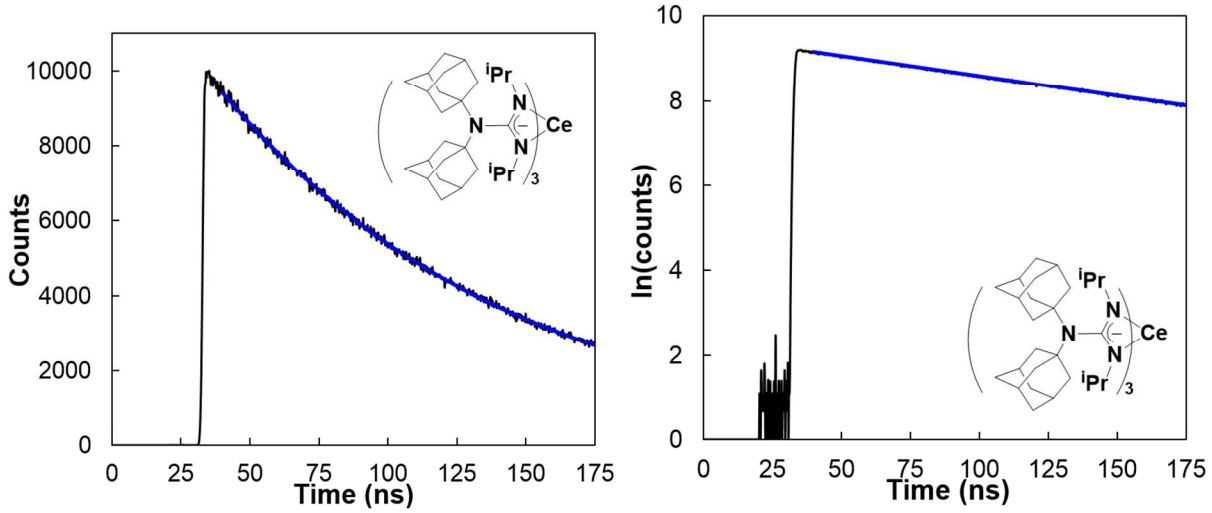

Figure S60. (left) Time-resolved emission intensity decay of **{[$(C_{10}H_{15})_2$N]C($N^iPr)_2$}$_3$Ce^{III}** in toluene shown in black trace. The decay data was collected at 460 nm upon 380 nm excitation. A single exponential fit from 40 ns to 175 ns is given as blue lines, affording τ = 95.21 ± 0.03 ns. (right) The ln(counts) versus time plot of time-resolved emission intensity decay for **{[$(C_{10}H_{15})_2$N]C($N^iPr)_2$}$_3$Ce^{III}** in toluene is shown in the black trace with the model shown as the blue solid line (R^2 = 0.9984).

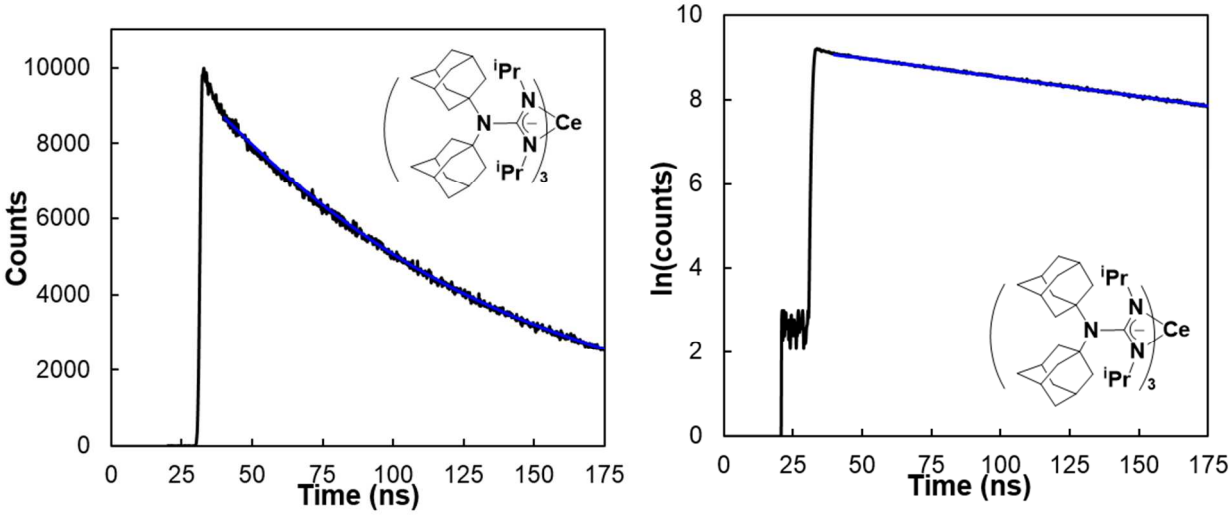

Figure S61. (left) Time-resolved emission intensity decay of **{[$(C_{10}H_{15})_2$N]C($N^iPr)_2$}$_3$Ce^{III}** in toluene-d_8 shown in black trace. The decay data was collected at 460 nm upon 380 nm excitation. A single exponential fit from 40 ns to 175 ns is given as blue lines, affording τ = 104.6 ± 0.1 ns. (right) The ln(counts) versus time plot of time-resolved emission intensity decay for **{[$(C_{10}H_{15})_2$N]C($N^iPr)_2$}$_3$Ce^{III}** in toluene is shown in the black trace with the model shown as the blue solid line (R^2 = 0.9987).

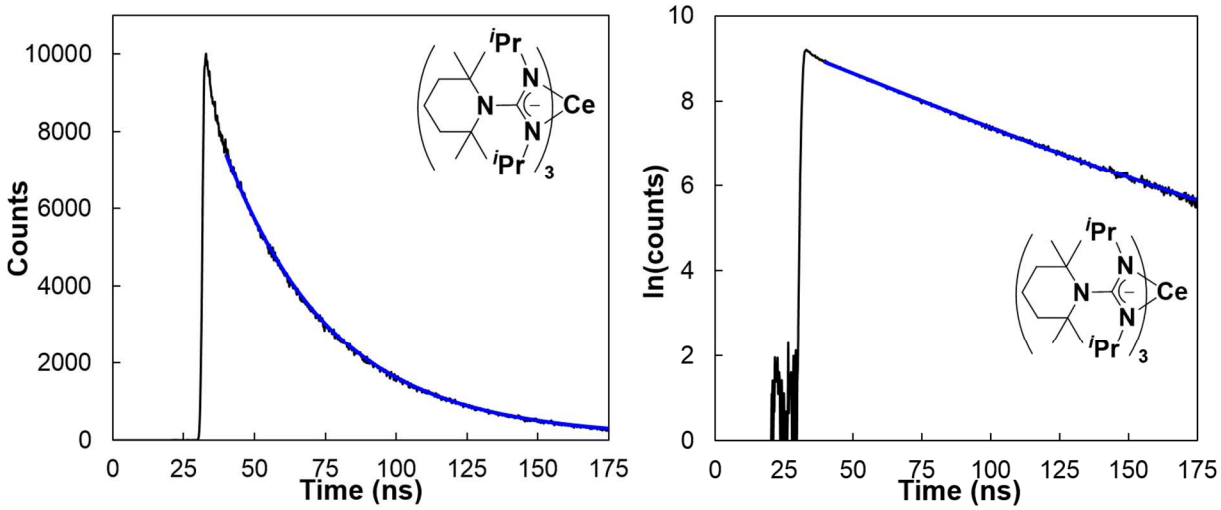

Figure S62. (left) Time-resolved emission intensity decay of **$[(C_9H_{18}N)C(N^iPr)_2]_3Ce^{III}$** in toluene shown in black trace. The decay data was collected at 510 nm upon 380 nm excitation. A single exponential fit from 40 ns to 175 ns is given as blue lines, affording τ = 37.31 ± 0.03 ns. (right) The ln(counts) versus time plot of time-resolved emission intensity decay for **$[(C_9H_{18}N)C(N^iPr)_2]_3Ce^{III}$** in toluene is shown in the black trace with the model shown as the blue solid line (R^2 = 0.9982).

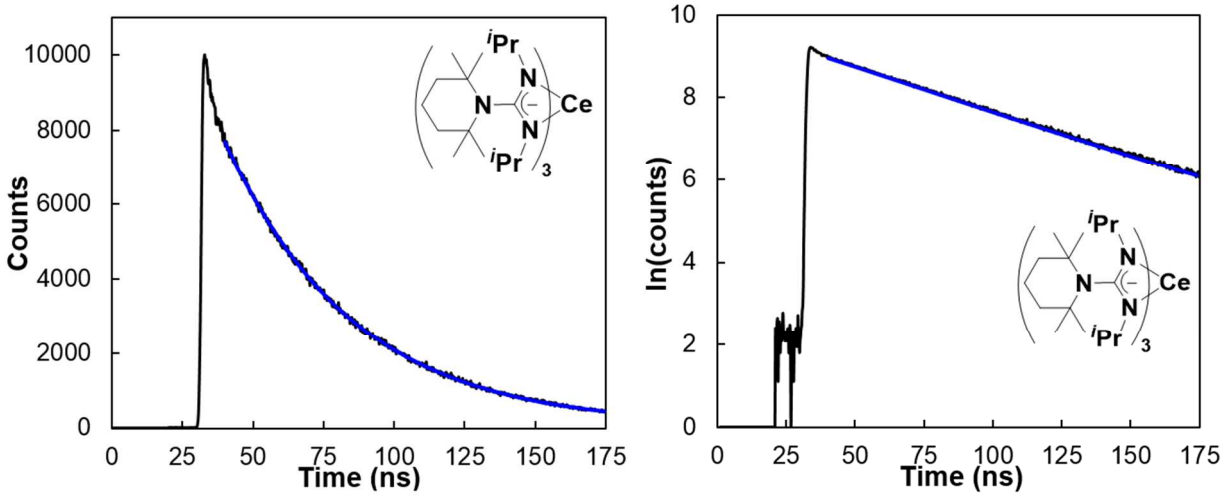

Figure S63. (left) Time-resolved emission intensity decay of **$[(C_9H_{18}N)C(N^iPr)_2]_3Ce^{III}$** in toluene-$d_8$ shown in black trace. The decay data was collected at 510 nm upon 380 nm excitation. A single exponential fit from 40 ns to 175 ns is given as blue lines, affording τ = 43.60 ± 0.04 ns. (right) The ln(counts) versus time plot of time-resolved emission intensity decay for **$[(C_9H_{18}N)C(N^iPr)_2]_3Ce^{III}$** in toluene is shown in the black trace with the model shown as the blue solid line (R^2 = 0.9983).

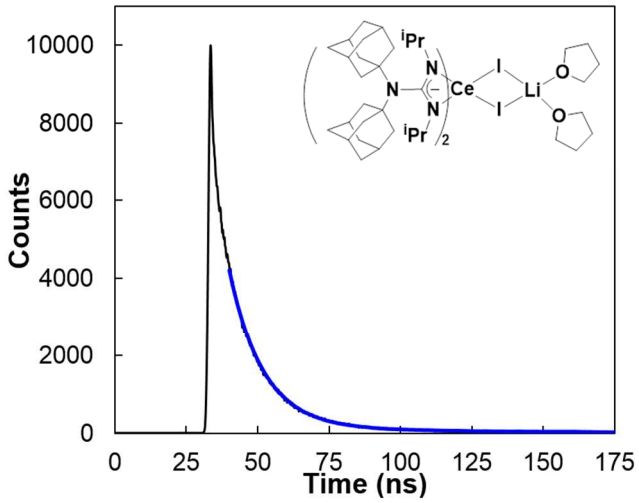

Figure S64. Time-resolved emission intensity decay of **{[$(C_{10}H_{15})_2$N]C($N^iPr)_2$}$_2$$Ce^{III}$($\mu^2$–I)$_2$Li(THF)$_2$** in toluene shown in black trace. The decay data was collected at 470 nm upon 380 nm excitation. A single exponential fit from 40 ns to 175 ns is given as blue lines, affording τ = 11.25 ± 0.03 ns (R^2 = 0.9968).

8. Summary of Spectroscopy Data

Table S8. Observed Radiative Decay Rates (k_r^{tol} and $k_r^{tol\text{-}d8}$), Nonradiative Decay Rates (k_{nr}^{tol} and $k_{nr}^{tol\text{-}d8}$), Differences in Nonradiative Decay Rates (Δk_{nr}) and α Angles for Complexes **1**–**4** in toluene and toluene-d_8.

complex	k_r^{tol} ($\times 10^6$ s^{-1}) [a]	$k_r^{tol\text{-}d8}$ ($\times 10^6$ s^{-1}) [a]	k_{nr}^{tol} ($\times 10^6$ s^{-1}) [a]	$k_{nr}^{tol\text{-}d8}$ ($\times 10^6$ s^{-1}) [a]	Δk_{nr} ($\times 10^6$ s^{-1}) [b]	α Angle (°)
1	9.1(2)	8.4(2)	2.2(2)	2.0(2)	0.2(2)	71.3
2	7.36(14)	8.12(13)	8.31(14)	7.51(13)	0.80(14)	65.5
3	3.04(2)	3.06(2)	7.48(2)	6.33(2)	1.15(2)	61.6
4	4.6(1)	4.6(2)	22.4(1)	18.3(2)	4.1(2)	60.0

[a] k_r and k_{nr} were obtained from the equations $k_r = \varphi_{PL}/\tau$, $k_{nr} = (1 - \varphi_{PL})/\tau$. [b] $\Delta k_{nr} = k_{nr}^{tol} - k_{nr}^{tol\text{-}d8}$. Standard deviations are shown in parentheses.

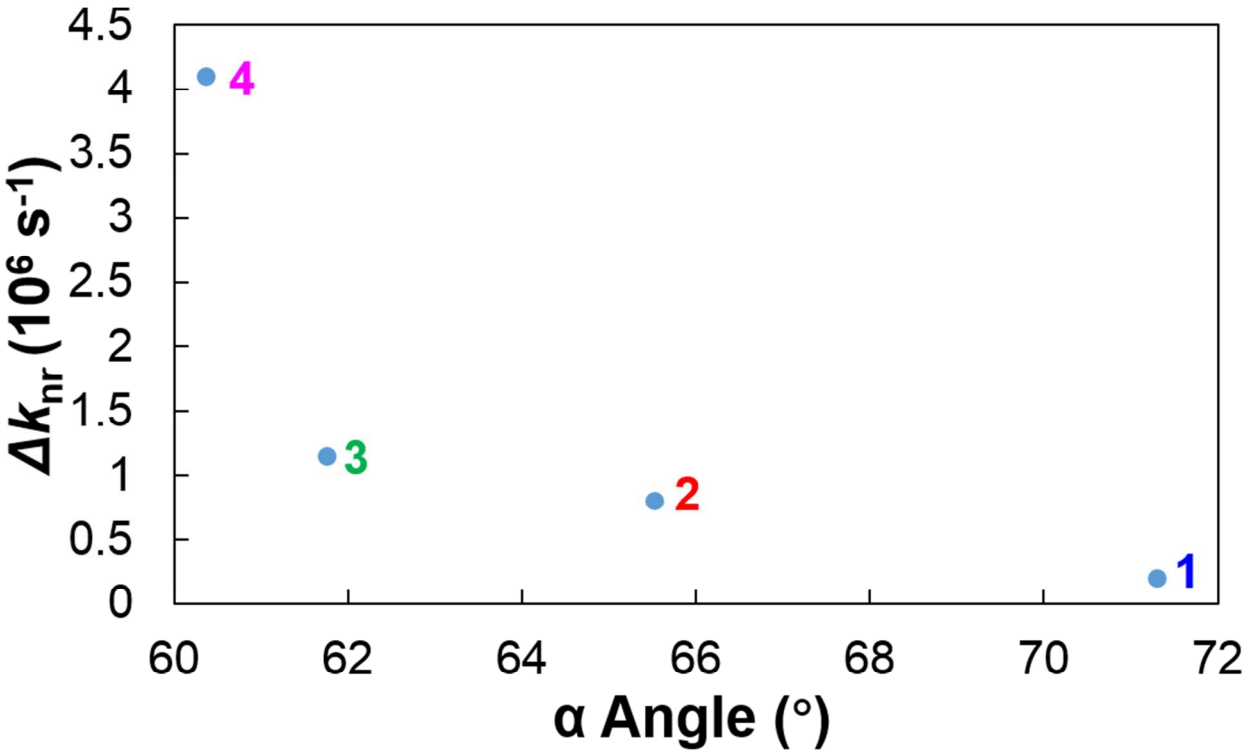

Figure S65. Correlation plot of the Δk_{nr} versus α angles for complexes **1–4.**

Table S9. Summary of spectroscopy data for **1**, **2**, **3**, **4** and **3-I** in toluene.

		1	**2**	**3**	**4**	**3-I**
Spectra data	λ_{abs} /nm (ε M^{-1} cm^{-1})	424 (595) 363 (355)	426 (512) 376 (287)	436 (586) 395 (258)	433 (412) 402 (280)	410 (635)
	λ_{emi} /nm	459	462	475	476	481
Stokes shift /nm		35	36	39	43	71
Fit of Emission data	$\rightarrow {}^2F_{5/2}$ /cm^{-1} (HWHM cm^{-1})	21914 (713)	21606 (744)	21131 (782)	21195 (776)	21266 (1054)
	$\rightarrow {}^2F_{7/2}$ /cm^{-1} (HWHM cm^{-1})	20264 (1427)	19919 (1386)	19466 (1415)	19591 (1479)	19646 (1844)
Φ[a]		0.81	0.47	0.29	0.17	0.063
τ /ns		89	64	95	37	11
k_r [b]/$\times 10^6$ s^{-1}		9.1	7.4	3.0	4.6	5.6
k_{nr} [b]/$\times 10^6$ s^{-1}		2.2	8.3	7.5	22	83

a. Referenced to 9,10-diphenylanthracene (absolute quantum yield Φ = 0.97)[4] b. $\Phi = k_r/(k_r + k_{nr})$, $\tau = 1/(k_r + k_{nr})$

Table S10. Summary of photophysical data for **1**, **2**, **3**, and **4** in toluene-d_8.[a]

	$\Phi^{tol\text{-}d8}$	$\tau^{tol\text{-}d8}$ /ns	$k_r^{tol\text{-}d8}$ /$\times 10^6$ s^{-1}	$k_{nr}^{tol\text{-}d8}$ /$\times 10^6$ s^{-1}
1	0.81(2)	96.1(1)	8.4(2)	2.0(2)
2	0.52(1)	64.0(1)	8.12(13)	7.51(13)
3	0.337(2)	104.6(1)	3.20(2)	6.33(2)
4	0.20(1)	43.60(4)	4.6(2)	18.3(2)

a. Standard deviations are shown in parentheses.

9. Strickler-Berg Analysis. Radiative decay rates can be predicted from Strickler-Berg equation:

$$k_r^{SB} = 2.88 \times 10^{-9} n^2 \frac{\int I(\tilde{\upsilon}_f) d\tilde{\upsilon}_f}{\int I(\tilde{\upsilon}_f) \tilde{\upsilon}_f^{-3} d\tilde{\upsilon}_f} \int \varepsilon(\tilde{\upsilon}_a)\, \mathrm{dln}(\tilde{\upsilon}_a)$$

The absorption and emission bands are plotted on wavenumber scale and the lowest energy absorption band is fitted with Gaussian function to its low energy edge. An example of fitted absorption band is shown in Figure S69 in the literature.[7] Molar distinction coefficient $\varepsilon(\tilde{\upsilon}_a)$ and emission intensity $I(\tilde{\upsilon}_f)$ as functions of wavenumbers were applied for this equation. n stands for the refractive index of the solvent. Computed k_r^{SB} was listed in Table S2 and compared to k_r^{obs}. The results are on the same order of magnitudes.

We need to note that Strickler-Berg equation was developed for two-state systems (one excited state and one ground state) and assumed Born-Oppenheimer approximation. In the f→d emissive transitions for Ce^{3+} cations, the ground manifold is consisted of $^2F_{5/2}$ and $^2F_{7/2}$ states. The observed Stoke shifts also suggest the Born-Oppenheimer approximation does not hold in the series of compounds. Based on these considerations, we do not expect Strickler-Berg analysis to accurately describe the radiative decay rates in our complexes.

Table S11. Predicted Radiative Decay Rates k_r^{SB} from Strickler−Berg Analysis and Observed Radiative Decay Rates k_r^{obs} and Nonradiative Decay Rates k_{nr}^{obs} for Complexes **1–4**.[c]

complex	k_r^{obs} (×10^6 s^{-1})[a]	k_r^{SB} (×10^6 s^{-1})[b]	k_{nr}^{obs} (×10^6 s^{-1})[a]
1	9.1(2)	2.2	2.2(3)
2	7.36(14)	1.7	8.31(14)
3	3.04(2)	2.1	7.48(2)
4	4.6(1)	1.8	22.4(1)

[a] k_r and k_{nr} were obtained from the equations $k_r = \varphi_{PL}/\tau$, $k_{nr} = (1 - \varphi_{PL})/\tau$. [b] k_r^{SB} was calculated from the Strickler-Berg analysis. [c] Standard deviations are shown in parentheses.

10. Determination of Structural Metrics.

Percent buried volume was determined by SambVca 2.0.[23] In calculating percent buried volume, the ligand structure was taken from the crystal structure. Cerium atom was set as the atom coordinated to the center of the sphere so that distance of the coordination point from the center of the sphere was set to 0 Å. Bondi radii were scaled by 1.17 and mesh spacing for numerical integration was 0.05. Hydrogen atoms were included. %V_{bur} of each ligand was calculated and summed up to the %V_{bur} of the complex. The results are shown in Table S12.

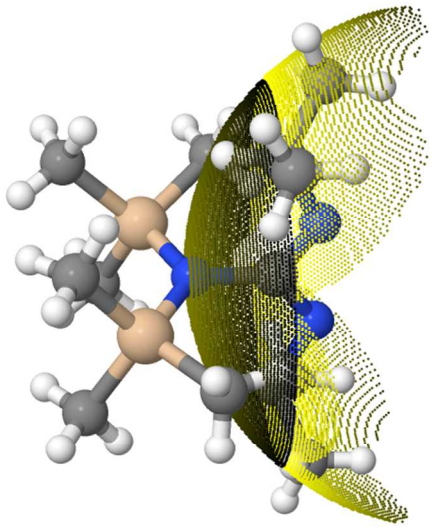

Figure S66. Representative sphere (R = 4.5 Å) occupied by carbodiimide moiety of complex **1** (gray = carbon, blue = nitrogen, yellow = silicon, white = hydrogen, and purple = cerium).

Table S12. Summary of percent buried volumes for **1**-**8**.

	1	**2**	**3**	**4**	**5**[a]	**6**	**7**	**8**
L1	28.6	29.4	29.8	29.6	29.5	28.4	29.2	28.0
L2	29.5	28.9	29.8	29.2	28.1	28.4	28.3	27.7
L3	29.8	29.1	29.6	29.6	26.8	28.4	28.8	28.3
%V_{bur}	87.9	87.4	89.2	88.4	84.4	85.2	86.3	84.0

a. Determined without hydrogen atoms.

The cone angle (θ) was computed by a Mathematica package FindConeAngle.[24,25] θ of each ligand was calculated and was averaged. Hydrogens are not considered. The results are shown in Table S13.

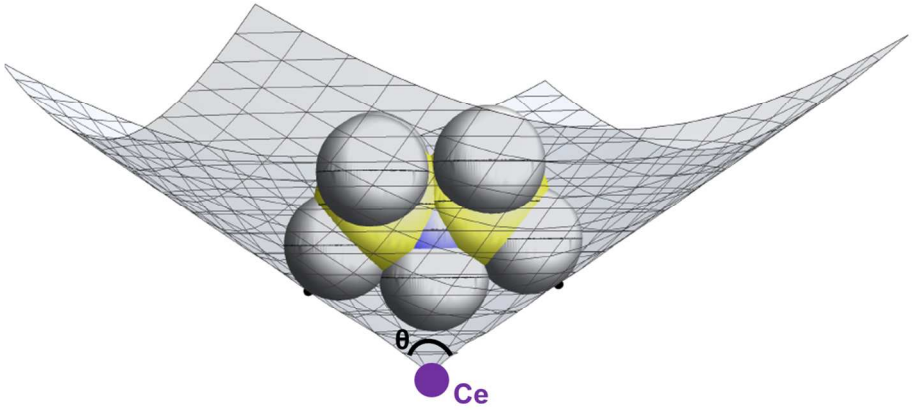

Figure S67. The cone angle of the amide ligand of complex **1** (gray = carbon, blue = nitrogen, and yellow = silicon) centered at cerium (purple). The cone is dependent on two atoms in the ligand

Table S13. Summary of the cone angles for **1**-**8**.

	1	**2**	**3**	**4**	**5**	**6**	**7**	**8**
L1	111.2	109.6	110.5	101.6	90.6	100.9	90.3	64.6
L2	112.4	111.1	110.9	100.8	94.3	100.9	87.1	64.7
L3	110.9	110.4	110.1	101.6	94.3	100.9	78.1	65.0
θ angle/ °	111.5	110.4	110.5	101.3	93.1	100.9	85.2	64.8

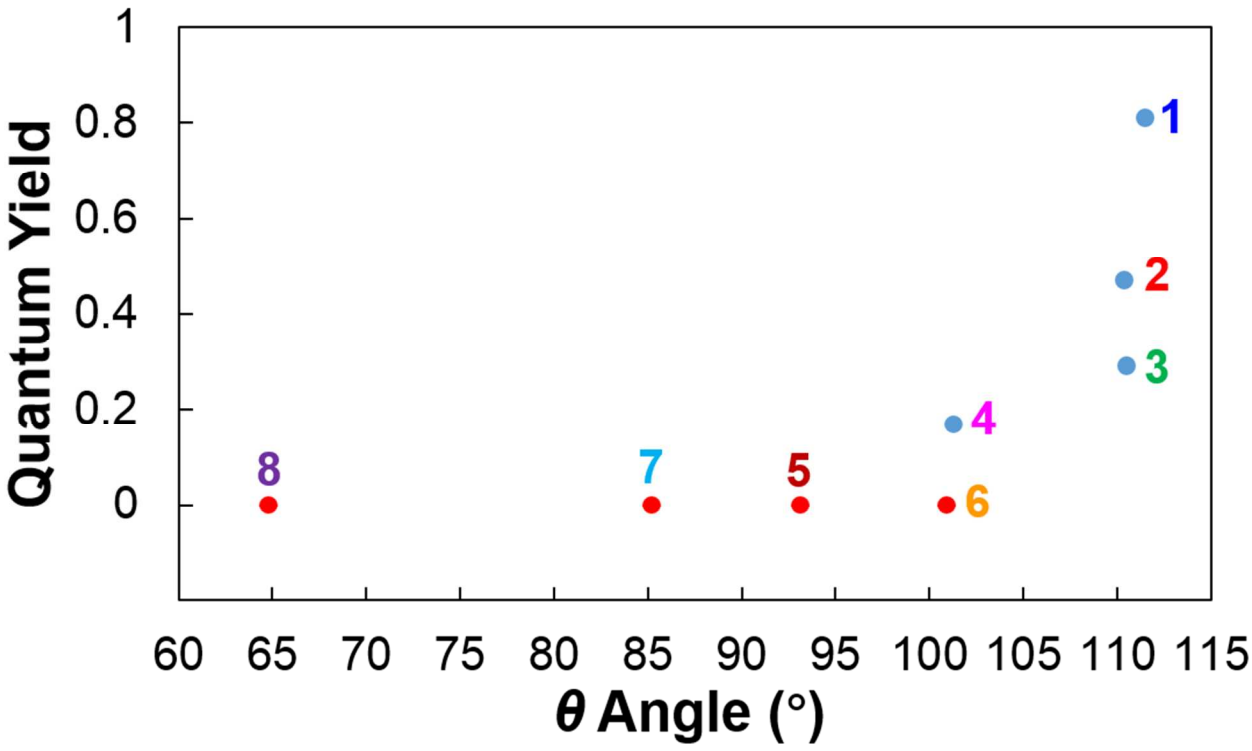

Figure S68. Correlation plot of the quantum yields versus *θ* angles for complexes **1–8.**

α angles were measured from crystal structures visualized in Mercury software. The *α* angle shown in the main text was the average of the values from three ligands.

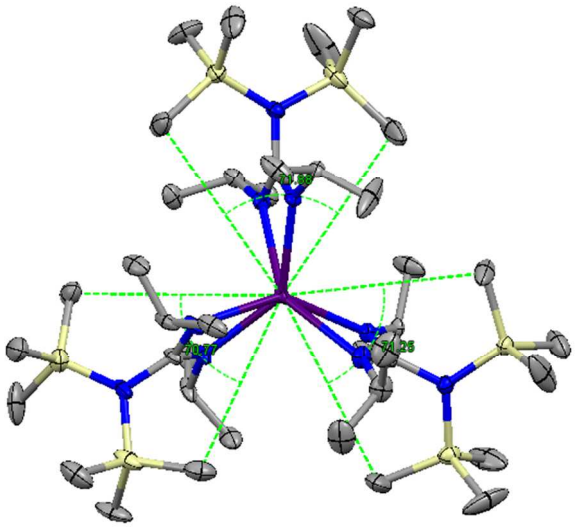

Figure S69. Determination of *α* angle of complex **1**.

Table S14. Summary of *α* angle for **1**-**8**.

	1	**2**	**3**	**4**	**5**	**6**	**7**	**8**
α angle/ °	71.9 70.8 71.2	64.7 66.2 65.6	61.8 61.5 61.5	60.2 60.2 59.6	53.6 57.9 58.8	55.7 55.7 55.7	53.3 50.7 44.6	26.9 26.9 27.0
Average *α* angle/ °	71.3	65.5	61.6	60.0	56.8	55.7	49.5	26.9

11. Computational Details for GA and GOAr Cerium(III) Complexes.

Density functional theory calculations. For the **GA** and **GOAr** cerium(III) complexes, density functional theory (DFT) and time-dependent DFT (TD-DFT) calculations were performed using the Turbomole (TM) program package.[26] In all calculations, the Ce center was modeled by a scalar-relativistic ECP28MWB effective core potential[27] with an accompanying ecp-28-mwb valence basis set (12s11p9d8f/9s8p6d5f) from the TM basis set library. For all other atoms, 6-31G* all-electron split-valence basis sets[28,29] were used. Ground state DFT calculations were performed to obtain equilibrium geometries for the **GA** and **GOAr** cerium(III) complexes (see Figure 1 in the main article). The BP86[30,31] and B3LYP[32,33] exchange-correlation functionals, the latter only for the **GA** complexes, were used for these optimizations. For each complex, the vertical absorption spectrum was calculated at the ground state equilibrium geometry with TD-DFT, using B3LYP and the Tamm-Dancoff approximation.[34] The lowest-energy bright excited states (*i.e.* the first excited states that have appreciable oscillator strengths) were then subjected to geometry optimization, and the resulted excited state equilibrium geometries were used to calculate vertical emission spectra. The BP86 functional was used for most of the excited state geometry optimization while the emission energies were calculated with B3LYP. For the **GA** series, excited state optimizations were also carried out with B3LYP. The excited-state equilibrium structures were very similar between BP86 and B3LYP, but the hybrid functional produced, in addition to absorption, emission energies in better agreement with the experimental data. For brevity, the (TD-)B3LYP//(TD-)B3LYP and (TD-)B3LYP//(TD-)BP86 notations will be used to underline the functional used for the energy calculation and for the geometry optimization respectively. Details of the various electronic states of interest, *e.g.* orbital occupations, electronic configurations, atomic charges, etc., were explored via natural bond orbital (NBO) population analyses[35] of the B3LYP electronic structures.

Comments on the calculated absorption spectra for the GOAr cerium(III) complexes. The absorption spectra are predicted to be rather similar to those of the **GA** series concerning the λ^1_{abs} bands. That is, they occur at similar wavelengths and they have the same assignments, *i.e.*, $4f \rightarrow 5d_{z^2}$ transitions. The λ^2_{abs} bands are found to be of LMCT nature for the C_3 and nearly C_2 symmetric complexes **CeOAr$_3$** and **CeOAr$_2$G** respectively, and of essentially $4f \rightarrow 5d$ nature for the C_1 symmetry **CeOArG$_2$** complex. We noticed that these latter kinds of transitions also lead to intense absorption bands in the spectra of the former two complexes, but at slightly

lower wavelengths than the LMCT transitions (331 nm *vs.* ~350 nm, see Table S19 below). In fact, between the two $4f \rightarrow 5d$ absorption bands of **CeOAr$_3$** and **CeOAr$_2$G**, we predict two sets of LMCT bands assigned to transitions from **OAr**-based MOs into either a 4f or a $5d_{z^2}$ Ce acceptor orbital. The former type of LMCT bands correspond to λ^2_{abs} of **CeOAr$_3$**, while the latter type corresponds to λ^2_{abs} of **CeOAr$_2$G**. For a clearer view, Figure S69 (shown below) displays the Kohn-Sham donor and acceptor orbitals that give rise to λ^1_{abs}, λ^2_{abs} and λ^4_{abs} absorption bands (see Table S19 shown below) in the spectrum of the **CeOAr$_3$** complex.

Accuracy of the calculated absorption band maxima. The calculated λ^1_{abs} and λ^2_{abs} vertical excitation energies are overall in very good agreement with the experimental band maxima for both series of cerium(III) complexes, with an average deviation below 0.2 eV for the **GA** complexes (Tables S17, S18 shown below), and below 0.1 eV for the **GOAr** complexes (Table S19 shown below). The deviations may be due to the used exchange-correlation functionals or a systematic mismatch between the calculated vertical absorption energy and the experimental band peak position. Nonetheless, they are well within the error bars expected for TD-DFT calculations with standard functionals.

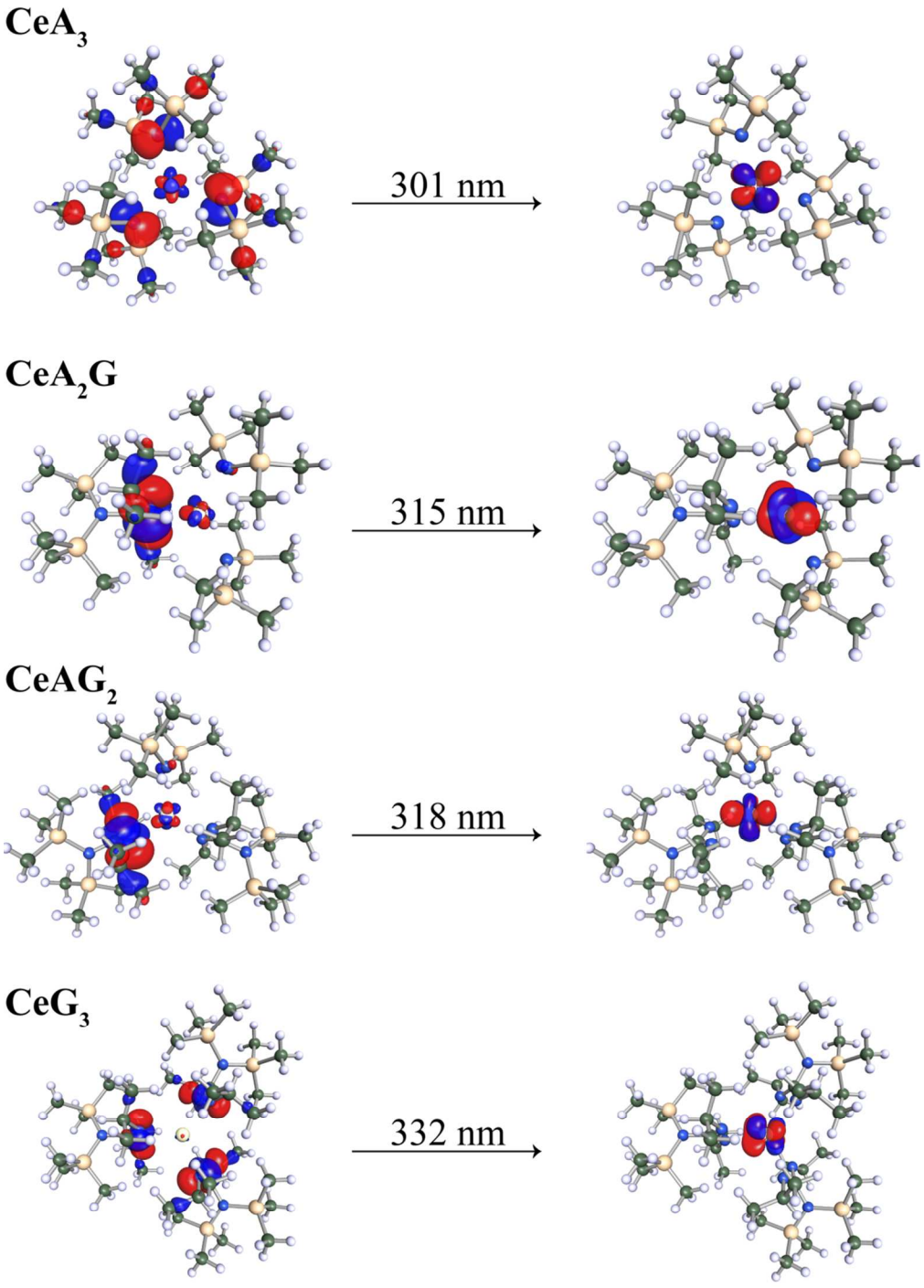

Figure S70. Kohn-Sham donor (left) and acceptor (right) orbitals that give rise to the lowest lying LMCT bands in the absorption spectra of the **GA** cerium(III) complexes. The isosurface value is ±0.04.

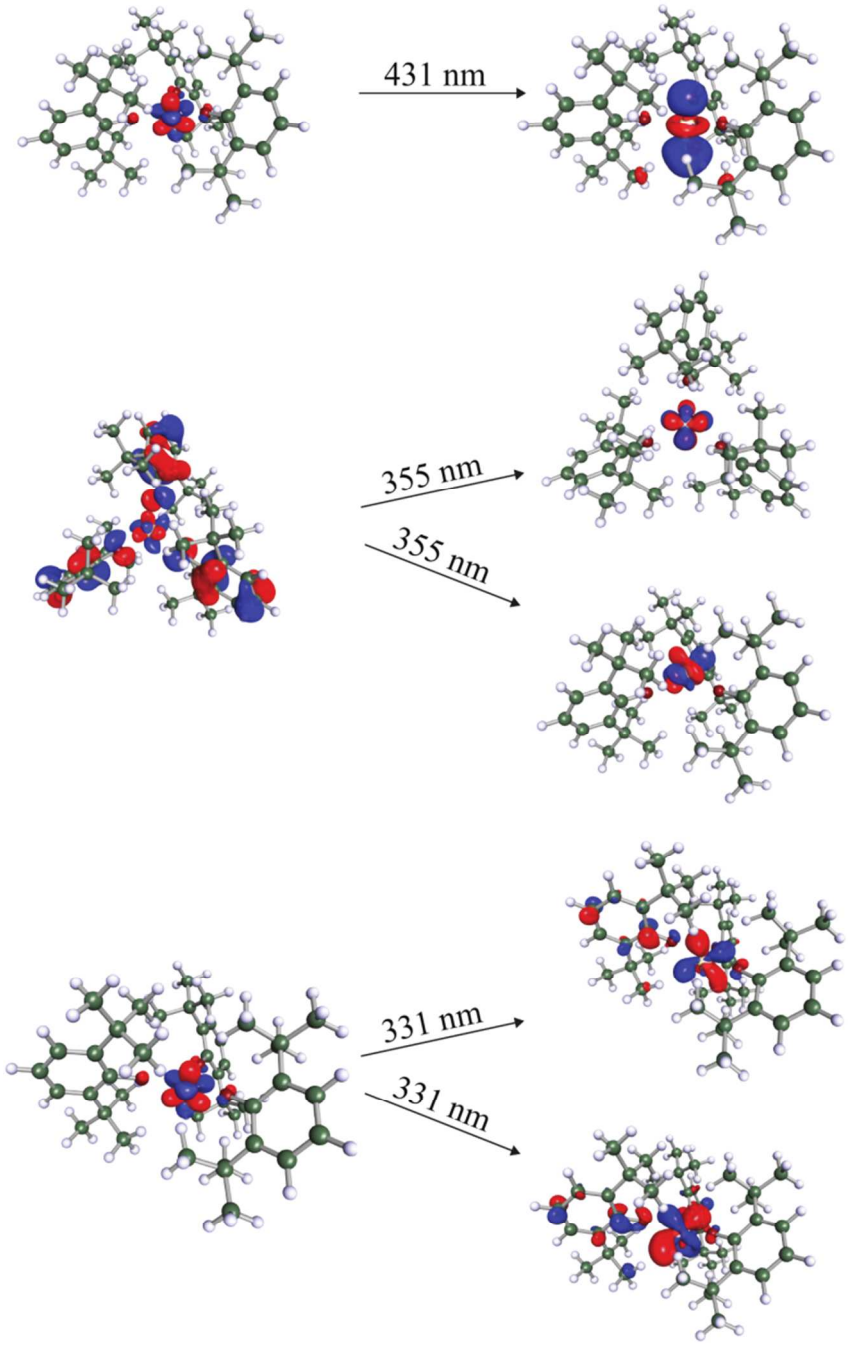

Figure S71. Kohn-Sham donor (left) and acceptor (right) orbitals that give rise to λ^{1}_{abs}, λ^{2}_{abs}, and λ^{4}_{abs} (see Table S19 below) absorption bands in the spectra of the **CeOAr$_3$** complex. The isosurface value is ±0.04.

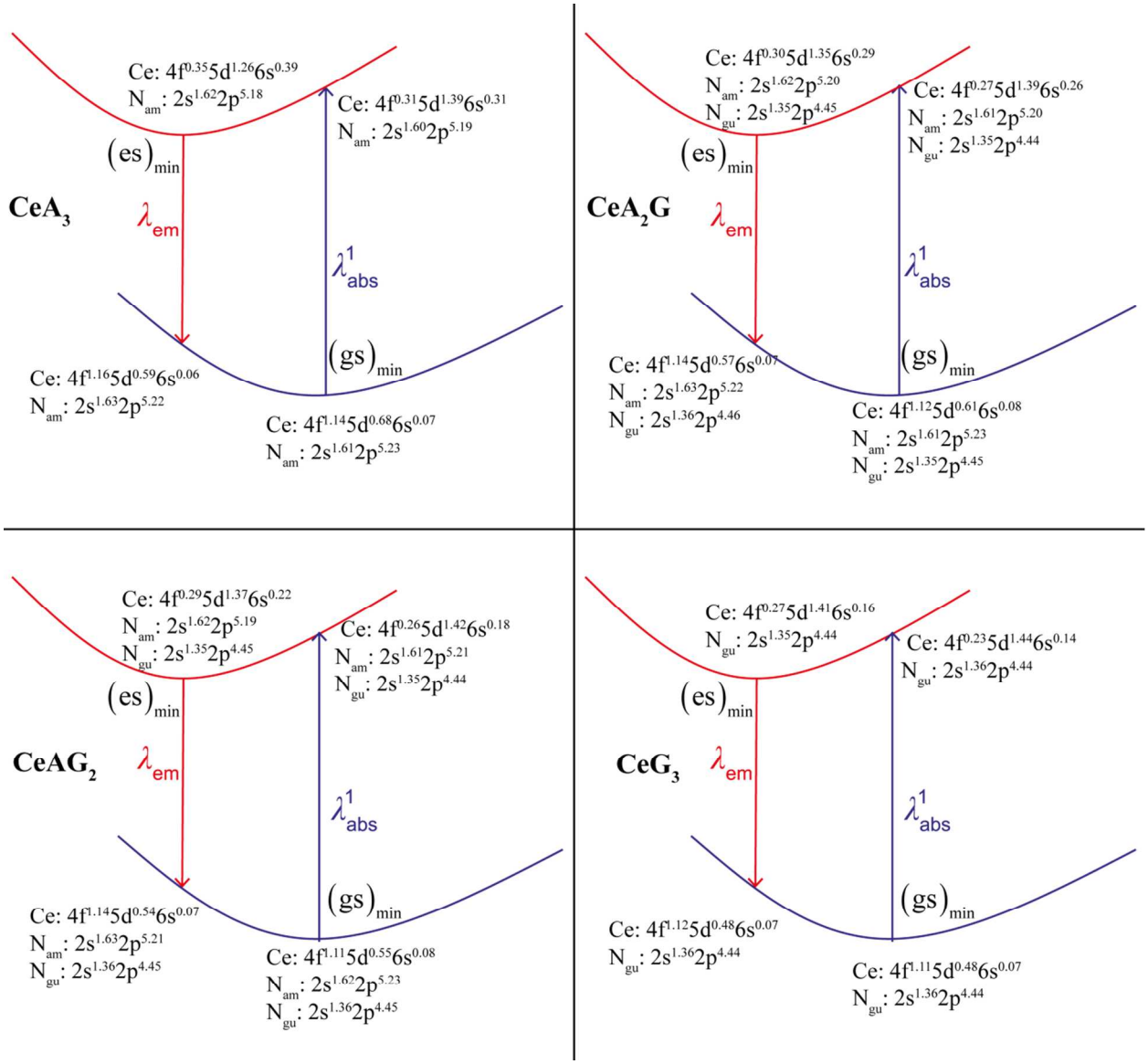

Figure S72. NBO populations, for the Ce and coordinating N atoms, obtained for the ground state and the emitting excited state in the **GA** complexes at their corresponding equilibrium geometries.

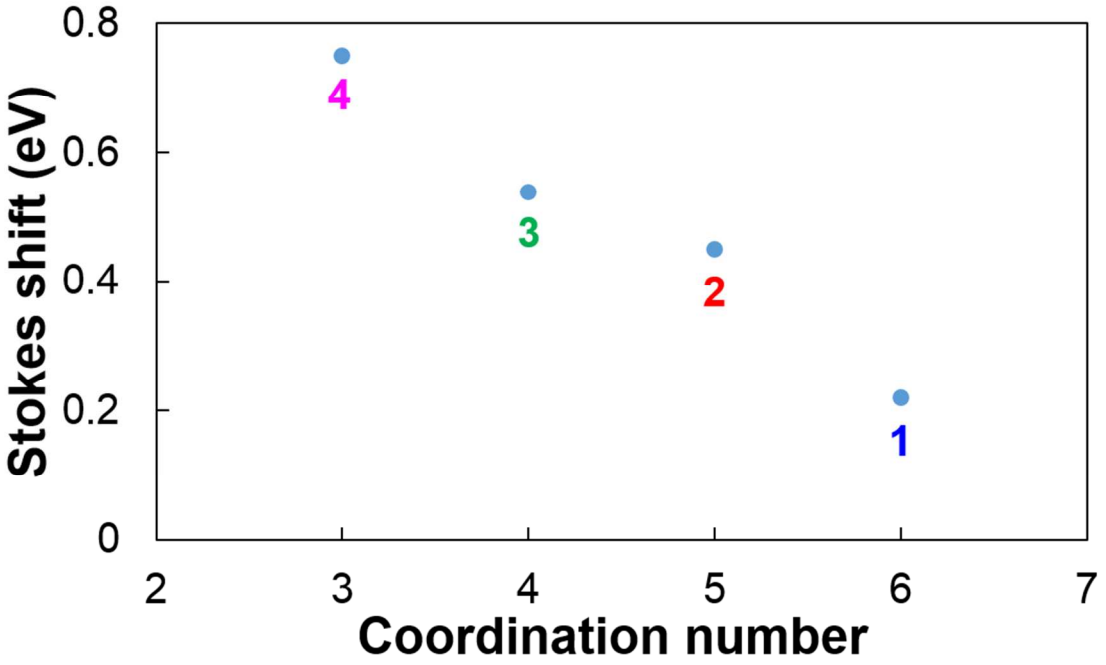

Figure S73. Correlation plot of the Stokes shift versus coordination number for complexes **1–4.**

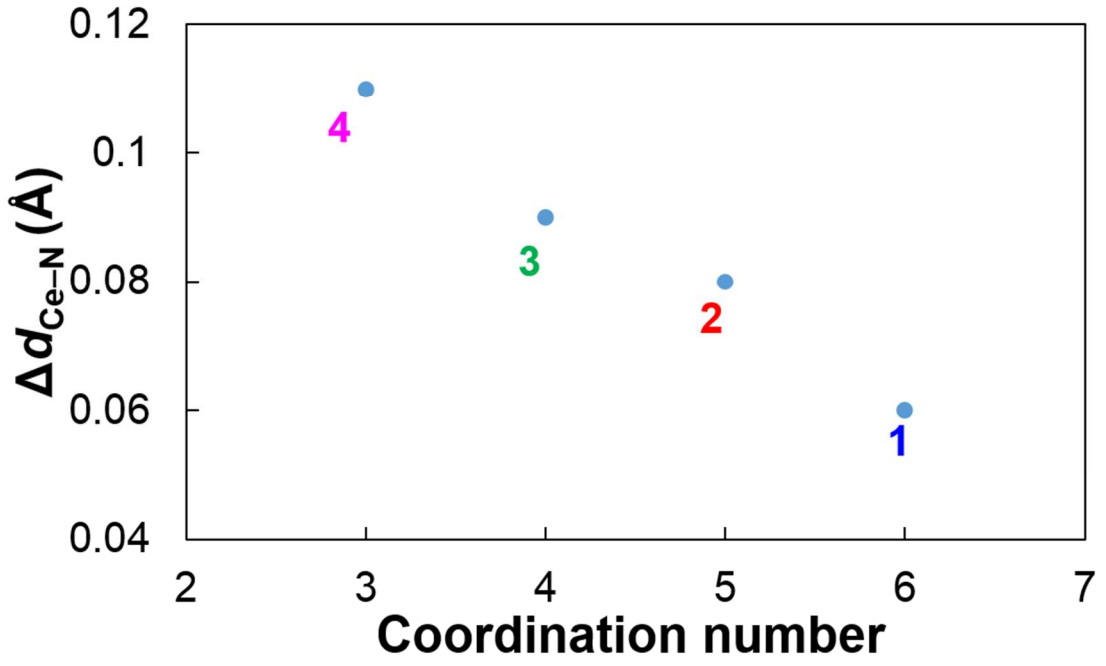

Figure S74. Correlation plot of the contraction of Ce–N bond *(Δd_{Ce-N})* versus coordination number for complexes **1–4.**

Table S15. Optimized ground state (gs) and emitting excited state (es) geometrical parameters, bond lengths (in Å) between the Ce atom and the amide/guanidinate N atoms (N_{am}/N_{gu}) of the first coordination sphere, and the differences of the average Ce–N bond distances between the calculated (B3LYP) ground-state and the excited-state structures (Δd_{Ce-N}). Where available, experimental X-ray diffraction (XRD) data are given for comparison.[a]

Complex[b]	Parameter[c]	El. State	BP86	B3LYP	Δd_{Ce-N}	XRD
CeA_3	$\bar{r}(\text{Ce-N}_{am})$	gs	2.33	2.34	0.11	2.32
		es	2.22	2.23		-
CeA_2G	$\bar{r}(\text{Ce-N}_{gu})$	gs	2.49	2.49	0.09	2.46
		es	2.43	2.43		-
	$\bar{r}(\text{Ce-N}_{am})$	gs	2.35	2.36		2.36
		es	2.23	2.25		-
$CeAG_2$	$\bar{r}(\text{Ce-N}_{gu})$	gs	2.53	2.54	0.08	2.49
		es	2.41	2.47		-
	$r(\text{Ce-N}_{am})$	gs	2.35	2.37		2.36
		es	2.28	2.25		-
CeG_3	$\bar{r}(\text{Ce-N}_{gu})$	gs	2.56	2.57	0.06	2.53
		es	2.46	2.51		-

[a]From ref 7. [b]See labeling in Figure 1 (main article). [c]Top bar denotes an average over all distances.

Table S16. Optimized ground state (gs) and emitting excited state (es) geometrical parameters, bond lengths (in Å) between the Ce atom and the guanidinate N atoms (N_{gu}) or aryloxide O atoms of the first coordination sphere. Where available, experimental X-ray diffraction (XRD) data are given for comparison.[a]

Complex	Parameter[b]	El. state	BP86	XRD
$CeOAr_3$	$\bar{r}$(Ce-O)	gs	2.17	-
		es	2.05	-
$CeOAr_2G$	$\bar{r}$(Ce-O)	gs	2.19	2.17
		es	2.11	-
	$\bar{r}$(Ce-N_{gu})	gs	2.47	2.44
		es	2.44	-
$CeOArG_2$	r(Ce-O)	gs	2.21	2.20
		es	2.14	-
	$\bar{r}$(Ce-N_{gu})	gs	2.52	2.48
		es	2.41	-

[a]From ref 7. [b]Top bar denotes an average over all distances.

Table S17. Calculated vertical absorption (λ^n_{abs}) and emission (λ_{em}) energies and wavelengths for the various **GA** cerium(III) complexes. Experimental values are given in parentheses.[a,b]

Complex	Band	Δ*E* (eV)	*λ*(nm)	*f*[c]	Assignment	Stokes shift[d]
CeA_3	λ^1_{abs}	3.02 (2.99)	411 (415)	0.0024	$4f \rightarrow 5d_{z^2}$	
	λ^2_{abs}	3.63 (3.43)	341 (362)	0.0040	$4f \rightarrow 5d$	
	λ^3_{abs}	4.12 (>3.87)	301 (<320)	0.0019	LMCT, $N_{am} \rightarrow 4f$	
	λ_{em}	2.08 (2.24)	597 (553)	0.0025	$5d_{z^2} \rightarrow 4f$	186 (138)
CeA_2G	λ^1_{abs}	3.00 (2.93)	413 (423)	0.0036	$4f \rightarrow 5d_{z^2}$	

	λ^2_{abs}	3.55 (3.38)	349 (367)	0.0045	$4f \rightarrow 5d$	
	λ^3_{abs}	3.94 (>3.87)	315 (<320)	0.0024	LMCT, $N_{gu} \rightarrow 4f$	
	λ_{em}	2.36 (2.39)	526 (518)	0.0030	$5d_{z^2} \rightarrow 4f$	113 (95)
$CeAG_2$	λ^1_{abs}	3.01 (2.89)	412 (429)	0.0039	$4f \rightarrow 5d_{z^2}$	
	λ^2_{abs}	3.89 (3.52)	319 (352)	0.0012	$4f \rightarrow 5d$	
	λ^3_{abs}	3.90 (≥3.87)	318 (≤320)	0.0066	LMCT, $N_{gu} \rightarrow 4f$	
	λ_{em}	2.51 (2.44)	494 (508)	0.0028	$5d_{z^2} \rightarrow 4f$	82 (79)
CeG_3	λ^1_{abs}	3.14 (2.92)	395 (424)	0.0020	$4f \rightarrow 5d_{z^2}$	
	λ^2_{abs}	3.66 (3.42)	338 (363)	0.0046	$4f \rightarrow 5d$	
	λ^3_{abs}	3.74 (~3.87)	332 (~320)	0.0060	LMCT, $N_{gu} \rightarrow 4f$	
	λ_{em}	2.89 (2.70)	430 (459)	0.0025	$5d_{z^2} \rightarrow 4f$	35 (35)

[a]From ref 7. [b]TD-B3LYP//(TD-)B3LYP calculations. [c]Oscillator strength in dipole-length representation. [d]Expressed in nm, calculated as the difference between λ_{em} and λ^1_{abs}.

Table S18. Calculated vertical absorption (λ^n_{abs}) and emission (λ_{em}) energies and wavelengths for the various **GA** complexes. Experimental values are given in parentheses.[a,b]

Complex	Band	Δ*E*(eV)	*λ*(nm)	*f*[c]	Assignment	Stokes shift[d]
CeA_3	λ^1_{abs}	2.99 (2.99)	414 (415)	0.0024	$4f \rightarrow 5d_{z^2}$	
	λ^2_{abs}	3.62 (3.43)	343 (362)	0.0042	$4f \rightarrow 5d$	
	λ^3_{abs}	4.26 (>3.87)	291 (<320)	0.0022	LMCT, $N_{am} \rightarrow 4f$	
	λ_{em}	2.10 (2.24)	591 (553)	0.0025	$5d_{z^2} \rightarrow 4f$	177 (138)

CeA_2G	λ_{abs}^1	2.97 (2.93)	417 (423)	0.0037	$4f \rightarrow 5d_{z^2}$	
	λ_{abs}^2	3.52 (3.38)	352 (367)	0.0047	$4f \rightarrow 5d$	
	λ_{abs}^3	4.12 (>3.87)	301 (<320)	0.0042	LMCT, $N_{gu} \rightarrow 4f$	
	λ_{em}	2.33 (2.39)	533 (518)	0.0025	$5d_{z^2} \rightarrow 4f$	116 (95)
$CeAG_2$	λ_{abs}^1	2.99 (2.89)	415 (429)	0.0039	$4f \rightarrow 5d_{z^2}$	
	λ_{abs}^2	3.86 (3.52)	321 (352)	0.0016	$4f \rightarrow 5d$	
	λ_{abs}^3	4.00 (≥3.87)	310 (≤320)	0.0033	LMCT, $N_{gu} \rightarrow 4f$	
	λ_{em}	2.44 (2.44)	509 (508)	0.0024	$5d_{z^2} \rightarrow 4f$	94 (79)
CeG_3	λ_{abs}^1	3.13 (2.92)	396 (424)	0.0029	$4f \rightarrow 5d_{z^2}$	
	λ_{abs}^2	3.61 (3.42)	343 (363)	0.0047	$4f \rightarrow 5d$	
	λ_{abs}^3	3.86 (~3.87)	321 (~320)	0.0079	LMCT, $N_{gu} \rightarrow 4f$	
	λ_{em}	2.55 (2.70)	487 (459)	0.0077	$5d_{z^2} \rightarrow 4f$	91 (35)

[a]From ref 7. [b]TD-B3LYP//(TD-)BP86 calculations. [c]Oscillator strength in dipole-length representation. [d]Expressed in nm, calculated as the difference between λ_{em} and λ_{abs}^1.

Table S19. Calculated vertical absorption (λ_{abs}^n) and emission (λ_{em}) energies wavelengths for the various **GOAr** complexes. Experimental values are given in parentheses.[a,b]

Complex	Band	Δ*E*(eV)	Δ*E*(nm)	*f*[c]	Assignment	Stokes shift[d]
$CeOAr_3$	λ_{abs}^1	2.88 (3.02)	431 (410)	0.0025	$4f \rightarrow 5d_{z^2}$	
	λ_{abs}^2	3.50 (3.50)	355 (3.54)	0.0047	LMCT, $_{Ar}O \rightarrow 4f$	
	λ_{abs}^3	3.65	340	0.0026	LMCT, $_{Ar}O \rightarrow 5d_{z^2}$	
	λ_{abs}^4	3.75	331	0.0114	$4f \rightarrow 5d$	
	λ_{em}	2.20 (2.38)	562 (522)	0.0026	$5d_{z^2} \rightarrow 4f$	131 (112)
$CeOAr_2G$	λ_{abs}^1	2.76 (2.86)	449 (434)	0.0041	$4f \rightarrow 5d_{z^2}$	
	λ_{abs}^2	3.54 (3.57)	350 (347)	0.0030	LMCT, $_{Ar}O \rightarrow 5d_{z^2}$	
	λ_{abs}^3	3.72	333	0.0030	LMCT, $_{Ar}O \rightarrow 4f$	

	λ^4_{abs}	3.75	331	0.0130	$4f \rightarrow 5d$	
	λ_{em}	2.34 (2.43)	531 (510)	0.0032	$5d_{z^2} \rightarrow 4f$	82 (76)
$CeOArG_2$	λ^1_{abs}	2.89 (2.80)	429 (443)	0.0053	$4f \rightarrow 5d_{z^2}$	
	λ^2_{abs}	3.66 (3.57)	339 (347)	0.0046	$4f \rightarrow 5d$	
	λ_{em}	2.32 (2.43)	535 (511)	0.0039	$5d_{z^2} \rightarrow 4f$	106 (68)

[a]From ref 7. [b]TD-B3LYP//(TD-)BP86 calculations. [c]Oscillator strength in dipole-length representation. [d]Expressed in nm, calculated as the difference between λ_{em} and λ^1_{abs}.

Table S20. NBO population and charge analysis for the electronic ground-state (gs) and the emitting excited-state (es) in the **GOAr** cerium (III) complexes at their corresponding equilibrium geometries.[a]

Complex	El. state	Ce charge	Ce populations	N_{gu}/O charge[b]
$CeOAr_3$	gs	2.17	$4f^{1.18}5d^{0.51}6s^{0.06}6d^{0.09}$	-/−0.98
	es	1.95	$4f^{0.45}5d^{1.15}6s^{0.39}6d^{0.07}$	-/−0.94
$CeOAr_2G$	gs	2.21	$4f^{1.15}5d^{0.50}6s^{0.06}6d^{0.08}$	−0.84/−0.99
	es	2.02	$4f^{0.36}5d^{1.20}6s^{0.33}6d^{0.08}$	−0.82/−0.95
$CeOArG_2$	gs	2.22	$4f^{1.13}5d^{0.49}6s^{0.07}6d^{0.08}$	−0.83/−0.98
	es	2.11	$4f^{0.34}5d^{1.23}6s^{0.21}6d^{0.09}$	−0.83/−0.95

[a](TD-)B3LYP//(TD-)BP86 calculations. Populations in units of electrons. [b]Natural charge averaged over all N_{gu}/O centers of the Ce first coordination sphere.

Multiconfigurational wave-function theory (WFT) calculations. To obtain a more complete picture of the electronic structures of the **GA** complexes, in particular regarding the influence of the spin-orbit coupling (SOC), *ab initio* WFT calculations based on a contracted spin-orbit configuration interaction approach were carried out at both the BP86 and B3LYP equilibrium geometries. The state-averaged complete active space self-consistent field (CASSCF) method,[36] was employed to generate a set of multi-configurational SOC-free electronic states. The active spaces used in these calculations comprised one electron in the seven 4f-dominant Ce-centered orbitals and additionally i) three Ce 5d-based orbitals that have $5d_{z^2}$, $5d_{xz}$ and

$5d_{yz}$ character for the **CeA_3** complex, ii) two Ce 5d-based orbitals that have $5d_{z^2}$ and $5d_{xz}$ character for the complex **CeA_2G**, iii) two Ce 5d-based orbitals that appear to have $5d_{z^2}$, $5d_{xz}$ and $5d_{x^2-y^2}$ character for the complex **$CeAG_2$** and, finally, iv) two Ce 5d-based orbitals that appear to have $5d_{z^2}$, $5d_{yz}$ and $5d_{x^2-y^2}$ character for the complex **CeG_3**. That is, CASSCF(1, 10) and CASSCF(1, 9) calculations were performed. The state averaging scheme consisted of the maximum number of doublet roots that can be achieved with these active spaces, *i.e.* either 10 or 9. The obtained CASSCF wave functions were then used as a basis to construct the SOC operator matrix, followed by diagonalization to yield the electronic states and energies including the effects from SOC. In order to account for scalar-relativistic (SR) effects, the second-order Douglas-Kroll-Hess (DKH2) all-electron Hamiltonian[37–39] has been used in all wave-function-based calculations. For brevity, CAS-SO and CAS-SR aliases are used through the manuscript to specify respectively if the CASSCF calculations included a treatment for both the SR effects and SOC or only for the SR effects. The segmented all-electron relativistically contracted SARC-DKH-TZVP basis set[40] was used for the Ce atom, alongside the def2-TZVP basis[41, 42] for the remaining atoms. The WFT calculations were performed with the ORCA program package.[43]

The ground state CAS-SR wave functions (*i.e.* obtained at the ground and excited state equilibrium geometries) were found to have a pronounced multiconfigurational character, as one would expect from the distribution of an electron among the nearly degenerate 4f orbitals, with configuration weights spanning a wide range between ~5% and ~80%. Despite the multiconfigurational character of the electronic ground states, the DFT and TD-DFT calculations performed well, which may be attributed to fortuitous error cancellations and the fact that the ground and emissive excited states are dominated by formally non-bonding orbitals. A pronounced multiconfigurational character was also identified for the CAS-SR wave functions associated with the λ^1_{abs} and λ_{em} excited states, both at the absorbing and the emitting geometries. Nonetheless, in both the CAS-SR and CAS-SO calculations, the configurations with the largest weights are the $4f^1$ ones in the ground states and the $5d^1_{z^2}$ ones in the λ^1_{abs} and λ_{em} excited states. Therefore, the assignment of the first excitation and the emission bands remains the same as those derived from the DFT calculations. Since both the CAS-SR and CAS-SO calculations delivered excitations and emission energies in good agreement with the measurements, neither larger active spaces nor the effect of additional dynamic correlation (i.e.

which could be introduced with a multireference perturbation theory approach) were investigated.

Table S21. Maximum absorption (λ_{abs}^{n}) and emission (λ_{em}) wavelengths for the various **GA** complexes, obtained from CAS-SR calculations. Experimental data are given in parentheses.[a,b]

Complex	Band	Δ*E*(eV)	*λ*(nm)	*f*[c]	Assignment	Stokes shift[d]
CeA_3	λ_{abs}^{1}	3.02 (2.99)	411 (415)	0.0168	$4f \rightarrow 5d_{z^2}$	
	λ_{em}	2.27 (2.24)	547 (553)	0.0130	$5d_{z^2} \rightarrow 4f$	136 (138)
CeA_2G	λ_{abs}^{1}	3.10 (2.93)	400 (423)	0.0147	$4f \rightarrow 5d_{z^2}$	
	λ_{em}	2.56 (2.39)	484 (518)	0.0119	$5d_{z^2} \rightarrow 4f$	84 (95)
$CeAG_2$	λ_{abs}^{1}	3.00 (2.89)	413 (429)	0.0100	$4f \rightarrow 5d_{z^2}$	
	λ_{em}	2.60 (2.44)	477 (508)	0.0087	$5d_{z^2} \rightarrow 4f$	64 (79)
CeG_3	λ_{abs}^{1}	3.07 (2.92)	404 (424)	0.0128	$4f \rightarrow 5d_{z^2}$	
	λ_{em}	2.84 (2.70)	436 (459)	0.0126	$5d_{z^2} \rightarrow 4f$	32 (35)

[a]From ref 7. [b]The (TD-)B3LYP equilibrium geometries are used. [c]Oscillator strength. [d]Expressed in nm.

Table S22. Maximum absorption (λ^{n}_{abs}) and emission (λ_{em}) wavelengths for the various **GA** complexes, obtained from CAS-SO calculations. Experimental data are given in parentheses.[a,b]

Complex	Band	Δ*E* (eV)	*λ*(nm)	*f*[c]	Assignment	Stokes shift[d]
CeA_3	λ^{1}_{abs}	3.01 (2.99)	412 (415)	0.0342	$^2F_{5/2} \rightarrow {}^2D$	
	λ^{1}_{em}	2.04 (2.09)	608 (592)	0.0105	$^2D \rightarrow {}^2F_{7/2}$	
	λ^{2}_{em}	2.30 (2.27)	539 (545)	0.0208	$^2D \rightarrow {}^2F_{5/2}$	127 (138)
CeA_2G	λ^{1}_{abs}	3.14 (2.93)	395 (423)	0.0257	$^2F_{5/2} \rightarrow {}^2D$	
	λ^{1}_{em}	2.34 (2.23)	530 (555)	0.0156	$^2D \rightarrow {}^2F_{7/2}$	
	λ^{2}_{em}	2.59 (2.43)	479 (509)	0.0221	$^2D \rightarrow {}^2F_{5/2}$	84 (95)
$CeAG_2$	λ^{1}_{abs}	3.06 (2.89)	405 (429)	0.0242	$^2F_{5/2} \rightarrow {}^2D$	
	λ^{1}_{em}	2.39 (2.32)	530 (535)	0.0180	$^2D \rightarrow {}^2F_{7/2}$	
	λ^{2}_{em}	2.64 (2.48)	479 (501)	0.0222	$^2D \rightarrow {}^2F_{5/2}$	74 (79)
CeG_3	λ^{1}_{abs}	3.14 (2.92)	395 (424)	0.0244	$^2F_{5/2} \rightarrow {}^2D$	
	λ^{1}_{em}	2.66 (2.51)	466 (494)	0.0213	$^2D \rightarrow {}^2F_{7/2}$	
	λ^{2}_{em}	2.91 (2.72)	426 (456)	0.0237	$^2D \rightarrow {}^2F_{5/2}$	31 (32)

[a]From ref 7. [b]The (TD-)B3LYP equilibrium geometries are used. [c]Oscillator strength expressed as sum over the oscillator strengths corresponding to excitations/de-excitations between the $^2F_{5/2}$/$^2F_{7/2}$ Kramers states and the ^2D SOC state. [d]Expressed in nm, calculated as the difference between λ^{2}_{em} and λ^{1}_{abs}.

Table S23. Maximum absorption (λ^{n}_{abs}) and emission (λ_{em}) wavelengths for the various **GA** complexes, obtained from CAS-SR calculations. Experimental data are given in parentheses.[a,b]

Complex	Band	Δ*E*(eV)	*λ*(nm)	*f*[c]	Assignment	Stokes shift[d]
CeA_3	λ^{1}_{abs}	2.99(2.99)	415(415)	0.0168	$4f \rightarrow 5d_{z^2}$	
	λ_{em}	2.31(2.24)	538(553)	0.0134	$5d_{z^2} \rightarrow 4f$	123(138)
CeA_2G	λ^{1}_{abs}	3.07(2.93)	404(423)	0.0149	$4f \rightarrow 5d_{z^2}$	
	λ_{em}	2.54(2.39)	489(518)	0.0119	$5d_{z^2} \rightarrow 4f$	85(95)
$CeAG_2$	λ^{1}_{abs}	2.98(2.89)	417(429)	0.0100	$4f \rightarrow 5d_{z^2}$	
	λ_{em}	2.57(2.44)	482(508)	0.0092	$5d_{z^2} \rightarrow 4f$	65(79)
CeG_3	λ^{1}_{abs}	3.05(2.92)	407(424)	0.0128	$4f \rightarrow 5d_{z^2}$	
	λ_{em}	2.72(2.70)	455(459)	0.0118	$5d_{z^2} \rightarrow 4f$	48(35)

[a]From ref 7. [b]The (TD-)BP86 equilibrium geometries are used. [c]Oscillator strength. [d]Expressed in nm.

Table S24. Maximum absorption (λ^{n}_{abs}) and emission (λ_{em}) wavelengths for the various **GA** complexes, obtained from CAS-SO calculations. Experimental data are given in parentheses.[a,b]

Complex	Band	Δ*E*(eV)	*λ*(nm)	*f*[c]	Assignment	Stokes shift[d]
CeA_3	λ^{1}_{abs}	3.01 (2.99)	412 (415)	0.0336	$^2F_{5/2} \rightarrow {}^2D$	
	λ^{1}_{em}	2.09 (2.09)	593 (592)	0.0118	$^2D \rightarrow {}^2F_{7/2}$	
	λ^{2}_{em}	2.34 (2.27)	530 (545)	0.0212	$^2D \rightarrow {}^2F_{5/2}$	118 (138)
CeA_2G	λ^{1}_{abs}	3.13 (2.93)	396 (423)	0.0258	$^2F_{5/2} \rightarrow {}^2D$	
	λ^{1}_{em}	2.32 (2.23)	534 (555)	0.0158	$^2D \rightarrow {}^2F_{7/2}$	
	λ^{2}_{em}	2.57 (2.43)	482 (509)	0.0220	$^2D \rightarrow {}^2F_{5/2}$	86 (95)
$CeAG_2$	λ^{1}_{abs}	3.05 (2.89)	407 (429)	0.0240	$^2F_{5/2} \rightarrow {}^2D$	
	λ^{1}_{em}	2.37 (2.32)	523 (535)	0.0190	$^2D \rightarrow {}^2F_{7/2}$	
	λ^{2}_{em}	2.62 (2.48)	473 (501)	0.0221	$^2D \rightarrow {}^2F_{5/2}$	66 (79)

CeG_3	λ^1_{abs}	3.13 (2.92)	396 (424)	0.0241	$^2F_{5/2} \rightarrow {}^2D$	
	λ^1_{em}	2.54 (2.51)	488 (494)	0.0213	$^2D \rightarrow {}^2F_{7/2}$	
	λ^2_{em}	2.80 (2.72)	443 (456)	0.0232	$^2D \rightarrow {}^2F_{5/2}$	47 (35)

[a]From ref 7. [b]The (TD-)BP86 equilibrium geometries are used. [c]Oscillator strength expressed as sum over the oscillator strengths corresponding to excitations/de-excitations between the $^2F_{5/2}$/$^2F_{7/2}$ Kramers states and the ^2D SOC state. [d]Expressed in nm, calculated as the difference between the λ^2_{em} and λ^1_{abs}.

12. References

1. Antolini, P. B.; Hitchcock, A. V.; Lappert, M. F.; *Eur. J. Inorg. Chem.* **2003**, 3391.
2. Sarker, H.; Greer, M. L.; Blackstock, S. C. *J. Org. Chem.* **1996,** *61,* 3177.
3. Lappert, M. F.; Slade, M. J.; Singh, A.; Atwood, J. L.; Rogers, R. D.; Shakir, R. *J. Am. Chem. Soc*. **1983**, *105*, 302.
4. Seaman, L. A.; Fortier, S.; Wu, G.; Hayton, T. W. *Inorg. Chem.*, **2011**, *50*, 636.
5. Cendrowski-Guillaume, S. M.; Gland, G. L.; Nierlich, M.; Ephritikhine, M. *Organometallics* **2000,** *19,* 5654.
6. Coles, M. P.; Hitchcock, P. B.; Khvostov, A. V.; Lappert, M. F.; Li, Z.; Protchenko, A. V. *Dalton Trans.*, **2010**, *39*, 6780.
7. Yin, H.; Carroll, P. J.; Manor, B. C.; Anna, J. M.; Schelter, E. J. *J. Am. Chem. Soc.* **2016**, *138*, 5984.
8. Thomson, R. K.; Scott, B. L.; Morris, D. E.; Kiplinger, J. L. *C. R. Chim.* **2010,** *13,* 790-802.
9. Wojdyr, M. *J. Appl. Crystallogr.,* **2010**, 43, 1126.
10. Lakowicz, J. R. *Principles of Fluorescence Spectroscopy*, 3rd Ed.; Springer: New York, **2006**.
11. http://www.horiba.com/fileadmin/uploads/Scientific/Documents/Fluorescence/quantumyieldstrad.pdf
12. Suzuki, K.; Kobayashi, A.; Kaneko, S.; Takehira, K.; Yoshihara, T.; Ishida, H.; Shiina, Y.; Oishi, S.; Tobita, S., *Phys. Chem. Chem. Phys.* **2009**, *11*, 9850.
13. Bruker, SAINT, Bruker AXS, Inc., Madison, WI, USA, **2009.**
14. Bruker, SHELXTL, Bruker AXS, Inc., Madison, WI, USA, **2009.**
15. Sheldrick, G. M. SADABS, University of Gottingen, Germany, **2007.**
16. Sheldrick, G. M. TWINABS, University of Gottingen, Germany, **2008.**
17. Sheldrick, G. M. *Acta Crystallogr. Sect. A* **2008,** 64, 112-122.
18. Sheldrick, G. M. SHELXL 2014/7; University of Gottingen, Germany, 2014.
19. Frisch, M. J.; Trucks, G. W.; Schlegel, H. B.; Scuseria, G. E.; Robb, M. A.; Cheeseman, J. R.; Scalmani, G.; Barone, V.; Mennucci, B.; Petersson, G. A.; Nakatsuji, H.; Caricato, M.; Li, X.; Hratchian, H. P.; Izmaylov, A. F.; Bloino, J.; Zheng, G.; Sonnenberg, J. L.; Hada, M.; Ehara, M.; Toyota, K.; Fukuda, R.; Hasegawa, J.; Ishida, M.; Nakajima, T.; Honda, Y.; Kitao, O.; Nakai, H.; Vreven, T.; Montgomery, Jr., J. A.; Peralta, J. E.; Ogliaro, F.; Bearpark, M.; Heyd, J. J.; Brothers, E.; Kudin, K. N.; Staroverov, V. N.; Kobayashi, R.; Normand, J.; Raghavachari, K.; Rendell, A.; Burant, J. C.; Iyengar, S. S.; Tomasi, J.; Cossi, M.; Rega, N.; Millam, J. M.; Klene, M.; Knox, J. E.; Cross, J. B.; Bakken, V.; Adamo, C.; Jaramillo, J.; Gomperts, R.; Stratmann, R. E.; Yazyev, O.; Austin, A. J.; Cammi, R.; Pomelli, C.; Ochterski, J. W.; Martin, R. L.; Morokuma, K.; Zakrzewski, V. G.; Voth, G. A.; Salvador, P.; Dannenberg, J. J.; Dapprich, S.; Daniels, A. D.;

Farkas, Ö.; Foresman, J. B.; Ortiz, J. V.; Cioslowski, J.; Fox, D. J. Gaussian 09, Revision A.02, Gaussian, Inc., Wallingford CT, **2009.**

20. Dolg, M.; Stoll, H.; Preuss, H. *J. Chem. Phys.* **1989,** *90,* 1730-1734; Cao, X.; Dolg, M.; Stoll, H. *J. Chem. Phys.* **2003,** *118,* 487-496.
21. Grigoriy, D. A. Z.; Zhurko, A. http://chemcraftprog.com/.
22. (a) Martin, R. L. *J. Chem. Phys.* **2003**, *118*, 4775. (b) Tretiak, S.; Saxena, A.; Martin, R. L.; Bishop, A. R., *Chem. Phys. Lett.* **2000**, *331*, 561.
23. https://www.molnac.unisa.it/OMtools/sambvca2.0/index.html.
24. Mathematica 8.0; Wolfram Research, Inc.: Champaign, IL, **2010**.
25. Bilbrey, J. A.; Kazez, A. H.; Locklin, J.; Allen, W. D. *J. Comput. Chem.* **2013**, *34*, 1189.
26. TURBOMOLE V5.7, a development of University of Karlsruhe and Forschungszentrum Karlsruhe GmbH, 1989-2007, TURBOMOLE GmbH, since 2007; available from http://www.turbomole.com", 2013.
27. Dolg, M.; Stoll, H.; Preuss, H. *J. Chem. Phys.* **1989,** *90,* 1730–1734.
28. Hariharan, P. C.; Pople, J. A. *Theoret. Chim. Acta* **1973,** *28,* 213–222.
29. Francl, M. M.; Pietro, W. J.; Hehre, W. J.; Binkley, J. S.; Gordon, M. S.; Defrees, D. J.; Pople, J. A. *J. Chem. Phys.* **1982,** *77,* 3654-3665.
30. Becke, A. D. *Phys. Rev. A* **1988,** *38,* 3098-3100.
31. Perdew, J. P. *Phys. Rev. B* **1986,** *33,* 8822-8824.
32. Becke, A. D. *J. Chem. Phys.* **1993,** *98,* 5648–5652.
33. Lee, C.; Yang, W.; Parr, R. G. *Phys. Rev. B* **1988,** *37,* 785–789.
34. Hirata, S.; Head-Gordon, M. *Chem. Phys. Lett.* **1999,** *314,* 291-299.
35. Reed, A. E.; Weinstock, R. B.; Weinhold, F. *J. Chem. Phys.* **1985,** *83,* 735-746.
36. Roos, B. O.; Taylor, P. R.; Siegbahn, P. E. M. *Chem. Phys.* **1980,** *48,* 157-173.
37. Douglas, M.; Kroll, N. M. *Ann. Phys.* **1974,** *82,* 89-155.
38. Hess, B. A. *Phys. Rev. A* **1985,** *32,* 756-763.
39. Hess, B. A. *Phys. Rev. A* **1986,** *33,* 3742-3748.
40. Pantazis, D. A.; Neese, F. *J. Chem. Theory Comp.* **2009,** *5,* 2229–2238.
41. Weigend, F.; Ahlrichs, R. *Phys. Chem. Chem. Phys.* **2005,** *7,* 3295-3305.
42. Weigend, F. *Phys. Chem. Chem. Phys.* **2006,** *8,* 1057–1065.
43. Neese, F. "ORCA – An *Ab initio*, DFT and Semiempirical SCF-MO Package, Version 4.0, Max-Planck-Institute for Chemical Energy Conversion, Mülheim an der Ruhr, Germany; available from https://orcaforum.cec.mpg.de", 2017.